UNIVERSITY OF LIVERPOOL

# Automatic Computer Vision Systems for Aquatic Research

Thesis submitted in accordance with the requirements of
the University of Liverpool for the degree of Doctor in Philosophy

by

**Qussay Salim Al-Jubouri**

September 2017

# Abstract

Recently, there has been an increase in biological research interest in fish, and zebrafish, as an efficient model in the investigation of a broad range of human diseases and genetic studies. Economically, the enormous number, low price and limited maintenance requirements of this fish species encouraged the researchers to use it extensively. The larva of this animal is also considered to be promising subjects for research that is not subject to same strict legal requirements as the adult fish. The importance of this animal in research has increased the demand for developing new computer vision tools and methods that could help researchers to perform more related investigations as well as understand behaviour for different experimental tests.

Computer vision is an efficient, economical and non-intrusive tool that can be applied to research in aquatic laboratories and aquaculture environments. However, in marine applications, this technology is still facing big challenges due to the free-swimming nature and unpredictable behaviour of the fish. This thesis presents a suite of novel and cost-effective tools for fish tracking and behavioural analysis, sizing, and identification of individual zebrafish. These main contributions this work is outlined briefly as follows.

The first part of this work deals with stimulation and physical activity analysis for fish larvae, a novel robust and automated multiple fish larva tracking system is proposed. The system is capable of tracking twenty-five fish larvae simultaneously and extracting all physical activity parameters such as; speed, acceleration, path, moved distance and active time. The system is used for further studies throughout local occurrence behaviour recognition and studying the behavioural of the fish larvae following electrical, chemical and thermal stimulation. The proposed tracking system has been adopted in the biologists' aquatic laboratory to be used as a robust tool for fish behaviour analysis when fish are exposed to several types of stimulation.

In the second part of the work, two novel practical and cost-effective models; orthogonal and stereo systems are designed and implemented to estimate the length of small free-swimming fish using off-the-shelf-components. The designed

models are accurate and easy to adapt use for small experimental tanks in laboratory settings. The models have been thoroughly tested and validated experimentally.

The third part of this thesis offers novel non-contact methods for recognition of individual free-swimming fish. Such systems can significantly reduce experts efforts and time required for fish tagging process and also offer a real-time recognition technique that can be alternative to the existing tagging methods used in this field.

Through the purposes of this suite of novel computer vision tools and models, this thesis has provided successful solutions for behavioural analysis, fish sizing, individual fish recognition related research problems. The proposed solutions addressed major research problems and provided novel and cost-effective solutions for these problems.

*To my*

*Beloved mother*

*Darling wife*

*Lovely children*

*Great brothers*

*and*

*Wonderful sister*

# Acknowledgements

I would like to express my gratefulness to all people who helped me achieve this work.

My deep thanks and appreciations go to my supervisor, Dr. Waleed Al-Nuaimy, who supervised and guided this work; his advice and suggestions have been invaluable. Many thanks and gratitude go to Dr. Iain S. Young for his encouragement, advice and constructive suggestions. His support has been invaluable for me. Special thanks also go to Prof. Majid Al-Taee for his valuable advice.

Many thanks go to Prof. Lynne U. Sneddon and Dr. Javier Lopez-Luna from the Institute of Integrative Biology, University of Liverpool, UK, for their valuable advice and support; Dr. Jonathan Buckley from the Institute of Functional and Comparative Genomics, University of Liverpool, for his constructive comments.

My deepest gratitude goes to my lovely family: my mother for pleasant words, my wife for her unconditional love and support, great brothers and sister and to my children.

I gratefully acknowledge financial support from the University of Technology, Ministry of Higher Education and Scientific Research, Iraq, that made this research possible and enable me to obtain this degree.

To all I would like to say, **thank you very much.**

Qussay Salim Al-Jubouri
Liverpool - UK
2017

# Contents

# List of Figures

# Chapter 1

# Introduction

## 1.1 Overview

Aquatic animals are becoming increasingly popular in biological studies and drug testing and as well as in aquaculture [1, 2, 3, 4]. Small aquatic animals and zebrafish (*Danio rerio*) in particular, have become the default experimental subject for a wide spectrum of studies.

The usage of a huge number of fish in research labs becomes an acceptable practice and over half a million fish are involved in scientific procedures annually in the UK alone [5]. Particularly, zebrafish become a preferable model for pain, stress, and welfare assessment in animals due to similarities between its nociceptive apparatus and that of mammals [6, 7]. Among these studies, the behavioural analysis of zebrafish larvae when exposed to different types of stimulation has also been of particular importance for biologists. However, accurate tracking and monitoring of the behaviour of these larvae have been a challenging process, mainly due to

its small size and transparency. Thus, the demand is increased for developing new computer vision systems for monitoring, recognition, tracking, sizing, and behavioural analysis of fish [8, 9, 10, 11, 12].

Over the past decade, video measurement and tracking has been widely used in aquaculture for fish product evaluation and have played a significant role in the enhancement of fish welfare. Furthermore, computer vision has become increasingly important in the monitoring of different analysis aspects including animal growth and health problems. This continuous growth in fish research has highlighted the need for monitoring devices and a non-destructive tools that can acquire relevant information remotely as reported in [13, 14, 15]. This is mainly due to the absence of disturbances related to the capture, transport, handling in various aquaculture processes [16, 17].

## 1.2 Motivation

Unlike large aquatic animals, small fish have not been thoroughly explored in the literature in terms of behaviour analysis, sizing and individual recognition. This is mainly due to the challenges of (i) their small size and (ii) fast and unpredictable movement. Similarly, the majority of existing conventional techniques for sizing and physical tagging of such fish used manual techniques which are considered a source of stress and pain and also might damage the subject under test.

In contrast, computer vision technology offers non-destructive and fast tool for fish research and aquaculture applications. However, this technology has not been thoroughly explored yet for such small size. In this project, unlike existing

computer vision systems, the proposed system addresses three key automation requirements:

- Behaviour analysis of larval fish when exposed to different type of stimulation
- Automated sizing systems of small free-swimming fish
- Recognition of individual adult zebrafish

These applications can be described as follows.

1. **Behaviour analysis** - physical activity monitoring for zebrafish larvae is a vital issue in animal research by which the pain/stress of stimulated animals under test can be quantified. In this project, a novel electrical stimulation hardware and software platform are designed and implemented. Unlike existing tracking systems, our developed system is fully automatic and does not require any manual adjustments. In addition, it is capable of estimating and monitoring physical activity of twenty-five larvae simultaneously.

2. **Sizing** - two cost-effective fish sizing systems are designed and implemented experimentally to address the fish-length estimation problem for small fish in lab tank. The first one introduces a new method for estimating the length of free swimming fish and outline its potential application to small fish (zebrafish) sizing. A mathematical model is derived that accounts for the fish-length projection error caused by light refraction during the measurements of subject length. Camera-distance calibration is also assessed experimentally and the performance of the entire sizing system is evaluated using a couple of free swimming zebrafish.

The second novel fish length estimation system is developed using the same cameras with the stereoscopic setup. The first camera in this system is placed perpendicularly at the front of the tank with desired distance while the second one is tilted with an angle to obtain the required intersection field of view at the rear end of the tank. For this setup, a new mathematical model is derived to estimate camera-fish distance which represents the most important parameter in the fish length estimation process. Furthermore, automatic calibration is also applied in this system to map the image pixels to metric dimensions.

3. **Recognition** - two new recognition methods for individual adult zebrafish are proposed as an alternative to the physical fish tagging. In the former one, blue stripes pattern exists around the central left or right side of the fish is adopted for feature extraction. This is achieved by using image color-space transformation (from RGB colour space to L*a*b* colour space) to obtain a more accurate segmentation using k-means clustering approach. The pixels values and locations of the blue stripes are characterized to extract a single feature that is considered to be as a unique feature that can be used to recognize the individual adult zebrafish.

   The latter method is based on using Speed-Up Robust Feature (SURF) matching which was proved as a robust invariant-scale and orientation for image recognition applications. In our proposed method, a set of local features are extracted from a sequence of image frames of the entire fish body. Then, the pre-extracted sets of features are stored as a reference database and the matching process between the computed features of the current image and corresponding stored features are performed according to the biggest ratio of matched features pairs between two images. The decision

of matching is performed throughout using threshold value which represents the minimum similarity between images.

## 1.3 Aims and Objectives

This thesis aims at developing and applying computer vision techniques to support biologist researchers to obtain more behavioural intelligence and extend their experimental knowledge about zebrafish under test. Three important application problems involving behavioural analysis of fish larvae, sizing, and recognition of individual adult zebrafish are studied as shown in Figure 1.1. The work also aims to track adult fish in three dimension to increase the richness of the behavioural data collected.

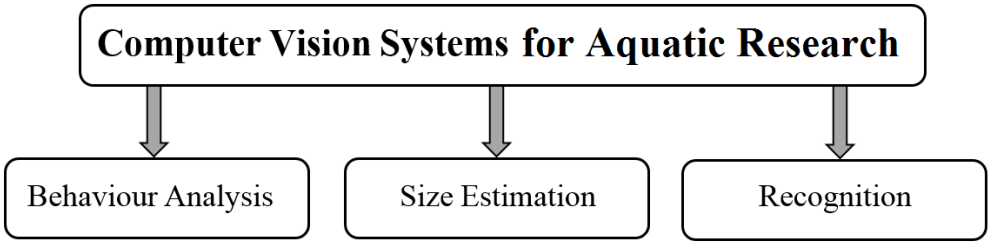


FIGURE 1.1: Overview of the proposed vision systems

The research described in this thesis is focused on proposing novel automated cost-effective behaviour analysis platform, fish sizing and fish identification based on new computer vision techniques. Towards this end, the following specific objectives have been identified:

- **Fish Larvae Behaviour Analysis**: Design a novel electrical stimulator hardware platform aided with robust automatic tracking and data analysis

software for physical activities of fish larvae and proposing a new method to investigate the effect of intensity of electric shock signal on the behaviour of zebrafish larvae.

- **Fish length estimation**: Design and implement novel cost-effective computer vision systems using automatic image calibration for both orthogonal and stereo camera setup for the purpose of automated small fish sizing.
- **Recognition of individual adult zebrafish**: Propose new automatic computer vision techniques to identify individual adult zebrafish swimming freely in real-time.

## 1.4 Contributions

This thesis has addressed a range of pressing research and practical challenges. The main contributions of this research can be summarized as follows:

- A novel tracking software based on an object automated detection, tracking, and monitoring algorithm is developed for this project. The algorithm is divided into four different stages, namely pre-processing, object detection, post-processing, and monitoring of the object physical activity.
- Design and develop a new automatic electrical stimulator that capable of stimulating 25 fish larvae simultaneously. This platform is considered as a novel approach for the stimulation and analysis of larval fish and can contribute to better understanding of the behaviour of zebrafish larvae.
- Design and develop two cost-effective fish sizing systems (orthogonal and stereo cameras setup) with automatic measurements calibration that capable

of real-time length estimation for small free swimming fish in the lab using web cameras.

- Proposing two new methods for individual adult zebrafish fish recognition as an alternative to the physical tagging by extracting single or set of features from the fish image. The first proposed method depends on the extraction of the blue stripe patterns feature while in the second recognition method local features matching are used based on Speed-Up Robust Feature (SURF) method.

- Assessing validity and performance of the developed systems experimentally with aid of consultant specialists in the department of life sciences / University of Liverpool.

These contributions are reflected by publishing the following research papers in peer-reviewed journals and referred international conferences:

### 1.4.1 List of Publications

(i) **First author**

(1) Q. Al-Jubouri, W. Al-Nuaimy, M. Al-Taee1 and I. Young, "An Automated vision system for measurement of small-fish length using low-cost orthogonal web cameras," Journal of Aquaculture Engineering, 2017, vol 78, part B, pp. 155-162

(2) Q. Al-Jubouri, W. Al-Nuaimy, M. Al-Taee1 and I. Young, "A new stereo-imaging system for length estimation of small free-swimming fish," Journal of Aquaculture Engineering, 2017, (Submitted).

(3) Q. Al-Jubouri, W. Al-Nuaimy, M. A. Al-Taee, J. Lopez-Luna and L. Sneddon, "Occurrence density index for behaviour classification of zebrafish larvae" Proc. IEEE Int. Multi-Conference on Systems, Signals, and Devices (SSD), Leipzig, Germany, March 2016, pp. 645 - 649.

(4) Q. Al-Jubouri, W. Al-Nuaimy, M. Al-Taee1 and I. Young, "Computer stereo vision system for 3D tracking of free-swimming zebrafish," Proc. IEEE Conference on Developments in eSystems Engineering, Paris, France, June 2017.

(5) Q. Al-Jubouri, W. Al-Nuaimy, M. Al-Taee I. Young, "Recognition of individual zebrafish using speed-up robust feature matching," Proc. IEEE Conference on Developments in eSystems Engineering, Paris, France, June 2017.

(6) Q. Al-Jubouri, W. Al-Nuaimy, M. Al-Taee, I. Young, H. Al-libawy and B. Al-Saaidah,"Identification and extraction of a new feature for zebrafish discrimination," Proc. Conference on Developments in eSystems Engineering, Liverpool and Leeds, UK, September 2016. (Best paper award)

(7) Q. Al-Jubouri, W. Al-Nuaimy, M. A Al-Taee, J. Lopez-Luna and L. Sneddon, "An automated pattern detection method for behavioural analysis of zebrafish larvae," Proc. IEEE Conference on system, signals, and devices (SSD), Leipzig, Germany, March 2016.

(8) Q. Al-Jubouri, W. Al-Nuaimy, M. A Al-Taee, J. Lopez-Luna and L. Sneddon, "Automated electrical stimulation and physical activity monitoring of zebrafish larvae," Proc. IEEE Conference on Applied Electrical Engineering and Computing Technologies (AEECT), Amman, Jordan, November 2015.

(9) Q. Al-Jubouri, W. Al-Nuaimy, H. S. AlZu'bi, O. Zahran and J. Buckley, "Towards automated monitoring of adult zebrafish," Proc. IEEE Workshop on Computational Intelligence (UKCI), Bradford, UK, September 2014.

(ii) **Second author**

(1) J. Lopez-Luna, Q. Al-Jubouri, W. Al-Nuaimy and L. Sneddon, "Reduction in activity by noxious chemical stimulation is ameliorated by immersion in analgesic drugs in zebrafish," Journal of Experimental Biology, vol. 220, pp. 1451-1458.

(2) J. Lopez-Luna, Q. Al-Jubouri, W. Al-Nuaimy and L. Sneddon, "Impact of analgesic drugs on the behavioural responses of larval zebrafish to potentially noxious temperatures," Journal of Applied Animal Behaviour Science. (*doi.org*/10.1016/*j.applanim*.2017.01.002)

(3) J. Lopez-Luna, Q. Al-Jubouri, W. Al-Nuaimy and L. Sneddon, "Swimming activity of larval zebrafish after exposure to irritant chemicals and analgesics," figshare, (2016), (*doi.org*/10.6084/*m*9.*figshare*.4285778.*v*3).

(4) J. Lopez-Luna, Q. Al-Jubouri, W. Al-Nuaimy and L. Sneddon, "Impact of stress, fear and anxiety on the nociceptive responses of larval zebrafish,", Journal 'PLOS ONE' , 2017, (Aceptted).

## 1.5 Thesis Organization

The thesis is organized into eight chapters as follows:

**Chapter 2** presents a literature review of state-of-the-art in the field computer vision techniques used for aquatic animals in both aquaculture and research. It focuses on the impact of applying computer vision systems on the aquatic research area. Challenges associated with painful stimulation and physical activities analysis for fish larvae and sizing approaches and, fish individual recognition methods are also presented in this chapter. It also provides an overview of the proposed vision system applications for small aquatic animals.

**Chapter 3** provides a detailed description for a new electrical stimulator hardware platform developed for experiments carried out in this research. It describes the design and construction of a new electrical stimulator that is used to study the physical behaviour of fish larvae when they are exposed to a different level of stimulation density.

**Chapter 4** proposes a novel software tracking package that is designed and developed by the author is presented in this chapter. The developed package helps developing new behavioural analysis approaches for fish larvae can be investigated.

**Chapter 5** deals with detailed description of the developed orthogonal vision system of fish-length estimation model with derived correction mathematical model.

**Chapter 6** deals with the design and development of stereo-vision for fish-length estimation. Mathematical modelling, calibration, and verification are presented and discussed in this chapter.

**Chapter 7** presents two new recognition methods for adult zebrafish individuals using CIELAB color space clustering and Speed-Up Robust Feature for feature extraction. The methodology of this work and the obtained results are presented and discussed in this chapter.

Finally, **Chapter 8** draws conclusions from the work presented in this thesis and suggests new areas for future work.

# Chapter 2

# Background

## 2.1 Introduction

Fish have become increasingly popular because of their importance in biology studies and drug test as well as in fish farming studies. Small aquatic animals and zebrafish (*Danio rerio*) in particular, have become the second experimental animal for a wide spectrum of studies. This kind of fish is used as the most common biological model in the laboratories worldwide after mice [3, 18, 19, 20]. This chapter reviews the studies that have been done before the development of this work. In particular, it summarizes study material, ideas and concepts of computer vision implementation that is used in fish research. The state-of-the-art and impact of computer vision systems which are commonly used for behavioural analysis, sizing and recognition in fish research are presented. It also provides an overview of computer vision applications and methods that form the main contributions of this research.

## 2.2 Aquatic Animals in Research

Small aquatic animals and zebrafish, in particular, have become the default experimental subject for a wide spectrum of studies. This is mainly because of its reduced latency to the expression of phenotype, short life-cycle, small size, low cost, subject to many tractable gene function analysis techniques as well as its amenability to oncogenic and chemical modifiers [6, 21, 1, 22]. It has also proved to be a great resource for the facilitation of drug discovery and psychotropic drugs screening [3] and aquatic toxicology studies. Such studies may provide insights into the development of smoking-related disease and could provide a cost-effective, high-throughput platform for the future evaluation of tobacco products [23]. An example image for an adult zebrafish is shown in Figure 2.1.

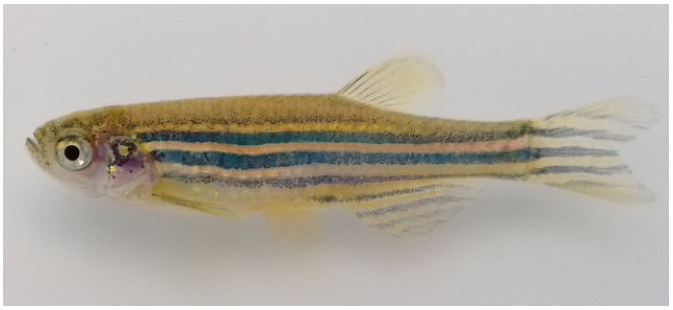

FIGURE 2.1: Zebrafish (*Danio rerio*)

The usage of a huge number of zebrafish in research becomes an acceptable practice. Approximately, over half a million fish are involved in scientific procedures annually in the UK alone [5]. This type of fish has also become a preferable model for pain, stress, and welfare assessment in animals due to similarities between its nociceptive apparatus and that of mammals [6, 7]. As a result, these have been a growing demand for developing new techniques for monitoring, recognition, tracking, sizing and behavioural analysis of this kind of fish [8, 9, 10, 11, 12].

Furthermore, the use of larval zebrafish shown in Figure 2.2 as a model organism in high-throughput behavioural screen has also grown rapidly due to:

- Development and availability of commercial and academic analytical platforms designed to assess locomotor activity [24, 25]
- Its large number of embryos produced from a single mating which led to the development of high-throughput testing of large numbers of experiments.
- Under European legislation on the protection of animals (Directive 2010/63/EU) these animals are not protected until 5 days post fertilization (dpf) [26]. Thus they are not subject to the legal requirements that adults are such as; handling of fish shall be kept to a minimum, water flow should be re-circulatory systems or filtration, temperature shall be maintained within optimal range, suitable lighting and noise levels shall be kept to a minimum noise and others.

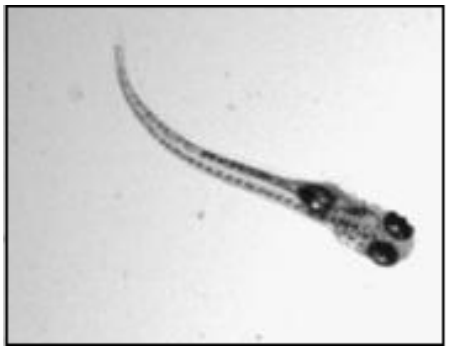

FIGURE 2.2: Example for larval zebrafish (5 days post fertilisation) [27]

Among these studies, the behavioural response of zebrafish larvae after exposed to different stimulation methods have also been of particular importance. In addition, their responses to a wide range of stimuli are robust and they have a significant potential for high-throughput screening by existing computer vision tools. However, accurate tracking and monitoring of the behaviour of these larvae

have been a challenging process, mainly due to its small size and transparency as shown in Fig.2. These circumstances allow developing high-throughput testing of large numbers of animals and offer more flexible experimental conditions.

## 2.3 Computer Vision for Aquatic Animals

Computer vision is an image processing/analysis technique which has been used as an efficient, economical and non-destructive tool in aquacultural applications and fish research. It becomes increasingly important in the monitoring of various aspects including animal growth and health problems. Over the past decade, video measurement and tracking has also been widely used in aquaculture for fish product evaluation and played a significant role in the enhancement of fish welfare. An example of continuous growth in fish research that highlighted the need for monitoring devices and tools that can acquire relevant information remotely was reported in [13, 14, 15]. Other vision systems have also been found to be particularly effective in remote monitoring under various operational conditions are reported when compared to existing manual approaches. This is mainly due to the absence of disturbances related to capturing and handling fisheries for various aquaculture applications [16, 17]. Moreover, the growth of aquaculture activities in offshore cages, for example, highlights the need for monitoring devices and procedures that can be remotely operated.

Application of vision systems to behavioural analysis, sizing, and recognition of fish which are particular interest in this research is reviewed in the following sections.

## 2.4 Fish Behaviour Analysis

Several image processing techniques have been proposed and utilized to study behaviour of fish [24, 25]. The typical variables that are used to quantify the physical activity of the fish such as total distance moved, velocity, acceleration, time spent active are adequate to interpret some of the observed behaviours. These parameters are widely used as common features in altered motor fish behaviours analysis. In [28], a method was proposed to analyze the avoidance behaviour of zebrafish larvae automatically. This method is used to characterize the response of larvae to visual stimulation using swimming speed and spent time as main parameters in the analysis process.

A method to characterize the response of larvae to light stimuli using the location and orientation of larvae in twelve multiple well plates was proposed in [28]. The behaviour of larvae was evaluated according to the location of larva centroid about a midpoint of the arena in the analysis process. Another method was reported in [29] to detect the auditory response defect in zebrafish. In this process, a sound level was used as a parameter to assess fish startle response to acoustic stimulation. The picture of the fish before and after stimuli were presented in different colours. Spectral analysis of the motion of the plate supporting the fish containers was used to analyse the effect of sound stimuli on fish behaviour. Another an optomotor analysis system was reported in [30] to investigate the behaviour of larvae fish to light stimuli. The light stimulation is performed using LCD screen of the laptop and the larvae were imaged by high-resolution digital camera placed in front of laptop screen.

In [31] the author suggested an approach to quantify the development of a newly

hatched embryo zebrafish using the swimming speed only as a feature of the behaviour of the fish. In [32], the average of distance moved is only used to analyze the behaviour changes in the response of zebrafish for long-term.

It was reported that the movement of the fish was measured automatically with the aid of an existing algorithm called LSRtrack [33] by adopting a similar set of motion parameters. The LSRtrack algorithm was also used in [34] as a tracking tool in motor function quantification for larval zebrafish. However, this tracking system depends on using infrared videography at 2 frames/sec which miss a large amount of physical activity information. Furthermore, in literature, LSRtrack algorithm is used mainly to track fish larvae of 7 days post-fertilization (dpf) which make it uncompilable for the other experiments which use unprotected larvae (i.e. 5 dpf larvae).

Several commercial tracking systems [35, 36, 37, 38] have also been introduced to track and analyze larvae fish. These products, however, are either of a high cost or prone to human error due to the requirement of precise manual procedures to specify dimensions of each test arena. For example, the Lolitrack v4 requires every arena to be defined manually with the objects that will be tracked. Certain RGB threshold values need to be adjusted manually prior to running the tracking process. In addition, the object is mirrored so that the user has to create a mask to avoid tracking outside the area of the test arena.

These studies emphasise that the use of the computer vision systems has become an essential technique in studying the behaviour analysis of zebrafish of large-scale experiments in this area. However, the need for robust, cost-effective, and easy setup remote observations tools is indispensable for the behavioural analysis of small size animals and zebrafish in particular.

## 2.5 Fish Sizing

Automatic computer vision for estimating the size of free swimming fish is considered as a sophisticated and high-cost system and is expected to have an error during observation process. Thus, manual image analysis and measurement which needs experts are adopted to obtain accurately fish size. As reported in [13], manual camera-based fish size measurement was used to estimate the length of Atlantic salmon using conventional dimensions of the lateral profiles of the fish body. The authors concluded that the use of multi-factor regression equations for mass prediction of individual dead fish is more accurate than using single-factor, suggesting that calibration equations will be different according to the structural difference in strain. A stereovideo system for free-swimming southern blue-fin tuna and other fish in both wild fisheries and aquacultural situations were proposed in [39]. The features of interest in this system, however, need to be pre-specified manually.

Several computer vision scenarios for fish sizing has been proposed and applied successfully using conventional dimensions measurement tools [40]. However, only a few of them have been developed as semi-automatic systems based on different imaging scenarios and size estimation techniques. In [14], a semi-automatic system for fish size estimation was developed using point distribution model (PDM). This system is based on the segmented edge distribution of fish body. Estimation accuracy of this model, however, which is affected by the manual placement of the initial position of the PDM as well as by the effect of neighboring fish images that force the final fitting away from the correct edges of the used template. A support vector machine (SVM) technique for size and the mass prediction was reported in [41]. This technique was based on 13 extracted dimensional features for simultaneous top and side images of individual and oriented dead fish.

An underwater stereo-vision system was also reported in [42] to estimate the mass of fish from their total length by using two orthogonal cameras. With this system, an interesting point such as caudal-fin points on the fish image was obtained to be a key step for the fish-segmentation process. Three parameters; total area, maximum axis length and circularity were suggested in [43] for binary image segmentation in fish-length estimation. A fixed threshold is adopted in their image filtering and segmentation process and they used pre-specified landmark point that utilized for 3D geometry calculation.

Another stereo-video system to estimate the length of Blue-fin tuna fish in a commercial cage was reported [44]. Different cage-depth setups were used to measure the length of the object in terms of repeatability of multiple images of the same blue-fin tuna. It was concluded in this study that the snout and tail points should be manually marked in their length estimation system and the fish length error ratio was 5% if the tuna were up to 5.5 m away from the cameras.

Further applications of computer vision systems have also been considered to estimate the size of free swimming fish in real time. For example, a real-time underwater vision system is developed for common carp, tilapia and grey mullet by extracting size and orientation invariant features from fish shapes. Fish images were acquired by a computer vision system while fish swam through a narrow channel with their sides to the camera as reported in [45]. More recently, a technique for measuring a tunas snout to fork length (SNFL) in digital images using the hand-held camera was reported in [40]. The images were taken on the deck of tuna fishing vessels. As reported, this technique can be efficiently used to estimate the length of the large stock fish but not free-swimming small fish.

Although fish sizing systems have also been of interest to numerous researchers

for larger-sized commercial species of fish [42, 46, 47, 44], sizing for small fish found only a little attention in the literature. For instance, a manual separation, counting, and inspection process for small commercial tropical guppy fish have been reported [8, 9], as has gender classification based on extracting the shape and colour features for the same kind of fish species [48].

Another method was reported in [49], using a paired-laser photogrammetric for fish-length estimation. In this method, a set of digital photographs was taken for each fish individual by using a waterproof camera equipped with two parallel lasers that were mounted on both sides of the camera. It was claimed that accurate fish-length estimation was achieved with error $< 3\%$. However, this system requires a precise alignment of the laser beam and is expensive and cumbersome to setup.

To date, zebrafish growth development studies are carried out in laboratory conditions and the traditional method of size/mass measuring that relies on fish handling. As reported in [10], a manual length and weight measurement for adult zebrafish were performed to investigate the health of an organism in terms of development and growth as well as the behaviour of these fish and their offspring. Both weight and length were adopted to determine growth indices and significant findings were shown when the fish under test were fed to specific dietary ingredients, nutrients. These methods are still used in present growth rate evaluation and are considered to be a big source of stress for the fish that might change the normal behaviour of fish and give inaccurate research findings as well as it might be not approved ethically.

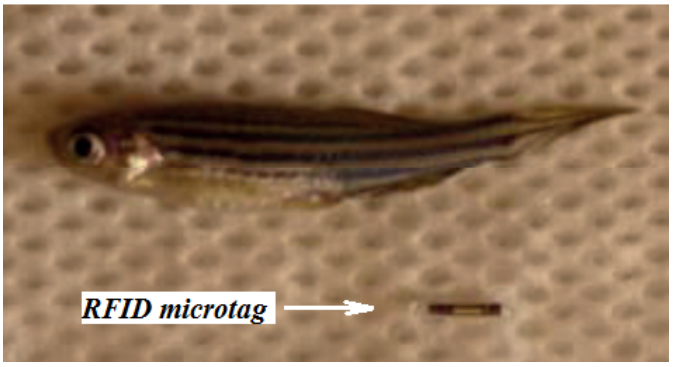


FIGURE 2.3: Radio Frequency Identification RFID micro tags for adult zebrafish [51]

## 2.6 Fish Recognition

Recent advancement in electronics and communications technology have led to developing of a small electronic tag [50] which meets the needs for small fish recognition. These tags are passive integrated transponders that use acoustic frequency and are embedded into zebrafish body and thus provides tracking and monitoring. Other types of tags used Radio Frequency Identification RFID micro tags shown in Figure 2.3, which were also deployed successfully in some studies [51]. These RFID tags are also embedded into the fish body by experts and then the tracking of corresponding fish can be achieved.

Despite these advances, tagging for small fish species has been found to have a negative overall impact on fish welfare. For this, the value and accuracy of collected data will be undermined as a result of influencing behaviour. Fluorescence microscope uses light emitting diode LED was built to recognise adult's zebrafish as a new method in the field of small fish recognition [52]. Fluorescent protein protocol gave simultaneous images of up to 5 swimming adults. Although this method has been able to solve the recognition problem of multiple adult zebrafish, animal welfare had not presented in these studies, underlining the need for further investigation. Therefore, as mentioned earlier, the similarity in shape and size of zebrafish in

addition to its rapid and unpredictable movement represent the challenge for identifying their individuals using computer vision and replacing the existing recognition techniques.

Two recognition approached are developed in this thesis based colour and local feature extraction methods. The theoretical concepts of these methods are described as follows.

### 2.6.1 Colour pace (L*a*b*) transform

Color spaces and numerical values are used to create, represent and visualize colours in two and three-dimensional space. The L*a*b*, or CIELAB, colour space is an international standard for colour measurements, adopted by the Commission International Eclairage (CIE) in 1976 [53]. However, application of this technique to fish recognition has not been explored in the literature yet.

CIELAB colour space is composite three layers L*, a*, and b* as shown in Figure 2.4. These layers are briefly described as follows:

1. L* represents the level from 0 to 100 for darkest black and brightest respectively. The true gray values can be obtained when the chromaticity components a* and b* are equal to zero.

2. The degree of redness-greenish is represented by a* and takes a positive value and negative value for greenish (from $-100$ to 100).

3. Yellowish-bluish degree is represented by b* which has the same range as a*. A positive value for yellowish and the negative value for bluish.

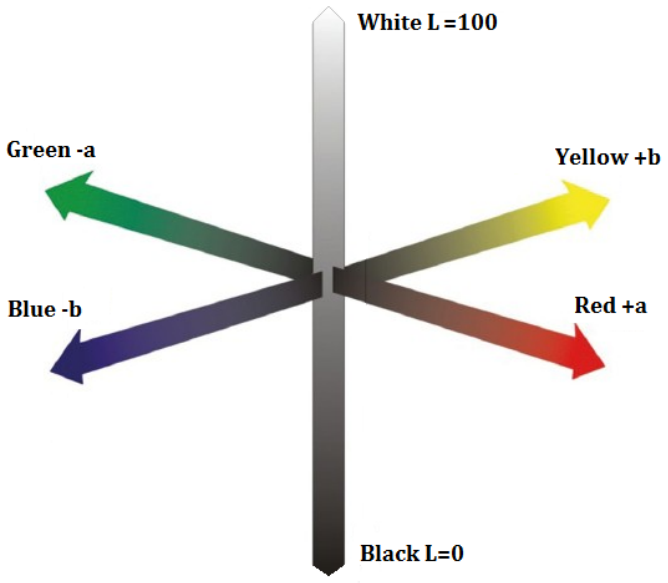


FIGURE 2.4: Graphical representation of the CIE L*a*b* color space [54]

Since the blue colour information exists in a* b* space, we will ignore L* values to obtain two dimensions new colour space. This reduction in colour space dimensions gave a significant benefit of obtaining fast clustering and accurate segmentation of blue stripes as will be discussed in the next subsection.

#### 2.6.1.1 Clustering

Clustering is a major data analysis tool used in such domains as marketing research, data mining, bioinformatics, image processing and pattern recognition. $k$-means is arguably the most popular clustering algorithm. It is intuitive and fast [55].

In this study, $k$-mean algorithm is used to extract the blue colour stripes on fish body efficiently. The algorithm mainly depends on minimizing the summation of squared distances between all points and cluster center. This procedure can be described in the four following steps [56]:

1. Initialize $k$ clusters center $c_1(1), c_1(2), \cdots, c_1(k)$

2. In each $n^{th}$ iteration, distribute the samples $q$ among the $k$ clusters using the following relation:

$$q \in U_j(n) \;\; if \; \|q - c_j(n)\| < \|q - c_i(n)\| \tag{2.1}$$

   For all $i = 1, 2, \cdots, k$; $i \neq j$ ; where $U_j(n)$ denoted the set of samples whose cluster center is $c_j(n)$.

3. Compute new clusters $c_j(n+1)$, $j = 1, 2, \cdots, k$ such that the sum of the squared distances from all points in $U_j(n)$ to the new cluster is minimized as follows:

$$c_j(n+1) = \frac{1}{N_j} \sum_{q \in U_i(n))}^{k} q, \quad j = 1, 2, 3, \cdots, k \tag{2.2}$$

   Where $N_j$ is the samples number in $U_j(n)$

4. The procedure is terminated once the algorithm converged,

$$c_j(n+1) = c_j(n), \quad for \;\; j = 1, 2, \cdots, k \tag{2.3}$$

   the procedure is terminated and proceeds to the feature extraction step, otherwise go to second step.

### 2.6.2 Speed-up robust feature (SURF) matching

Formation of feature vectors in this method is based on local patterns around certain key-points. The key-point detector and descriptor are the main stages

used to generate set of image features. These stages are described briefly as follows [57, 58]

- **Key-points detector**: At this step, the extracted key-points are detected using Hessian matrix approximation. The second order Gaussian derivatives for Hessian matrix are approximated using box filters. To locate the interest point, detected blob-like structures at locations where the determinant is at maximum. Integral images are used in Hessian matrix approximation, which reduce computation time drastically. Given a point $\mathbf{m} = (m, n)$ in an integral image $I$, the Hessian matrix $H(\mathbf{m}; \sigma)$ in $\mathbf{m}$ at scale $\sigma$ is defined by

$$H(\mathbf{m}, \sigma) = \begin{bmatrix} L_{mm}(m, \sigma) & L_{mn}(m, \sigma) \\ L_{mn}(mn, \sigma) & L_{nn}(m, \sigma) \end{bmatrix} \tag{2.4}$$

where $L_{mm}(m, \sigma)$ , $L_{mn}(m, \sigma)$ and $L_{nn}(m, \sigma)$ are the convolutions of the Gaussian second order partial derivatives $\frac{\partial^2}{\partial m^2} g(\sigma)$ with the image I in point x respectively. To reduce the computation time, a set of $9 \times 9$ box is used as the approximations of a Gaussian with $\sigma = 1.2$ and represents the lowest scale (i.e. highest spatial resolution) for computing the blob response maps. They denoted by $D_{mm}(m, \sigma)$, $D_{mn}(m, \sigma)$, and $D_{nn}(m, \sigma)$. The weights applied to the rectangular regions are kept simple for computational efficiency. This yields:

$$det(H_{approx}) = D_{mm} D_{nn} - (w \times D_{mn})^2 \tag{2.5}$$

where $H_{approx}$ represents Gaussian approximation and $w \approx 0.9$ is a weight for the energy conservation between the Gaussian kernels and its approximation [58].

- **Key-point descriptor**: Haar wavelet filters are used to compute two responses at m and n directions in this method. The descriptor extraction depends on constructing a square region located at the centre of the region of interest as shown in Figure 2.5. The original square area is divided into equally $4 \times 4$ square sub-regions. Harr wavelet responses are then computed for each sub-region. The filter responses in both horizontal and vertical directions are respectively represented by $dm$ and $dn$. These responses are then summed up and form a first set of entries in the feature vector over each sub-region. Polarity of the intensity changes is brought in using an additional extraction in which the sum of absolute values of the responses, $|dm|$ and $|dn|$ is used [57]. Thus, each sub-region ends up with four-dimensional descriptor vector given by

$$\mathbf{v} = \{\Sigma dm,\ \Sigma dm,\ \Sigma\,|dn|\,,\ \ \Sigma\,|dn|\} \tag{2.6}$$

This process is applied to all sub-regions of the region of interest.

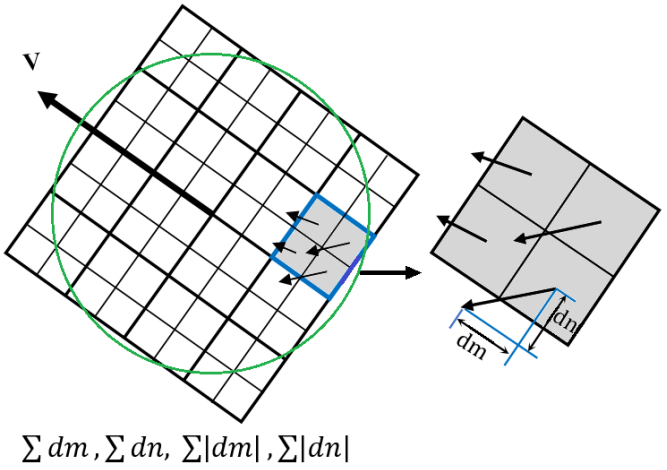


FIGURE 2.5: The demonstration of descriptor building

## 2.7 The Proposed Computer Vision Systems

The work proposed here addresses the urgent needs for developing a new non-destructive tools/methods for small aquatic animals and in particular zebrafish. This is achieved by design and developing robust methods and cost-effective tools for fish tracking and behavioural analysis, sizing, and recognition. These main contributions are shown in Figure 2.6 and are outlined briefly as follows.

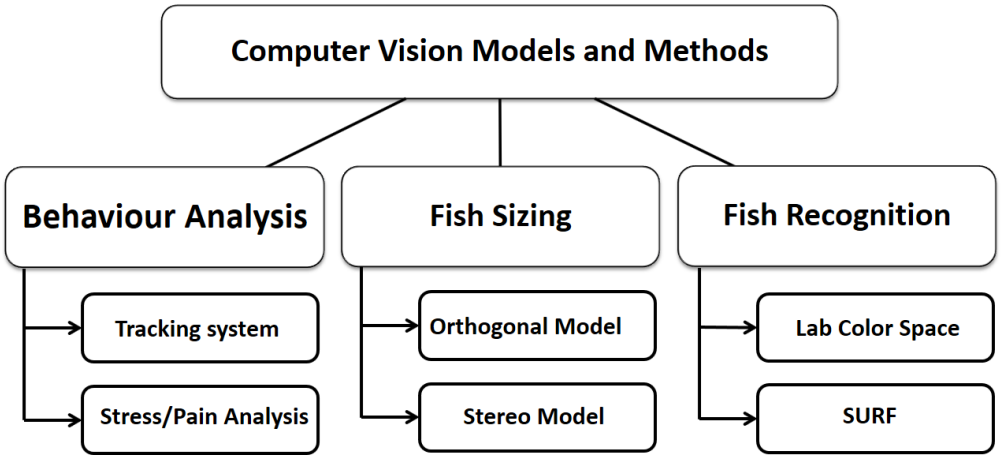


FIGURE 2.6: Overview of the proposed vision systems

1. Develop a novel tracking software based on an object automated detection, tracking, and monitoring algorithm capable of tracking, and providing the required behaviour physical activity parameters for twenty-five free-swimming individual fish larvae simultaneously of the object.

2. Design and implement a novel cost-effective electrical stimulator for behavioural analysis of 25 zebrafish larvae. Unlike the previously reported arena detection methods where the standard edge-detection techniques are utilized, a more efficient technique.

3. Design and implement novel cost-effective computer vision models (orthogonal and stereo) that are capable to calibrating the measured dimensions automatically to estimate the length of small free-swimming fish (zebrafish).

4. Propose two novel method for recognising individual adult zebrafish using L*a*b* colour-space transform and speed-up robust feature ($SURF$) feature extraction techniques. The former technique depends upon extracting individual features from the segmented pattern of the blue stripe that is occurred in the central detected batch area of the fish image. In contrast, the latter technique extracts the features of interest depending on the entire area of the fish image.

# Chapter 3

# Experimental Testbed

## 3.1 Introduction

For some species (rainbow trout, goldfish), evidence from empirical studies suggest that fish may have the capacity to experience painful stimuli and the associated discomfort [59, 60, 61]. Nociception, the detection of potentially harmful stimuli, is the basic mechanism for the sensation of pain, i.e., interpreting the nociceptive stimulus. The use of zebrafish in pain and nociception studies has dramatically risen in the last few years [62, 63, 64]. This is mainly due to the similarities that both the peripheral and central nociceptive processing systems of this species have with other vertebrates and mammals [62, 64]. The high number of adults used in these kinds of studies, however, should be drastically reduced due to ethical restrictions in research [65].

Research has recently reported that larval zebrafish demonstrate similar molecular responses of nociception similar to those of adults. It could therefore represent a

direct replacement of a protected adult fish with a non-protected form in pain and nociception-related research [18, 20]. Thermal, chemical, and electrical [66, 67, 68] stimulus are the most common technique in fish nociception studies. However, the electrical stimulation has only been reported in a very limited number of studies related to the activity response of adult fish and larvae [68].

This chapter presents a novel cost-effective electrical stimulator testbed aided with developed tracking software package for that is used to analyse the behavioural of zebrafish larvae for different types of stimulation. The developed package has the capability of estimating physical activities of multiple larvae, simultaneously.

## 3.2 Stimulation Techniques

As mentioned earlier, there have been several techniques in use for fish stimulation; of these, thermal, chemical, and more recently the electrical stimulation. These techniques which are typically used for pain and recovery studies and associated behavioural investigations are described as follows.

### 3.2.1 Thermal

Thermal stimulation can be described with the aid of Figure 3.1, as follows. The subjects under study (i.e. fish larvae) are placed in a mesh (length 16.5 mm, width 16.5 mm, depth 9 mm) of 25 wells on a custom-built plastic plate mounted to the side of a plastic tank. The plastic plate had a 53 $\mu$m mesh bottom which allows chemicals and water to be rapidly flushed in and out. The tank is positioned on the top of an infrared light stage (illumination area 450×210 mm) to maximize contrast

and facilitate tracking of dark targets on a light background. The behaviour of each larva is tracked using a digital monochrome infrared-sensitive camera (IDS UI-1240LE-NIR-GL; STEMMER IMAGING, Surrey, UK) with an attached lens (SPACE-COM JHF25M-5MP; SPACE inc., Tokyo, Japan).

After acclimation of the fish larvae under test, a 10-minute period is recorded to assess the pre-stimulation behaviour of each group of fish. Subsequently, to determine the effect of different potentially harmful temperatures on the response of the fish larvae, each group of 25 larvae are exposed to the different temperature water (10, 30 and 40 °C) for 1 minute by circulating water through the experimental tank. The actual water temperature in the experimental tank is controlled using a feedback controller that maintains the desired temperature at a certain degree depending on a prespecified set point. Post exposure of the subjects under test to the desired temperature, the behaviour of the subject is video recorded using the Infrared camera. The recorded video clip is then analysed to assess the impact of thermal stimulation on the fish behaviour using a range of cold/hot temperature levels. Further information on this kind of stimulation and its impact are reported in [18].

### 3.2.2 Chemical

Chemical stimulation of is the exposure of fish to water with different concentration levels of chemical agents. Structure of the chemical stimulator is generally similar to that of the thermal stimulator shown in Figure 3.1, except for using different chemical concentrations for stimulation rather than thermal. However, in this case,

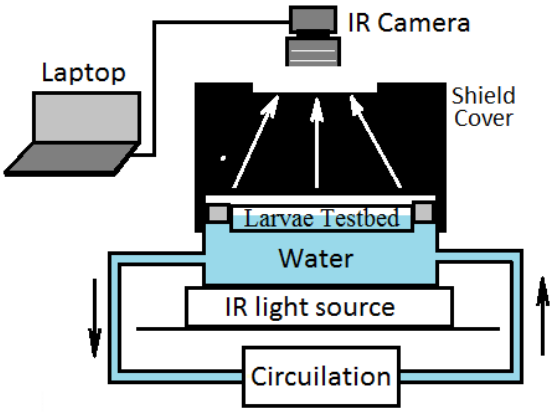


(a) Schematic diagram

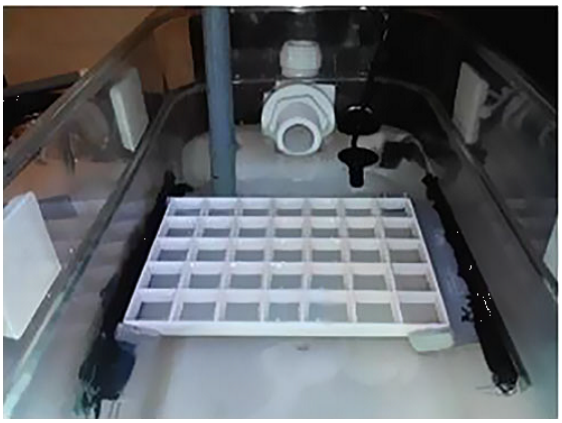

(b) Picture

FIGURE 3.1: System set-up for thermal and chemical stimulation

the temperature of circulating water should be constant at a certain temperature. This stimulation technique can be described briefly as follows.

Each group of 25 larvae is exposed to the chemical agent by adding it to water that circulated through the experimental tank. After acclimation, a 10-minute period is recorded to assess the pre-stimulation behaviour of the fish. Acetic acid at 0.01%, 0.1%, and 0.25% and citric acid at 0.1%, 1% and 5% concentrations are then added to the water tank. Once exposure to the agents started immediately, a second 10-minute period is also recorded to assess the post-stimulation behaviour. Further information on this kind of stimulation and its impact are reported in [20].

## 3.3 Electrical Stimulation

Electrical stimulation that is considered painful in mammals [69] is one of the methods used to study and assess nociceptive thresholds. So far, it is used in a limited number of studies for adult zebrafish [21] and larvae [70, 71]. In these studies, the classical endpoints that include tail-fin and escape responses were measured as a response to this stimulation. However, this method cannot be applied efficiently to larval zebrafish, due to: (i) challenges associated with unpredictable behavioral reactions to different intensities of the stimulation and, (ii) difficulty of capturing movement of such small fish due to transparency of its body.

In this work, a new electrical stimulation testbed is developed for the experiments carried out in this work. A new robust software is also developed to track and measure the physical activity parameters of multiple larvae, simultaneously. The hardware and software aspects of the developed system are described as follows.

### 3.3.1 Experimental testbed

The proposed testbed comprises of a digital infrared (IR) camera along with the desired setup (see Appendix A)., IR lamp, square-wave function generator, laptop, ON/OFF switching controller, and a test mesh of multiple arenas, as shown in Figure 3.2. The number of arenas used in this study (25 arenas) is recommended by the life sciences experts at the University of Liverpool.

A testbed mesh shown in Figure 3.3 is built to facilitate simultaneous electric shocks for all arenas. It comprises of 25 arenas of asymmetric volume with

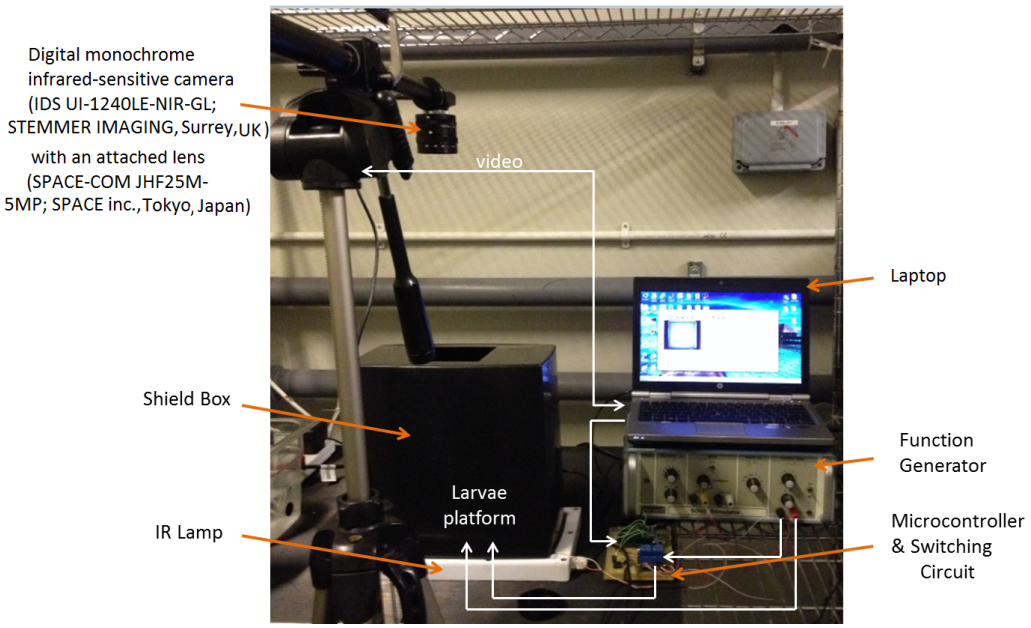


FIGURE 3.2: Experimental system set-up

dimensions $105 \times 105 \times 9$ mm. These arenas are connected to external stimulation terminals through a multicore coated copper wire of 0.1 mm diameter. The number of arenas can be easily expanded, simply by adding more rows and columns arenas to the existing mesh subject that the size of mesh is covered by the camera's field of view. The stimulation electrodes are fixed as shown in Figure 3.3(b) to ensure a simultaneous stimulation to all arenas.

The subjects under test are placed in the testbed arenas and exposed to different levels of stimulation in terms of the period of stimulation, voltage level and frequency. To enhance visibility of the stimulated subjects, the testbed cells are illuminated by infrared (IR) light that is placed beneath the testbed mesh, as illustrated in Figure 3.2. The IR camera, which is linked to a laptop, is placed over the testbed mesh, as illustrated. It collects video frames of subjects in the testbed arenas. The collected frames are used later to study behaviours of the subjects under test at different phases; before, during and after stimulation.

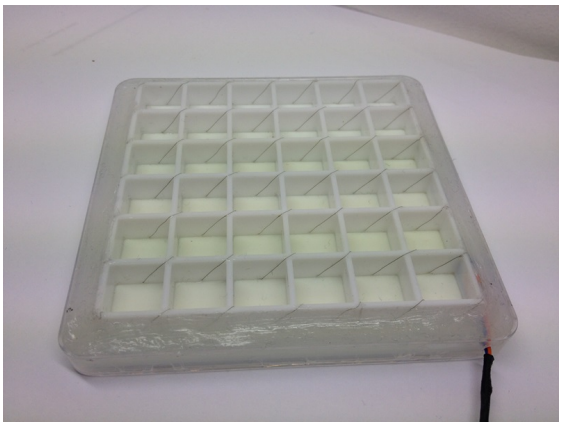

(a) Experimental mesh

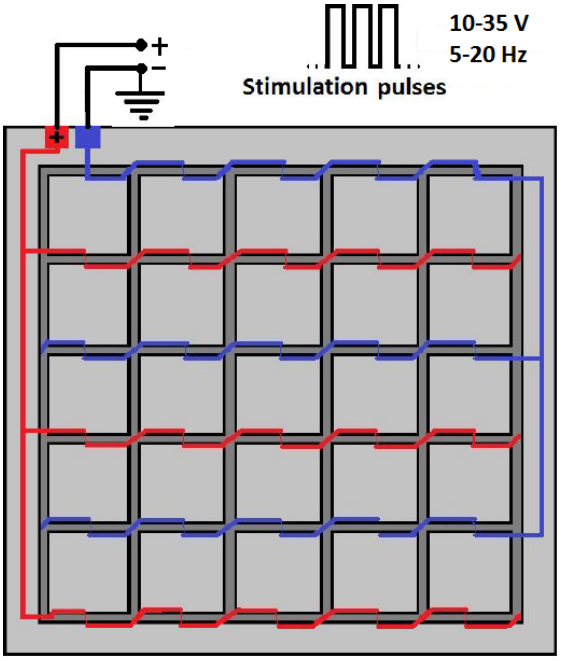


(b) Top view of mesh wire connection

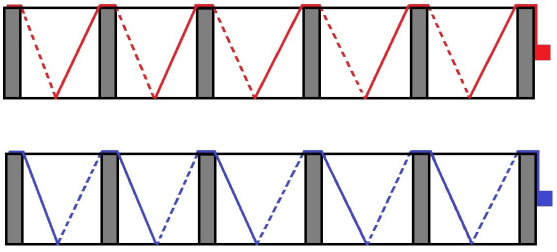

(c) Side view of mesh wire connection

FIGURE 3.3: Experimental Testbed with schematic connection

### 3.3.2 Experimental considerations

Several arrangements are considered to improve the quality of the collected video signals and to ensure that all experiments are conducted according to the guidelines of research ethics as approved by the Ethical Committee at the University of Liverpool (License PPL40/3534). These arrangements are outlined as follows.

1. On the day of egg collection from wild-type zebrafish, all the embryos were pooled and placed in a small tank at a temperature of 28.5 °C. The developmental stage is set as days post fertilization (dpf) based upon the staging system employed in this species of fish [72]. Only 5 dpf larvae are used in the conducted experiments.

2. The subjects under test are placed in individual testbed cells and allowed to exhibit their natural behaviour for the period of 30 min. Larval fish may initially experience elevated fear unrelated to the stimulus signal provided. After a 30 min acclimation period, the video recording begins and the stimulation signal is applied. The recording period for each experiment takes approximately 15 minutes.

3. The subjects under test are stimulated at different voltages amplitudes ($10-35$ V) and frequencies ($5-20$ Hz).

4. Testbed mesh is covered by a black box to improve quality of the collected video frames and reduce the effect of external light on the normal behaviour of the subjects during the stimulation period and beyond.

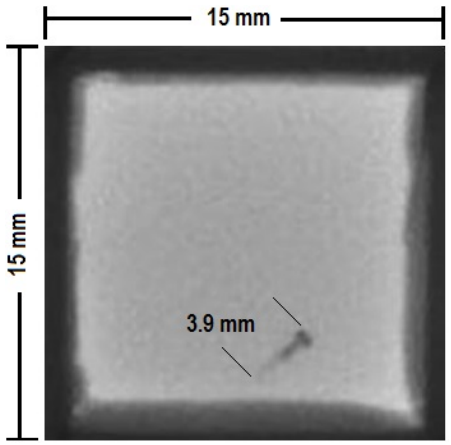


FIGURE 3.4: Example image of a zebrafish Larva in a test arena

### 3.3.3 Test subjects

The small size of embryos minimizes the cost and waste volume for drug and toxicant studies. Thus, minute amounts of expensive metabolites or new targeted drugs can be rapidly evaluated. Zebrafish has become a powerful model system for medium to high-throughput applications: (i) It has recently been used in experiments as a nociceptive or pain model due to a wide range of advantages including: the embryos are transparent and developed externally, (ii) permitting in vivo experiments right after the fertilization and, (iii) this fish has a relatively short regeneration time [62, 18]. These fish are small and their maintenance costs are relatively low compared to other vertebrates. The modest colony of fish can also produce hundreds or even thousands of embryos on a daily basis. After hatching, the free-swimming 3 to 5 day-old fish larvae display a range of behaviours that are important for finding food and avoiding predators. Some of these behaviours are robust and suitable for large-scale screening. An example image of the fish larvae under study is shown in Figure 3.4.

## 3.4 Subject Stimulation

Subject stimulation is controlled automatically through a micro-controller (Arduino UNO ATMEGA328) using pre-program schedule. This controller automates the application of the stimulation signal via ON/OFF switching controller, as illustrated in Figure 3.2. This part of the system software is initially developed using Matlab and then deployed in the micro-controller. The second part of the system software is developed and deployed on the laptop to control and synchronise operation of the micro-controller and the IR camera. In addition, it performs all computation tasks relevant to object tracking and monitoring process of all test objects in the testbed mesh. Further details on the design of the system software are given in the next section.

In order to study the physical activity of larvae while fulfilling the above-mentioned experimental considerations, an accurate and timely controlled stimulation process is required. Figure 3.5 shows a timing diagram for the proposed stimulation and data collection periods. The electrical stimulator is used to apply in the form of with a per-specified voltage level and frequency. At each experiment, the stimulation pulses are equally and simultaneously applied to all subjects under test.

The sequence of events performed during this process is shown in the flowchart of Figure 3.6. Once initiated by the user, this application starts reading the desired periods, which are pre-configured by the user via a user-friendly graphical user interface (GUI) depending on the experiment circumstances and requirements (see Appendix B (Figure B.1)). The first period of data collection will then be automatically started for a period $T_1$ given by

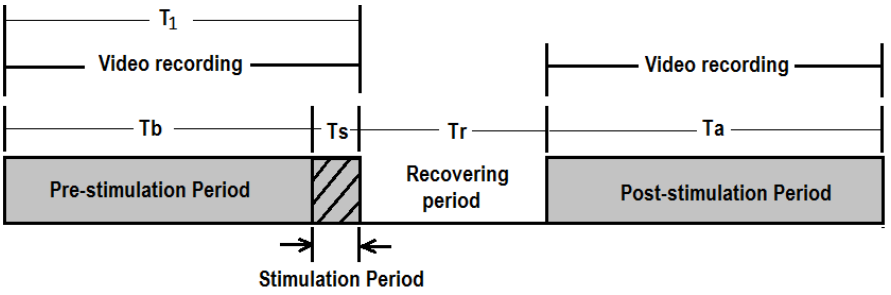


FIGURE 3.5: Stimulation and video recording time diagram

$$T_1 = T_b + T_s \tag{3.1}$$

where $T_b$ is the pre-stimulation period and $T_s$ is the stimulation period. Next, the second data collection period $T_a$ will start after a recovery period $T_r$. The entire period of the experiment $T$ is therefore given by

$$T = T_1 + T_r + T_a \tag{3.2}$$

## 3.5 Object Detection, Tracking and Monitoring

The developed object's detection, tracking and monitoring algorithm can be divided into four distinct stages (shown in Figure 3.7); pre-processing, object detection, post processing, and monitoring. These stages are described briefly as follows.

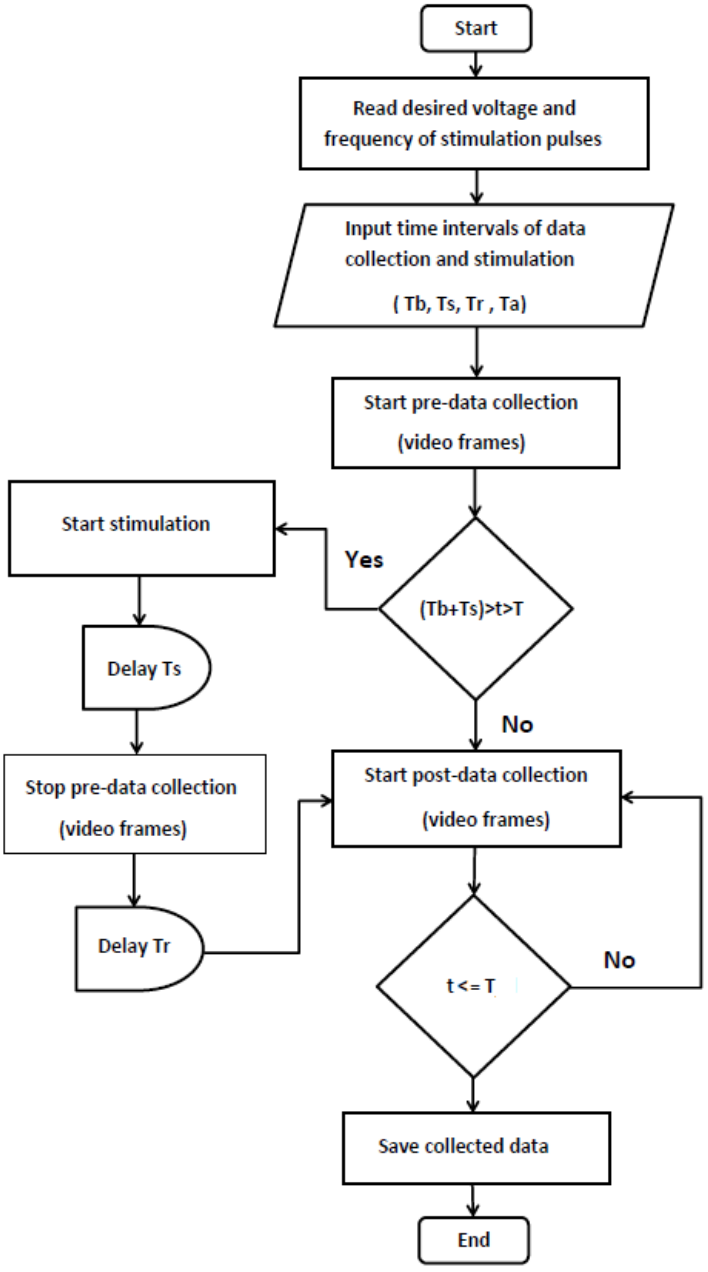


FIGURE 3.6: A flowchart for the data collection and stimulation process

### 3.5.1 Data collection

A digital USB2 IR camera is adjusted experimentally to have maximum frame rate 23.72 fps (see Appendix A) that provides sequences of video frames that are timely transferred via a USB port to the laptop. Each video clip has distinct recording periods that are coherent to the timing diagram of Figure 3.5. A

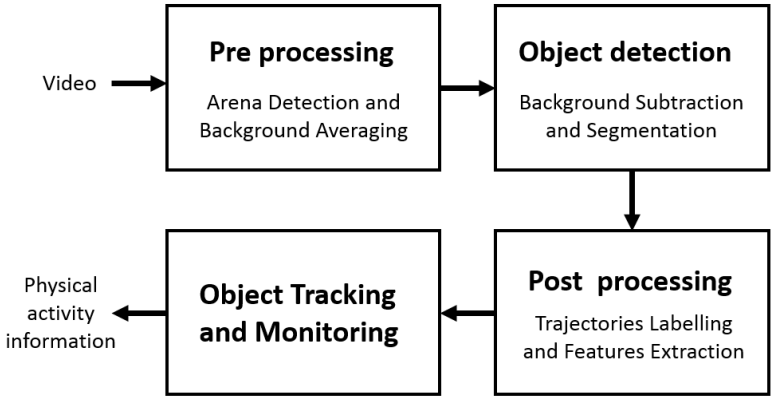


FIGURE 3.7: Tracking and monitoring algorithm

simplified flowchart for the data collection and stimulation process is shown in Figure 3.7.

### 3.5.2 Pre-processing

At this stage, two pre-processing stages are performed; (i) automatic arena detection and (ii) background averaging.

### 3.5.3 Arena detection

This process represents an important stage for individual fish larva tracking process which depends on the estimate area's boundaries to provide corresponding trajectory of tracked larval at the end. Computation of these boundaries is usually based on manual identification of each arenas boundary, this requires expert's effort and time. A new detection method is proposed and developed in this work that is capable of automatic identification of arena's boundary. This method is described as follows.

The infrared decoded raw frame of the collected video clip is converted to grayscale shown in Figure 3.8(a). The obtained image is then converted to a binary image ($I$) to identify the borders of the testbed as illustrated in Figure 3.8(b). In order to detect the pixel density distribution, ($D_x$) and ($D_y$) of the segmented image in both image axes, pixel summations for both rows and columns are calculated from

$$D_x(i) = \sum_{j=1}^{m} I(i,j) \tag{3.3}$$

$$D_y(j) = \sum_{i=1}^{n} I(i,j) \tag{3.4}$$

To detect the coordinates of central arena, shown in Figure 3.9(a), the calculated pixels density with detected image's centre are used to identify the initial region for arena's coordinates detection process. The centre of the image is used as an initial point in both axis directions. In each axis direction, the detection process is continued until matching the centre value of the central pixels density which is selected according to desired threshold to avoid the effect of distortion on coordinates detection process, as illustrated in Figure 3.9(b).

Knowing that the mesh arenas are uniformly distributed in the testbed mesh, the detected coordinates ($x_{c_1}$,$y_{c_1}$) and ($x_{c_2}$,$y_{c_2}$) of the central arena are then used to calculate width/height ($\triangle C$) that to be a reference of the entire mesh layout as follows.

$$X_L(u+1-n,j) = x_{c_1} - n\left|\triangle C\right|, \quad if \;\; 1 \leqslant n \leqslant u; \;\; j = 1 : N+1 \tag{3.5}$$

$$X_R(n,j) = x_{c_2} - n\left|\triangle C\right|, \quad if \;\; u+2 < n \leqslant N+1 \tag{3.6}$$

where $X_L$ and $X_R$ represent left and right arena coordinates vectors in x-axis. $u$

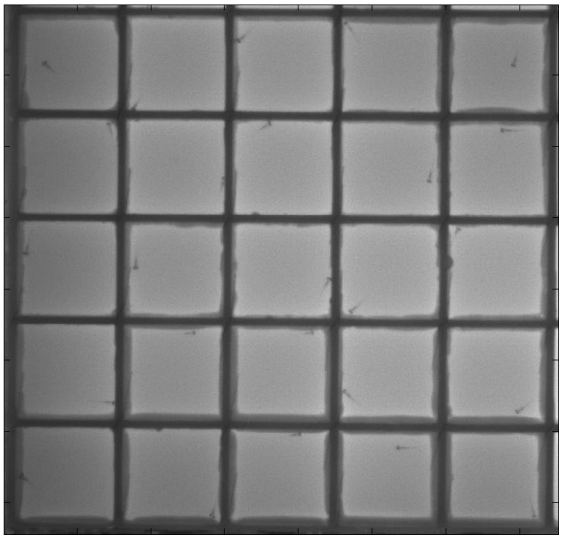

(a) Input: raw image

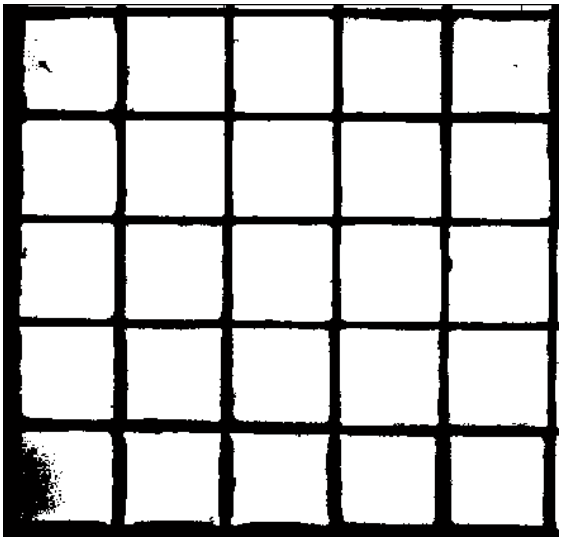

(b) Segmented binary image for the testbed arenas

FIGURE 3.8: Testbed's arenas detection steps

represents the number of the arena from the centre. Similarly, the other coordinates distribution in y-axis is given by

$$Y_U(i, u+1-n) = y_{c_1} - n\,|\triangle C|\,, \quad if \;\; 1 \leqslant n \leqslant u \;\; i = 1 : N+1 \tag{3.7}$$

$$Y_D(i, n) = y_{c_2} - n\,|\triangle C|\,, \quad if \;\; u+2 < n \leqslant N+1 \tag{3.8}$$

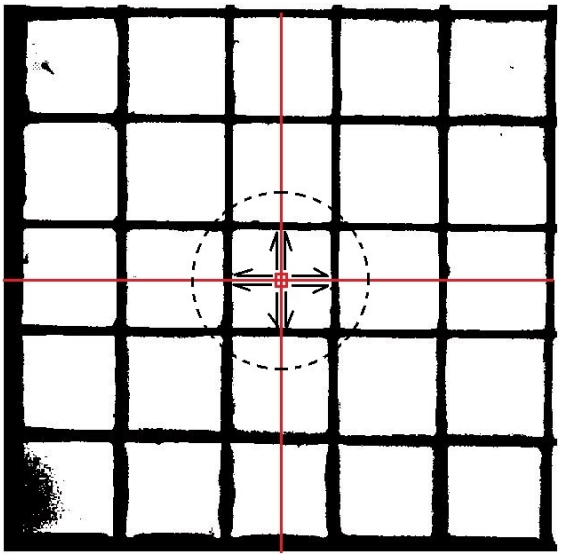

(a) Detection of central arena

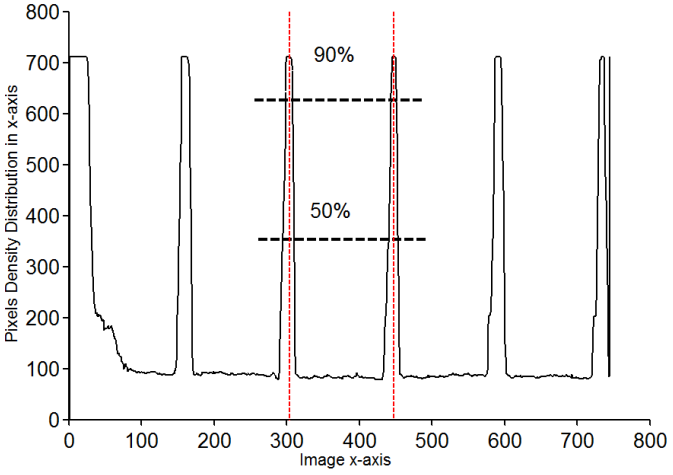


(b) Effect of threshold on the accuracy at central boundaries of the pixels density

FIGURE 3.9: Arenas' boundaries detection

where $Y_U$ and $Y_D$ represent left and right arena coordinates vectors in y-axis.

### 3.5.4 Subject detection

At this stage, the generated background frame is subtracted from the input frame in Figure 3.11(a) to detect the blobs areas. The corresponding centroids of each

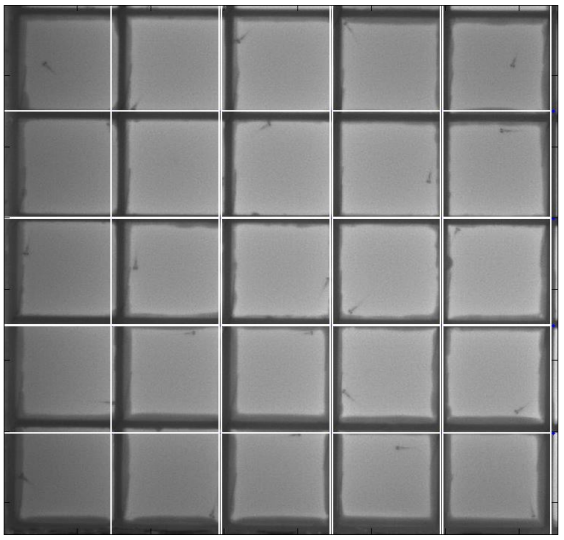

(a) The effect of low threshold on arenas boundaries detection

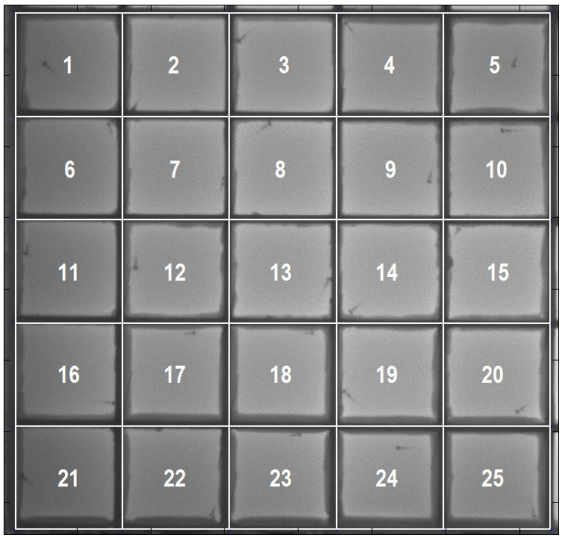


(b) Accurate arenas' boundaries detection with labeling

FIGURE 3.10: The effect of threshold on arenas' boundaries detection

subject are calculated and displayed on consecutive frame cumulatively to achieve synchronized monitoring, as illustrated in Figure 3.11(b). An example of tracking larva based on segmentation and detection process shown in Figure 3.11(c).

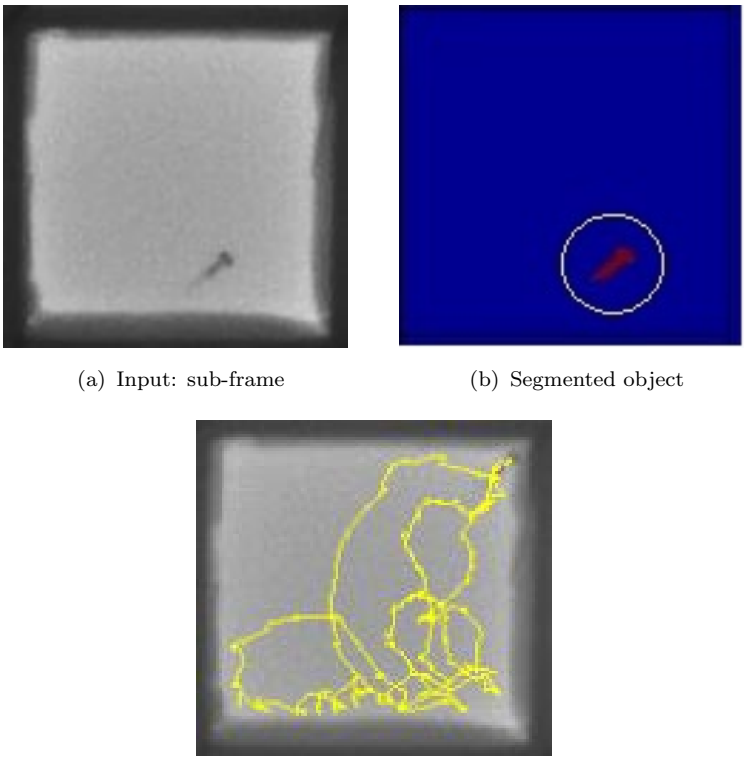

(a) Input: sub-frame (b) Segmented object

(c) Tracked object

FIGURE 3.11: Steps of object detection and extraction of its tracking path

### 3.5.5 Post processing

At this stage, the locations visited by each of the subjects under test are linked and saved in a data buffer created for this purpose. The physical activity features of each object in terms of velocity, acceleration, active/inactive periods and the total distance moved are then extracted using various kinematic equations. The motion trajectory of each fish is then obtained using the corresponding physical activity features.

### 3.5.6 Object tracking

In order to monitor the individual behaviour of the subjects under test, a user-friendly (GUI) is designed and developed using Matlab. It consists of the following two

sections:

1. 25-arenas monitor which displays the physical activity of all subjects under test.

2. Configuration and control panel that is used to start/stop the experiment configure the desired data collection and stimulation periods, and to upload the recorded video clips from the camera to the laptop computer for further processing.

The collected video clips for each arena is then processed individually, and the obtained tracking paths for each subject are then graphically displayed in the corresponding window (see Appendix B (Figure B.1).

## 3.6 Results and Discussion

The developed stimulation system and its object detection and tracking algorithms suggest a relatively has low experimental set-up for studying behaviour of larval zebrafish. Furthermore, the developed tracking system is capable of dividing the entire response time of individual larval fish which represent a new property for larvae recovering studies. Figure 3.12 shows examples of samples of time segmentation for the tracking period.

A significant change in the fish larvae behaviour occurs when they are exposed to testing electric shocks as shown in Figure 3.13. This means that the developed electrical stimulator is capable of delivering the expected stimulation signal successfully. Furthermore, the recovering time for the stimulated larvae can also be estimated

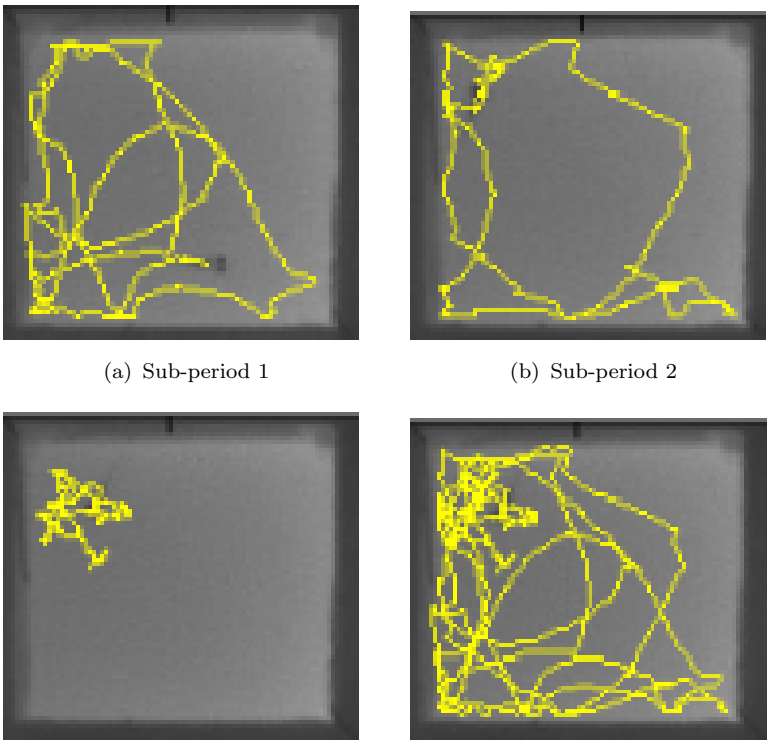

(a) Sub-period 1 (b) Sub-period 2

(c) Sub-period 3 (d) Total period

FIGURE 3.12: Samples of time segmentation of the tracking period

using the developed software with segmented time capability in the tracking process. Figure 3.14 shows a comparison example of the sampled distance moved of single larvae in pre- and post-stimulation, including the recovering period. The recovering time estimation could also help in providing a significant indication for the pain level in the stimulated larval fish.

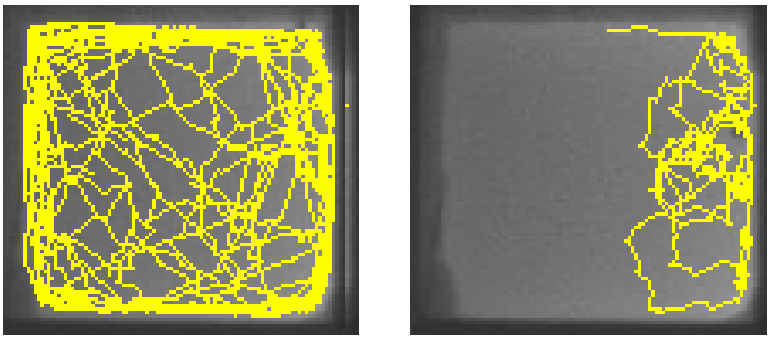

(a) Pre-stimulation (b) Post-stimulation

FIGURE 3.13: Samples of fish behaviour at pre- and post-stimulation

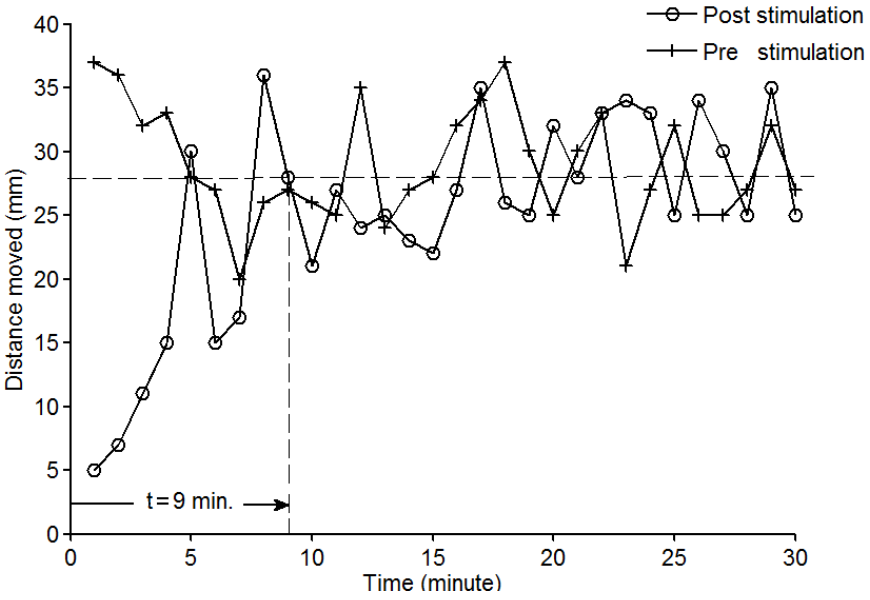


FIGURE 3.14: Example of using the developed tracking software time recovering estimation in electrical stimulation experiment

## 3.7 Conclusion

An automated electrical stimulation and physical activity monitoring of zebrafish larvae have been designed, prototyped and tested successfully. Despite that the test mesh allows 25 fish larvae for experiment, the obtained results demonstrated accurate tracking and effective monitoring of multiple larvae responses for various levels of painful stimulation.

The developed object tracking algorithm can be further improved using real-time

tracking to recognize and classify various behavioural patterns for larvae based on standard motion attributes including: velocity, acceleration, active/inactive times and the total distance moved by larvae(see Appendix B (Figure B.2) .

The developed electrical stimulation and data collection testbed offers several unique features including; flexible construction, cost-effective (see Appendix C), atomicity of stimulation signal application, and tracking physical activity of multiple larvae fish per experiment.

# Chapter 4

# Behavioural Analysis:

# Outer Zone Pattern Detection

## 4.1 Introduction

Despite the importance of using adult zebrafish as an efficient model for numerous studies in pain and different traits, the behavioural analysis of zebrafish larvae is not fully explored in the literature yet. The need for non-invasive computer vision tools and analysis methods remains an important challenge.

Electrical stimulation that is considered painful in mammals [69] is one of the methods used to study and assess nociceptive thresholds. So far, it is used in a limited number of studies for adult zebrafish [21] and larvae [71, 70]. In these studies, the classical endpoints that include tail-fin and escape responses were measured as a response to this stimulation. However, this can be difficult to assess in larval zebrafish due to challenges associated with small size and unpredictable

behavioral reactions with different intensities of the stimulation signal along with the difficulty of recording from such small individuals. Therefore, developing a more efficient method and tools to investigate responses of fish larvae to an electrical stimulus is timely and relevant. In this chapter, a new behavioural analysis method is developed to assess the pain nociception of zebrafish larvae when exposed to electric shock at different voltage intensities. The method aims to detect the pattern of fish behavior in the outer zone (also called thigmotaxis or wall hugging). Three distinct groups of fish larvae are used as test subjects in this study, and pre- and post-stimulation behaviors of the subjects under test are and analysed.

## 4.2 Materials and Method

Animals that are engaged in thigmotaxis behavior are typically avoid staying in the center of the test arena.They keep moving in close proximity to the boundaries of a novel environment, for instance, the walls [71]. Considering this type of behaviour, the outer zone pattern detection is therefore developed to study the effect the intensity level of the electric shock on the response of fish larvae. Experimentally, three distinct groups of fish larvae are used as test subjects in this study. Each of these groups are exposed to electric stimulation using different voltage levels. Pre-post stimulation behaviours of the subjects under test are initialy recorded using an infrared sensitive camera and analyzed. The proposed pattern detection method has four distinct stages: Tracking, outer patterns segmentation, patterns boundaries detection, patterns number estimation and pre-post patterns number comparisons. These stages are shown in the block diagram of Figure 4.1 and are

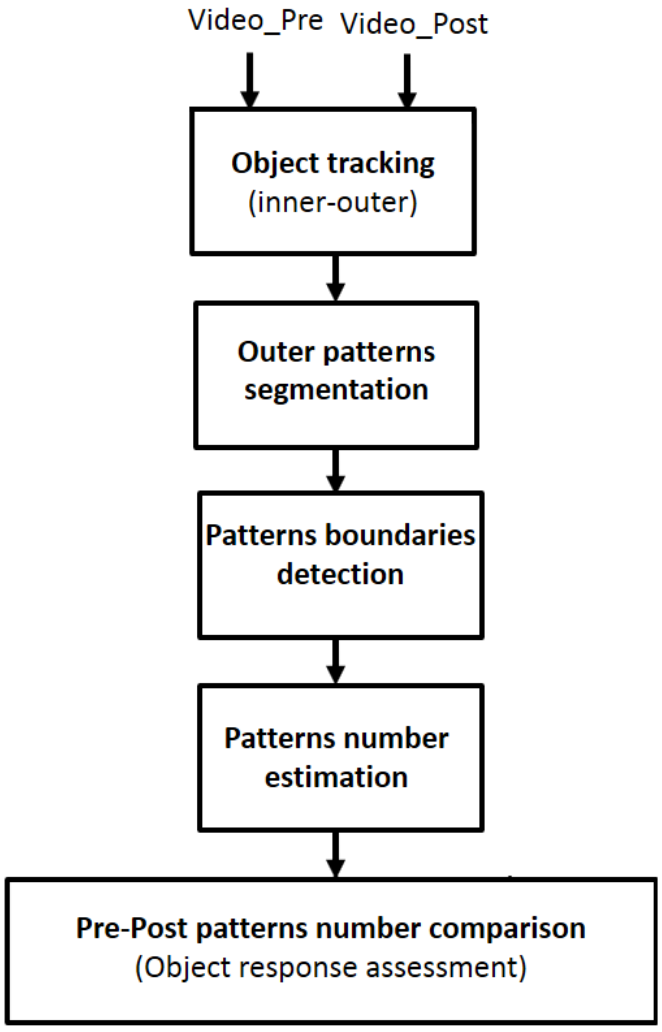


FIGURE 4.1: Stages of the proposed pattern detection method

described briefly as follows.

### 4.2.1 Object tracking

The developed tracking software is initially used to generate larvae trajectories vectors $P_n(x, y)$. It then divides them according to desired zones conditions into two labeled sets of larval location in different colour (blue and yellow) as shown in

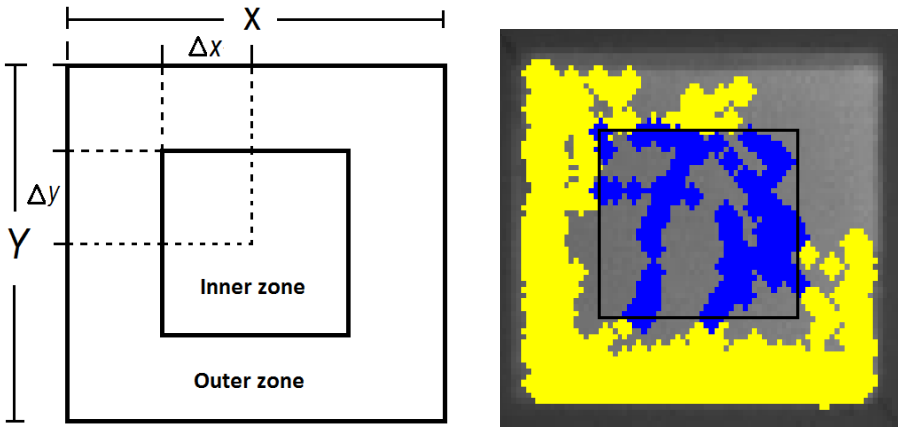


(a) Schematic of the arena zones within a single well in the testbed

(b) Zone boundary within single well in the testbed

FIGURE 4.2: Sample of conditional tracked larval fish in arena

Figure 4.2. The labelling for the outer $P_{out}(x, y)$ and inner $P_{in}(x, y)$ is processed according to following conditions.

**- For outer zone:**

$$P_{out}\left(x,y\right) = P_{n}\left(x,y\right), \quad (x,y) \in \left\{ \begin{array}{c} x,y : \Delta x \geq x > 0, \quad Y > y > 0; \\ X > x > 3\Delta x, \quad Y > y > 0; \\ 3\Delta x \geq x > \Delta x, \quad \Delta y \geq y > 0; \\ 3\Delta x > x > \Delta x, \quad Y > 3\Delta y \end{array} \right\} \tag{4.1}$$

**- For inner zone:**

$$P_{in}\left(x,y\right) = P_{n}\left(x,y\right), \quad (x,y) \in \{x,y : 3\Delta x \geq x > \Delta x, 3\Delta y > y > \Delta y\} \tag{4.2}$$

where $\Delta x$ and $\Delta y$ are the spaces of behaviour analysis requirements, $X$ and $Y$ are automated detected arena dimensions.

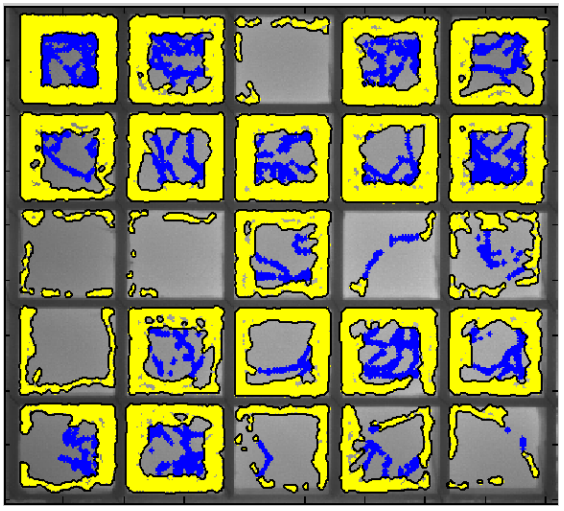

(a) Pattern segmentation

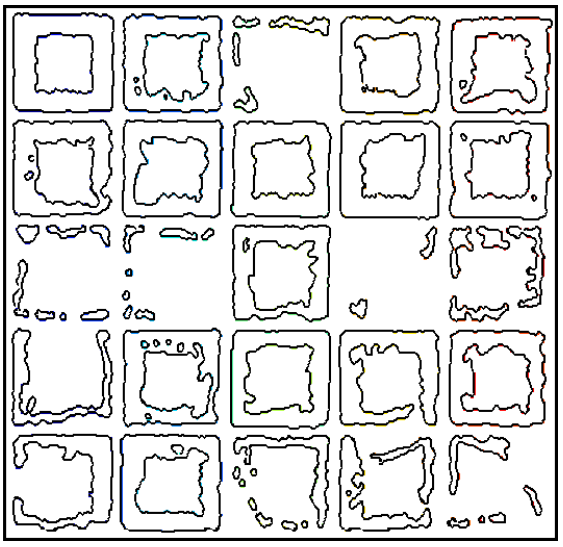

(b) Boundary detection

FIGURE 4.3: Example: Segmentation and boundary detection of the patterns in outer zone for 25 arena

### 4.2.2 Outer pattern segmentation

In this stage, the newly generated trajectories groups are replotted on the corresponding arena to produce a new trajectories pattern mapping which is used to detect boundaries of the patterns in outer zones as shown in Figure 4.3.

### 4.2.3 Pattern-number estimation

At this stage, an edge detection method, called Sobel [73], is applied to the new image to detect the boundaries of enclosed patterns. This obtains a smoothed connection (8-way connectivity) for the adjacent pixels of the detected boundaries in the outer zone, as illustrated in Figure 4.3(b). The set of the calculated pixels ($C_{pn}$) in each arena is then obtain from

$$C_{pn} = \{pn(1), pn(2), pn(3), ...pn(n)\} \tag{4.3}$$

where $n$ represents the number of the detected boundary per arena. The pre-post condition ($N_{pre,post}$) that represents the number of patterns adopted in each individual arena is given by

$$N_{pre,post} = \left\{ \begin{array}{ll} 1 & C_{pn} \geqslant \delta_b \\ 0 & else \end{array} \right\} \tag{4.4}$$

where $\delta_b$ is the prespecified threshold of the sum for pixels number of the adopted pattern boundary.

### 4.2.4 Assessment of detected patterns

In this stage, a percentage ratio of the change in detected pattern number (CPN%) is used to assess the effect of the stimulation signal intensity on the larvae response in pre- and post-stimulation in terms of the total number of the detected patterns. the CPN% ratio is given by

$$CPN\% = \frac{N_{pre} - N_{post}}{N_{pre}} \times 100\% \tag{4.5}$$

where $N_{pre}$ and $N_{post}$ represent the sum of detected patterns number in all arenas in the mesh for pre- and post-stimulation.

## 4.3 Results and Discussion

Three experiments are carried out in this study using three different groups of zebrafish larvae ($n = 25$ per group). Wach of these groups are stimulated under different voltage intensities; 25, 30 and 40 volts (a single stimulation voltage value per experiment). These voltage levels are selected based an experimental tests as well as recommendations given by domain knowledge experts at the Life Sciences Department/ University of Liverpool. The experimental tests demonstrated that 25 volts represents average minimum threshold for voltage effect on the fish activity while the 45 volts represents the average killing level of stimulation. However, it should be mentioned here that the applied voltages may vary across the test arena at both $x$ and $y$ planes, due to the freshwater conductance.

The pre-stimulation behavior of the subjects is considered as a reference that is used to evaluate the response of the fish larvae after stimulation. In each experiment, the subject trajectories are identified for a period of approximately 5 minutes (before and after stimulation).

1. **Experiment 1 (25 V variable stimulation signal)** No apparent change in the overall responses of subject can be noticed after the stimulation. This reflects that stimulation with this relatively low-voltage level had only a small effect on the subjects' activity. 22 and 21 pattern number are identified for the pre- and post-stimulation, respectively, as illustrated in Figure 4.4 shows

the detected patterns for pre and post stimulation.

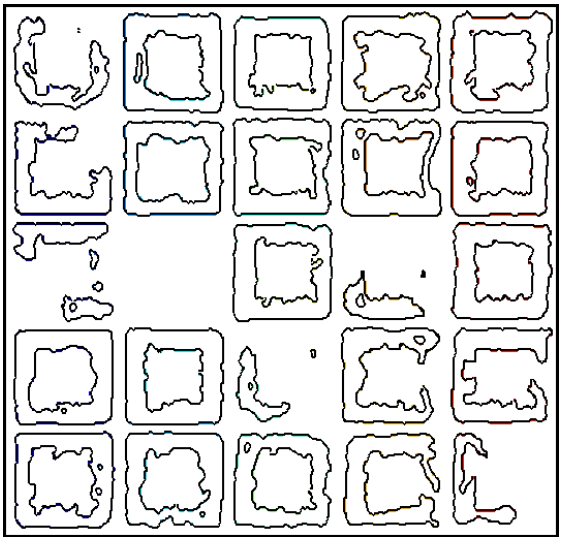

(a) Pre-stimulation

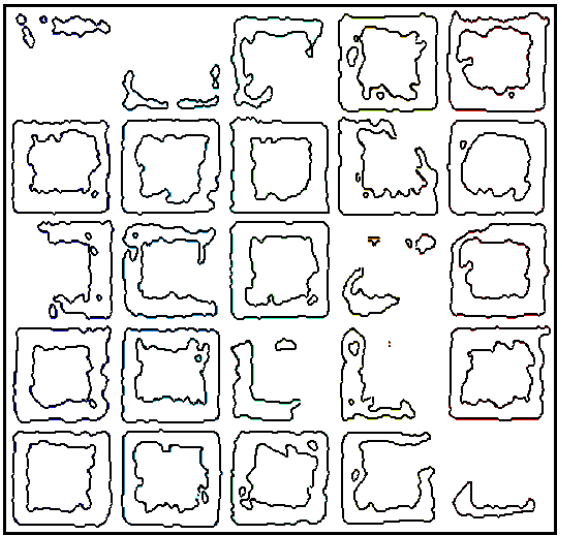

(b) Post- stimulation

FIGURE 4.4: Detected patterns for Experiment 1 after variable electrical stimulation up to 25V

2. **Experiment 2 (30 V variable stimulation signal)** A slight change can be noticed in the activity of subjects in post-stimulation with increasing the level of the stimulation signal. The numbers of patterns are 24 and 19 patterns for pre- and post-stimulation, respectively, as illustrated in

Figure 4.5.

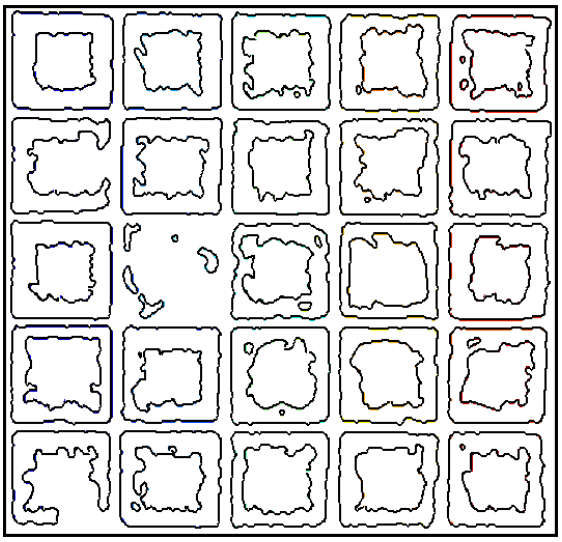

(a) Pre-stimulation

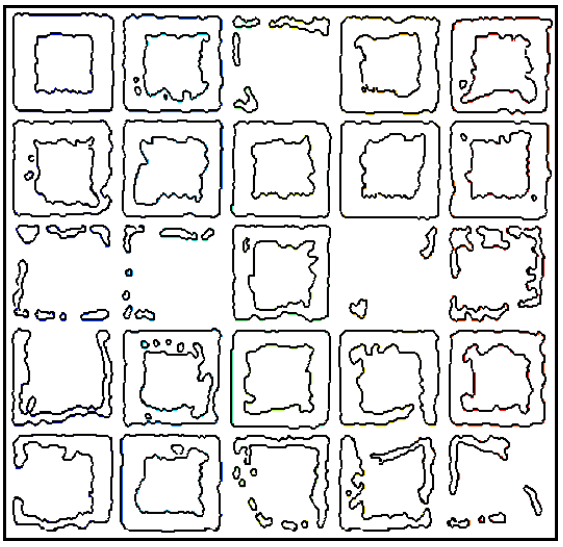

(b) Post- stimulation

FIGURE 4.5: Detected patterns for Experiment 1 after variable electrical stimulation up to 30V

3. **Experiment 3 (40 V variable stimulation signal)** In this experiment, the fish is exposed to higher voltage level, thus the subject appeared to move less in the outer zone after the stimulation, as shown in Figure 4.6(b). The stimulation effect is reflected by the number of detected patterns. It is

found that the number of patterns for pre- and post-stimulation are 24 and 16, respectively, as illustrated in Figure 4.6.

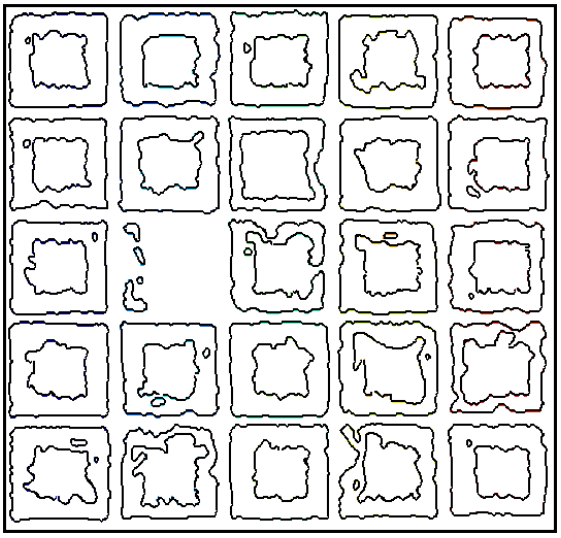

(a) Pre-stimulation

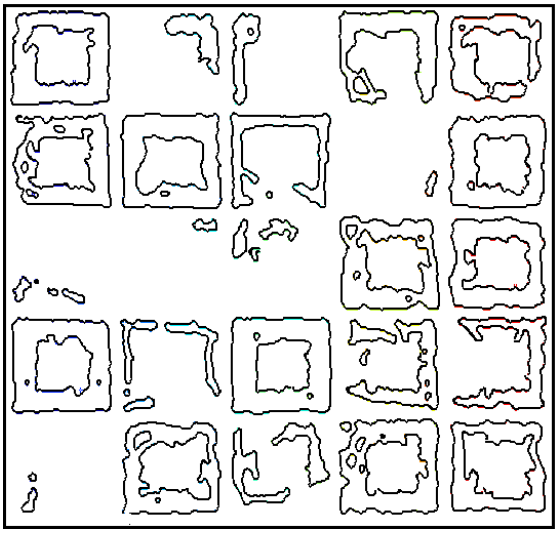

(b) Post- stimulation

FIGURE 4.6: Detected patterns for Experiment 1 after variable electrical stimulation up to 40V

In each experiment, the identified trajectories are labeled and counted automatically. The percentage differences between the number of detected patterns for both stages (pre- and post-stimulation) for the three experiments are shown in Figure 4.7.

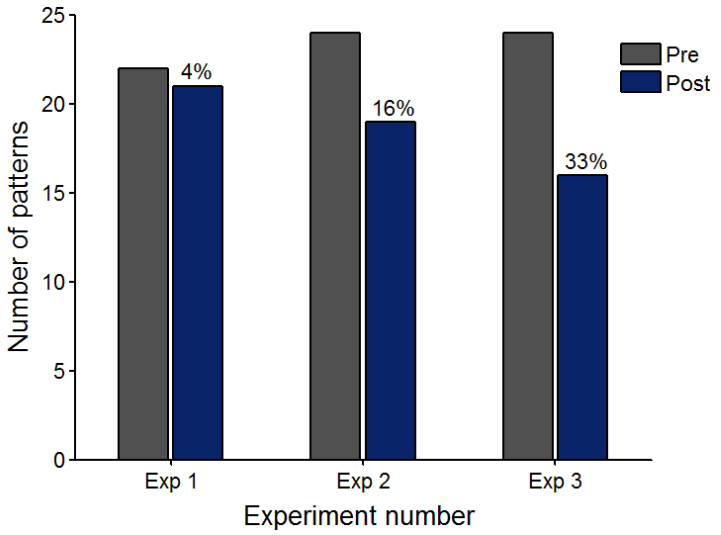


FIGURE 4.7: Detected patterns for three different experiments when zebrafish larvae were exposed to variable electrical stimulation less than 25V (Exp 1), 30V (Exp 2) and 40V (Exp 3). Data are shown for before stimulation and afterward with the percentage difference noted

These percentage values reflect the impact of the applied stimulation voltages ($< 25$, $< 30$ and $< 40$) on the behaviour of the subjects under study. These findings demonstrate the possibility of using the identified number of patterns in the outer-zone as a robust index for assessing the impact of electrical stimulation on behaviour of larvae.

Significant changes are identified between pre- and post-stimulation in the larvae behaviour based on this index. It should mentioned here that the distribution of electrical shock inside each arena is not uniform which make measurements of the instantaneous voltage corresponding to animal location is difficult. However, the obtained post-stimulation responses of the subjects under test demonstrated different behavioural patterns in the outer-zones of the arena mesh. Thus, the obtained findings can also be used for larvae thigmotaxis behaviour investigation as well as study the behaviour of the larvae under test as a group rather than investigating the individual behaviour. In other words, the behaviour within the group can be sorted into different states such as normal stressed responses

or other related behavioural state based on the detected number of behavioural patterns. Zebrafish and other species are known to decrease their activity following a nociceptive event, thus the behaviour of larvae is comparable to adults [2, 6].

## 4.4 Conclusion

There is an increasing demand automatic video analysis system that is capable of automatic detecting of various behavioral patterns of larval zebrafish when are exposed to various kinds of stimulation. Experimental tests based on the proposed pattern detection method have demonstrated a noticeable change in the larval reaction under different types of stimulus regarding the number of detected patterns in the outer zones of the arena cells. Such findings confirm the validity of the proposed pattern detection method.

# Chapter 5

# Fish-Length Estimation: Orthogonal Model

## 5.1 Introduction

This chapter presents a new low-cost automatic calibration computer vision system for estimating the length of small-fish length, using dual synchronized orthogonal web cams. The suggested calibration procedure that account for light-refraction during the fish length measurements is also presented along with camera-distance calibration. The experimental assessment for the developed vision system using a couple of free-swimming adult zebrafish is also presented and discussed in this chapter.

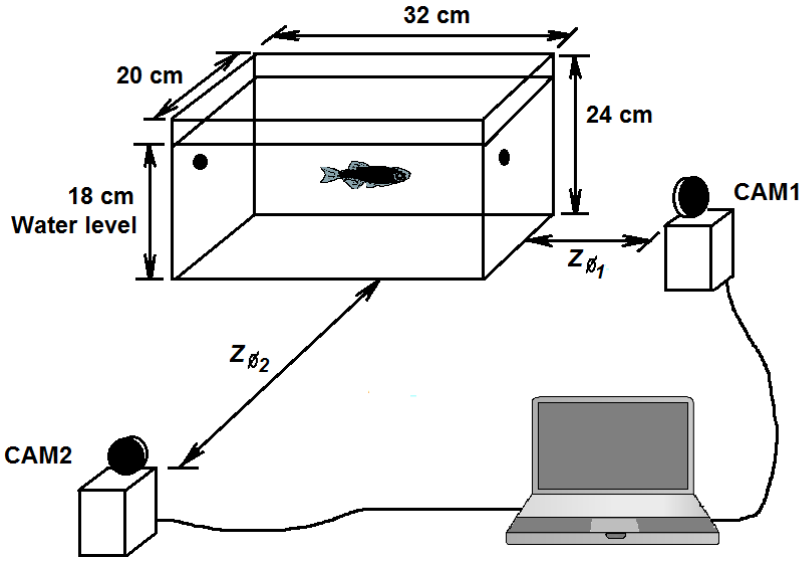


FIGURE 5.1: Experimental system setup

## 5.2 Material and Methods

The proposed system comprises a transparent-glass swimming container (i.e. water tank), two calibration objects, two web cameras and a computer. A generic laptop with Intel$^R$ Core$^{TM}$ i$^5$-3320$M$ CPU:2.6 GHz, 8.0 GB RAM, open-source MATLAB functions version 2013b (MathWorks, Inc.; Natick, MA, USA) and 64-bit Windows$^{TM}$7 operating system is used for data collection, processing, and monitoring purposes. The main components of this experimental setup are shown in Figure 5.1 and are described briefly as follows.

### 5.2.1 Water tank

This made up of 3 mm thick glass with dimensions of 32 × 20 × 24 cm (length, width and height), filled with water to a height of 18 cm. The top of the tank is open and exposed to ambient lighting while its bottom is clear. Two calibration

objects (i.e. coins with 2.03 cm diameter) are fixed to two adjacent sides of the tank, as illustrated.

### 5.2.2 Web cameras

Two generic low-cost webcams (TRIXES) with the following specifications are used in this study; video frame size of $640 \times 480$ pixels, 29 frames per second, and a focal length factor of $f = 3.85$ mm are used in this study. These cameras are fixed at the front and side views of the swimming container/tank with different camera-tank distance, which helped capturing a full-vision for both sides of the tank. The front camera is used as the main source of image capturing to measure length of the fish body while the side camera only measures location of the subject.

Knowing the cameras' depth of focus helps obtaining a clear image but such a specific information is not available in the technical specifications of the low-cost web camera used in this study, thus making calculation of this factor (i.e. the depth of focus) a difficult task. Instead, the depth of focus is assessed experimentally through immersing a coin object in the centre of the tank and adjusting the focal point manually until a clear image is obtained. Two snap images for first and last glass surface of the tank are then acquired to evaluate the effect of the obtained focal point on the detection quality of the front camera. Only a slight difference in the image quality was observed between the images taken at the first and last glass surfaces of the tank. The depth of focus for the front camera is therefore considered approximately equal to the depth of the tank.

Two coins are used as calibration objects. Utilisation of these objects to calculate the calibration factor (mm/pixel) helps in obtaining real physical metric of the

fish under test as well as estimating the camera-tank distances $Z_{\phi_1}$ and $Z_{\phi_2}$ automatically. A similar calibration procedure is adopted for objects tracking and length estimation by both cameras.

### 5.2.3 Test subjects

Since the main objective of this study is to develop a non-invasive fish length estimation, a single fish per test is considered. likewise, the number of the fish under test is also restricted by laboratory and funding availability. Thus, two free-swimming adult zebrafish with different lengths; 42 and 45 mm are individually used in this study. These fish are placed in two tanks with previously mentioned dimensions filled with room temperature $25°C$ and filtered water. The actual length of fish is measured by using additional small glass tank with $30 \times 11 \times 17$ cm (length, width and height) and a flat piece of white plastic is used to temporary confine the fish under test in a certain desired area closed to the ruler scale, as shown in Figure 5.2. The actual fish length can therefore be measured, using a ruler fixed at the front-side of the test tank. It should be mentioned here that this manual measurement is only required for comparison with the fish-length estimation by the proposed vision system.

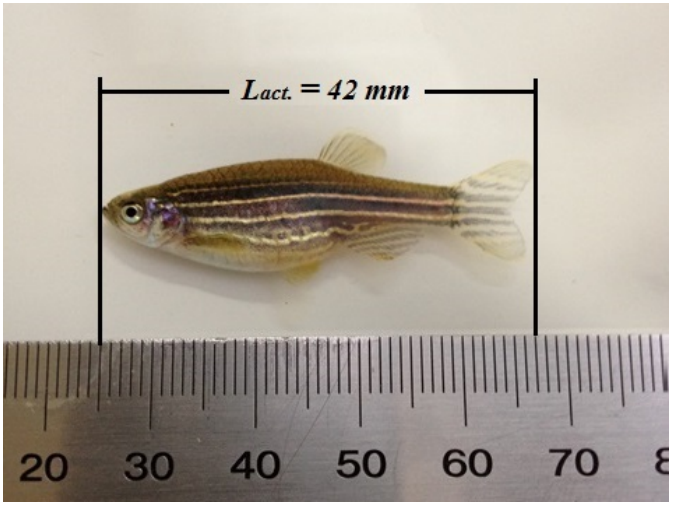


FIGURE 5.2: Actual length measurements ($L_a$) for the two-tested zebrafish

## 5.3 Mathematical Model

### 5.3.1 Challenges and assumptions

The typical inverse proportionality relationship between distance and apparent length is a common phenomenon in vision systems. In vision-based sizing systems, this phenomenon is therefore considered as a measurement challenge. In these systems, the actual length of fish needs to be reconstructed from a measured one that normally does not represent the actual length. In the present study, the refraction through glass is considered to be negligible due to the relatively small thickness of the wall's tank. The effect of water refraction is, however, a significant parameter. The proposed vision system is based on a mathematical model that is derived by the author, taking into consideration the following assumptions :

- Distances between the cameras and the tank are different $Z_{\phi 1} < Z_{\phi 2}$.
- The depth of focus of the front camera approximately equal to the depth of the tank.

- Parallax effect on the measurement of the target coordinates is reduced through pre-specifying boundaries of detection area for cameras.
- Calibration of fish-length is performed using an object with known diameter (coin)
- Subject under test should pass through the camera image center as condition for the image capturing process.

### 5.3.2 Camera-tank distance measurement

Calibration of the distance between the webcams and the tank's wall is performed by measuring the distance changes incrementally within a range of 5 to 90 cm with a step of 0.5 cm. The distance between the camera ($Z_\phi$) and the calibration object is inversely proportional to the measured distance, as shown in Figure 5.3(a). In mathematical form, this relationship is given by

$$Z_\phi \propto \frac{1}{d} \tag{5.1}$$

$$Z_\phi = \psi \frac{1}{d} \tag{5.2}$$

where $d$ represents diameter of the calibration object in pixels and $\psi$ is the proportionality constant. For the webcams used in this study, the value of $\psi$ is assessed through changing it value from 1 to 2000. At each step, the percentage of Relative Error (RE%) between the estimated and measured is calculated as with the aim of identifying the optimal value of $\psi$.

$$RE = \frac{|Measured - Actual|}{Actual} \times 100\% \tag{5.3}$$

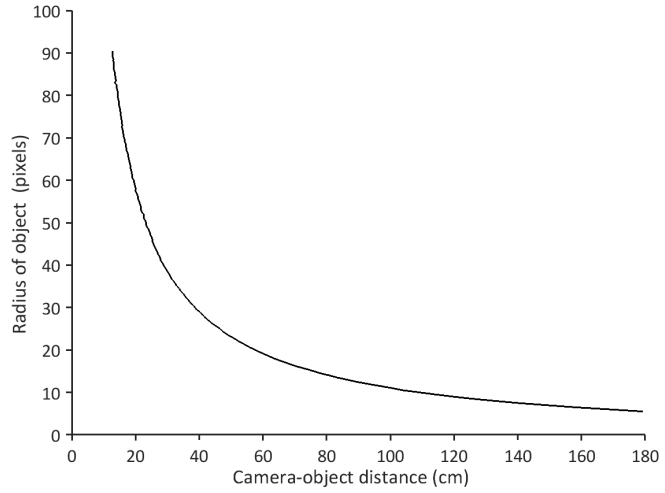


(a) Measured relationship between the calibration object

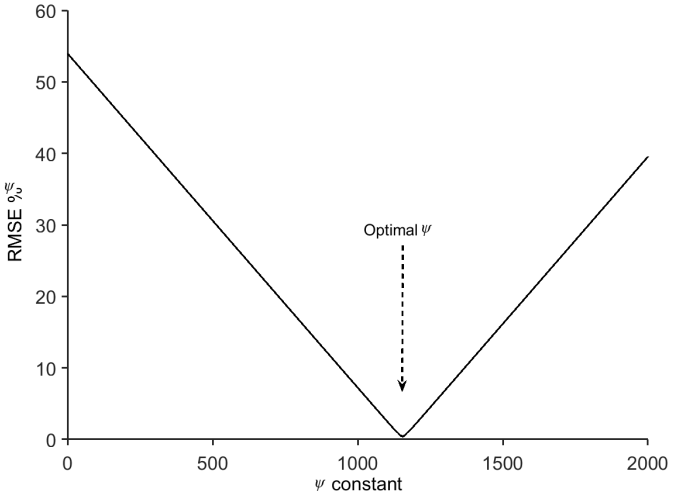


(b) Optimal value of $\psi$ for the camera distance and the calibration object

FIGURE 5.3: Optimized $\psi$ for automatic camera-tank measurement $Z_\phi$

Figure 5.3 demonstrates the findings of this experiment in which the optimal value of $\psi$ (at least RE%) is clearly illustrated.

### 5.3.3 Model derivation

Based on the data collected by CAM1 and CAM2, derivation of the proposed model can be described with the aide of Figure 5.1, as follows. 1 is used to measure the projected (measured) length ($L_m$) on which, the following relationships are derived

for the front camera CAM1. These relationships are equally applicable for CAM2. Figure 5.4(a) demonstrates the effect of distance and water refraction on actual fish length while Figure 5.4(b) provides correction model geometry. From this geometry, the angle of front projection $\theta_1$ can be calculated from:

$$\theta_1 = \tan^{-1}\left(\frac{L_m}{2Z\phi_1}\right) \tag{5.4}$$

The angle of interest ($\theta_2$) for length correction is obtained from

$$sin\theta_2 = \frac{L_m}{n\sqrt{L_m^2 + 4Z_{\phi_1}^2}} \tag{5.5}$$

where $n$ is the refractive index of the water which is equal to 1.33. Once ($Z_d$) is measured by the second camera, the estimated fish length ($L_{est.}$) is obtained from

$$L_{est.} = L_m + 2Z_d \tan\left\{\sin^{-1}\frac{L_m}{n\sqrt{L_m^2\left(1-\frac{1}{n^2}\right) + 4Z_{\phi_1}}}\right\} \tag{5.6}$$

## 5.4 The Vision System

The proposed vision system comprises of four distinct stages; pre-processing. subject segmentation, length-distance measurement, and length estimation. These stages are shown in the block diagram of Figure 5.5 and are described as follows.

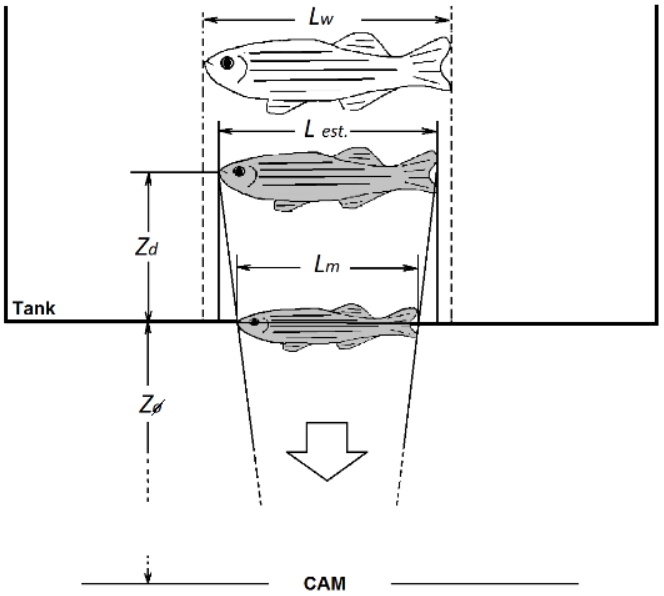


(a) Distance and refraction effect

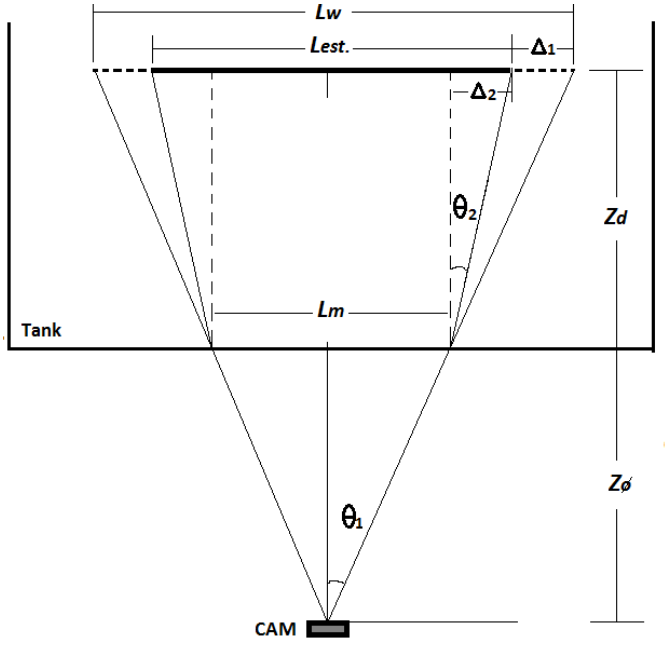


(b) Correction model geometry

FIGURE 5.4: Fish-length correction model ($L_{est.}$ estimated fish-length; $L_m$, fish-length measured by camera; $L_w$, fish-length affected by water refraction; $Z_o$, the distance between the camera and the tank wall; $Z_d$, the dynamic distance between the tank wall and the subject under)

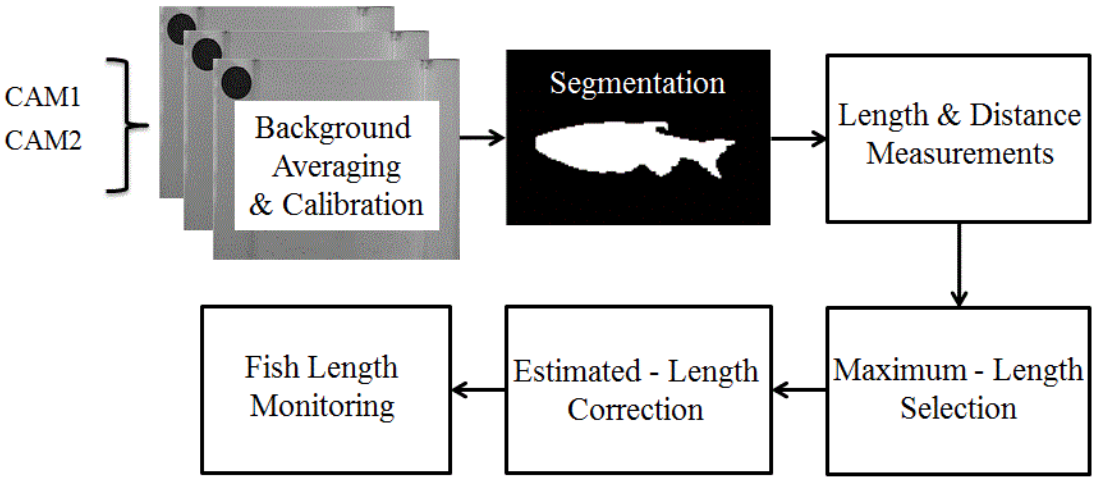


FIGURE 5.5: Block diagram of the proposed vision system

### 5.4.1 Pre-processing

This stage comprises of three main steps; calibration, camera-tank distance estimation, and background generation. These steps are outlined as follows.

1. **Camera-tank distance estimation**- it is achieved through automatic detection for the radius of calibration object and then using the measured relationship represented in Eq.5.2.

2. **Calibration**- focuses on obtaining a factor that coverts fish-length from pixels a metric unit (mm). This is achieved through performing the three sequential steps; (i) collecting a single snapshot from each camera, (ii) detecting and measuring diameter of the calibration object used in this study (coin) in the image, and (iii) calculating the calibration factor through dividing the actual diameter of the calibration object in millimeter by the measured diameter in pixels. As a result, the post-calibration maximum pixel-sizes are 457 and 253 micrometers for the front and side cameras, respectively.

3. **Background detection**- the decoded frames are added sequentially to artificial zero image (i.e. initial image) and then divided by the maximum value of resultant sum for normalizing. In mathematical terms, this process is given by

$$G = \sum_{i=1}^{f} \Omega_i \tag{5.7}$$

where, $\Omega_i$ is the grayscale of the individual RGB converted frame, $f$ is the number of selected frames. In this study, $f = 25$ frames is considered adequate for detection of the image background. The obtained value of $G$ is then normalized $G_b$ using the following formula

$$G_b = \frac{G}{G_{max}} \Omega_{max} \tag{5.8}$$

### 5.4.2 Subject segmentation

Post generation of both front and side backgrounds, each of the collected frame is subtracted from the corresponding background and the resultant image is threshold at 50% to convert the image into binary format. Figure 5.6 shows several images that demonstrate the implemented subject-segmentation process. As illustrated, the quality segmented-area image in Figure 5.6(b) is relatively poor due to some noise caused by transparency of some moving parts of the fish (i.e. fins and tail). The segmented binary image is then enhanced using two-morphological operations to eliminate noise in the detected regions, as illustrated in Figure 5.6(c). The first morphological operation is dilation with $3 \times 3$ structuring element that can be defined as below [74]:

$$A \oplus B = \{z \in E \mid (B_s)_z \cap A \neq \varnothing\} \tag{5.9}$$

where $B_s$ denotes the symmetric of B, which can be calculated as follow:

$$B_s = \{x \in E \mid -xB\} \tag{5.10}$$

A single iteration is used to prevent the growing region from crossing other boundaries. The second morphological operation was erosion with a $3 \times 3$ structuring element that is defined by

$$A \ominus B = \{z \in E \mid B_{z \subseteq A}\} \tag{5.11}$$

where $B_z$ is the translation of B by the vector z which can be calculated from:

$$B_z = \{b + z \mid b \in B\} \forall_z \subseteq E \tag{5.12}$$

Post-morphological enhancement, the resultant image is shown in Figure 5.6(d). This stage is not only enhanced the subject image but also improved measurement accuracy of the subject's length.

### 5.4.3 Length-distance measurements

At this stage, two properties of the segmented regions are used to measure the lengths and depths distances of the tracked subject, represented by $Z_d$ plus $Z_\phi$ for each camera (see Figure 5.3(b)). First, the 'BoundingBox property which determines the length $L_m$ (pixels) of the tracked area from one camera, considering the orientation of the moving subject. Second, the location property Centroid that obtains the corresponding subject distance $Z_d$ from the other camera. The BoundingBox property for the front camera is illustrated in Figure 5.6(d) -the Centroid detected by the other camera is not shown in this figure.

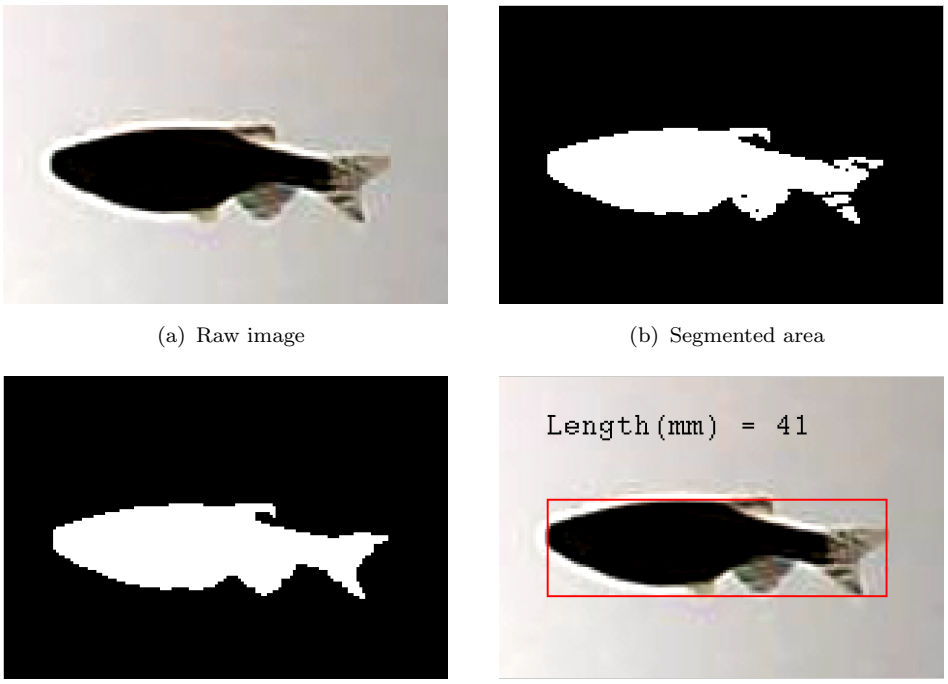


(a) Raw image (b) Segmented area

(c) Segmentation enhancement (d) Length measurement

FIGURE 5.6: Example of fish-length estimation based on major length of bounding box of the segmented fish body area

### 5.4.4 Length estimation

As illustrated in the block diagram of Figure 5.3(b), the estimated values of $L_m$ and $Z_d$ for each camera are used to estimate the fish length through the following steps:

1. **Per-camera length estimation**-the measured values of $L_m$ and $Z_d$ are used in Eq.5.3 to obtain the estimate length of the fish $L_{est}$.

2. **Maximum-length selection**-a new vector of the maximum estimated length $L_{est_{max}}(m)$ that represents the vector of the maximum values of the estimated length after using a certain threshold (see Figure 5.7(a)) is generated from

$$L_{est_{max}}(m) = \left\{ \begin{array}{ll} Select, & L_{est}(m) \geq THR \\ Ignore, & else \end{array} \right\} \tag{5.13}$$

where $THR$ represents the threshold that calculated from the first set $n$ of the estimated length values $L_{est}(n)$ as follows

$$THR = 0.5 \times max(L_{est.}(n)); \qquad n < m = 1:100 \tag{5.14}$$

The estimated length values are selected to represent the fish length at each instant as shown in Figure 5.6(a).

3. **Maximum-length mode**-post selection of the maximum length, the mode of the length values is computed and used to identify the final value of the fish length. Figure 5.6(b) demonstrates an example for the obtained results in this experiment

## 5.5 Results

Two individual adult zebrafish and 10 experiments are carried out to estimate the length of each fish. In order to maintain appropriate welfare condition for the fish under test, these experiments are conducted in a frequency of two experiments per day. In each experiment, the fish is moved into the testing tank for about an hour for acclimation. Next, the image capturing process is initiated until capturing 3000 frames that are considered adequate for the purpose of this study (i.e. fish-length estimation). It should be mentioned here that this process lasts for a period of up to an hour, depending on the swimming behaviour of the fish under test. The fish is then moved back to the pre-experiment environment. Finally, the acquired images are analysed using the developed vision system to estimate the fish length.

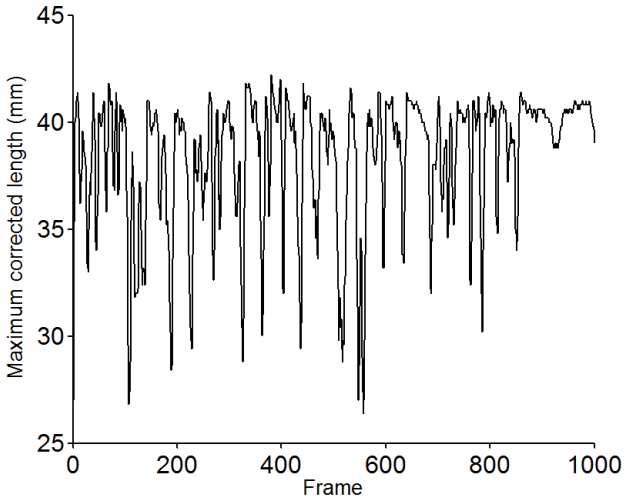


(a) Maximum selected length

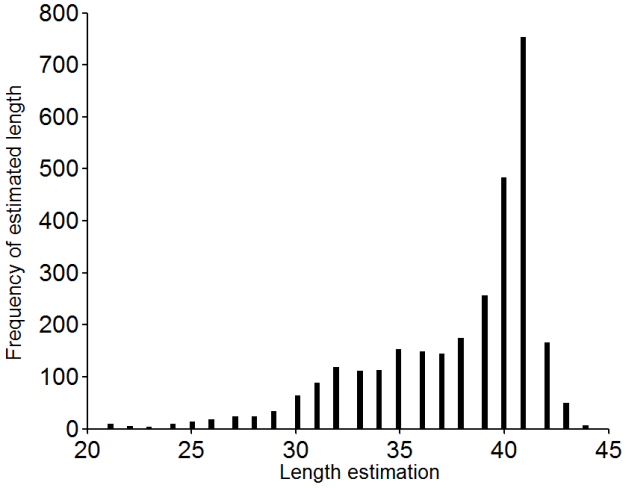


(b) Histogram of length estimation

FIGURE 5.7: Example of fish-length estimation based on histogram mode

Figure 5.8 compares the actual and estimated fish-length measurements. As illustrated a difference in the range of $2-4\%$ is demonstrated at this stage. This error that is comparable to that reported previously for large fish length/mass manual estimation [44] can be caused by several factors including: (i) camera resolution, (ii) accuracy of coin calibration, (iii) refraction-correction error during rapid movement of the fish, and (iv) distortion relevant to image segmentation at large depth distance and morphological operations. In this study, due to the above mentioned sources of error, further improvement for the measurement accuracy is

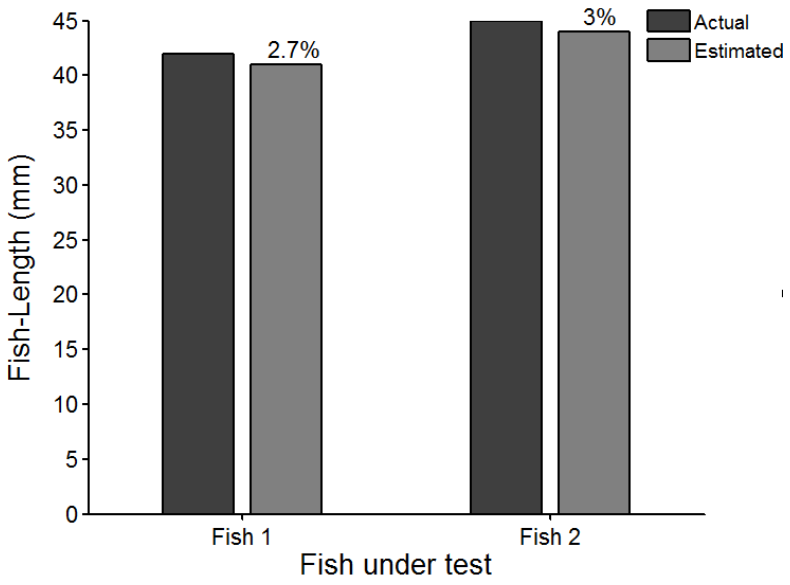


FIGURE 5.8: Comparison between actual and estimated fish-length

suggested to minimize the systematic measurement error through identifying a new error correction factor $\varepsilon$ and noting that the corrected $L_{cor}$ that length is slightly higher than the mode is obtained from

$$L_{cor} = Mode_{L_{est_{max}}(m)} + \varepsilon \times \sigma_{L_{est_{max}}(m)} \tag{5.15}$$

where $Mode_{L_{est_{max}}(m)}$ represents the most frequent value of the maximum estimated length vector $L_{est_{max}}(m)$ and $\sigma_{L_{est.max}}$ represents the standard deviation of this vector. $L_{cor}$ is the final corrected estimated length using error correction factor $\varepsilon$.

As shown in Figure 5.9, the optimization process of $\varepsilon$ is carried out through calculating the Percentage Relative Error (RE%) of the estimated length for a range of $\varepsilon$ values. It can be noticed that the minimum measurement error of the fish length is obtained with $\varepsilon$ value around 0.23. Table 5.1 summarises and emphasises the use of the identified value of the length estimation accuracy.

The average length estimation error is dropped from 3% to around 1%; 0.77%

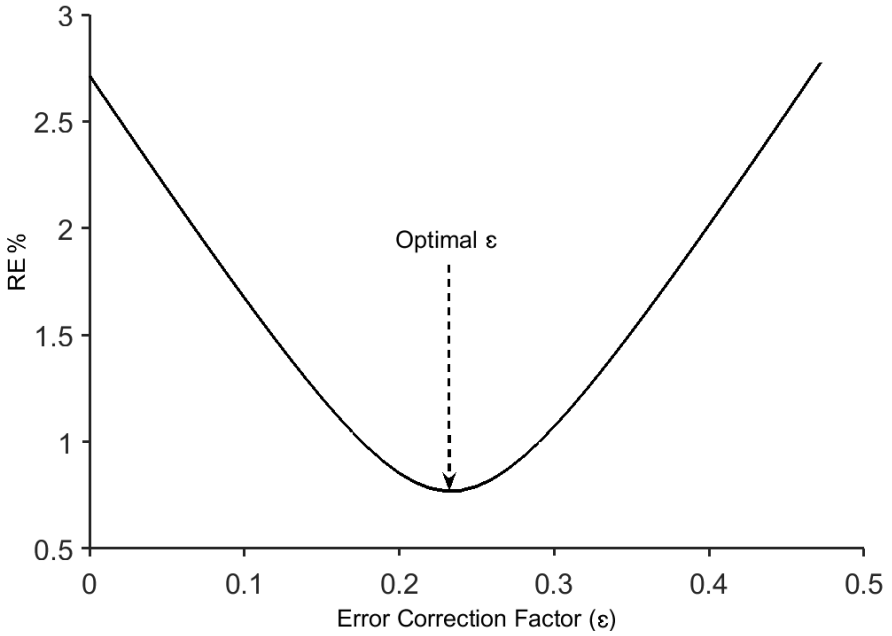


FIGURE 5.9: Optimization of the error correction factor ($\varepsilon$)

for a fish with a length of 42 mm and 1.08% for another fish with a length of 45 mm (see Figure 5.8) . These findings reflect a significant performance improvement compared to the state of the art. For example, in [49], the achieved length estimation error for small fish sizing using paired-laser photogrammetric method, around 3% and around 5% for a large fish (bluefin tuna) using direct linear transportation method as reported in [44]. Another study for larg fish, the estimation error was found to be 14%. as reported in [44].

## 5.6 Discussion

Dual orthogonal cameras were previously used for small fish tracking [75, 76]. In these studies, the cameras were positioned as side-view and top-view, and each individual track file from each camera then had to be manually synchronized and exported (as raw track data) into spreadsheets. In this setup, the cameras need to be started manually, and their synchronization was often difficult and required

TABLE 5.1: Relative percentage error RE% for two fish with different lengths

| **Test** | **Actual Length 42 mm** | | **Actual Length 45 mm** | |
|---|---|---|---|---|
| | **RE%** | | **RE%** | |
| | $\varepsilon = 0$ | $\varepsilon = 0.23$ | $\varepsilon = 0$ | $\varepsilon = 0.23$ |
| 1 | 2.38 | 0.19 | 2.22 | 0.21 |
| 2 | 2.38 | 0.04 | 4.44 | 2.08 |
| 3 | 2.38 | 0.27 | 4.44 | 2.20 |
| 4 | 4.76 | 2.18 | 2.22 | 0.09 |
| 5 | 2.38 | 0.23 | 2.22 | 0.22 |
| 6 | 2.38 | 0.80 | 2.22 | 0.14 |
| 7 | 2.38 | 0.46 | 2.22 | 0.16 |
| 8 | 2.38 | 0.27 | 2.22 | 0.42 |
| 9 | 2.38 | 0.09 | 4.44 | 1.47 |
| 10 | 2.38 | 0.14 | 2.22 | 0.12 |
| **Av.** | 2.71 | **0.77** | 3.06 | **1.08** |

careful pre-processing of recorded data. In a typical small fish experiment, many frames must be synchronised, thereby making it time-consuming and susceptible to human error. In the developed vision system, most of these practical difficulties have been addressed where the cameras are automatically synchronized and no manual camera-distance calibration is required. This is not only simplifying the system setup but also improves the estimation accuracy when compared to the state of the art.

The obtained experimental findings and observations have demonstrated the feasibility of using the proposed mathematical model to develop a robust and non-destructive fish-length estimation system at low cost. The obtained estimation accuracy for the subjects used in this study can be considered quite acceptable for small experimental tanks in laboratory settings to estimate length of small fish and easy to use for small experimental tanks in laboratory settings to estimate length of small fish.

Despite the fact that the proposed system offers an acceptable range of accuracy, it still has the following limitations that are currently under consideration by the on-going research of the authors. First, the time taken for each experiment is relatively long (up to 1 hour) which depends on the swimming behaviour of the fish under test which should pass through the camera image center. However, the experimental time can be reduced through further improvement of the mathematical model, taking into consideration the conditions when the fish is not directly in front of the camera. Second, the use of fixed generated background and detection threshold in the detection process. This makes the system prone to estimation error due to variations in the light intensity. This problem can be addressed through using a smarter detection based on a dynamic adaptation of both the background and the detection threshold.

## 5.7 Conclusion

An practical computer vision system based on orthogonal camera setup is developed for small experimental tanks and it can be considered in laboratory settings to estimate fish length. This system can be adopted for behavioural analysis of small fish as well as studying the relationship between the fish behaviour and its size. Overall, the developed orthogonal vision system can be considered practical, robust and a cost effective instrument for length estimation of small fish in a aquarium lab setting. It also forms a robust foundation for further developments and studies on behavioral and welfare of small fish.

# Chapter 6

# Fish-Length Estimation: Stereo Model

## 6.1 Introduction

This chapter presents a new stereo-imaging model for length estimation of small-size free-swimming zebrafish using low-cost web cameras. It also presents an automatic calibration module and performance assessment for proposed model through comparing the estimated length with a physical measurement of the fish length.

## 6.2 System Model

### 6.2.1 Camera-target distance measurement

In this study, a geometric model for the camera-target distance is derived and implemented. Figure 6.1 shows the following camera-target distance scenarios for the target's location :

1. Target at left-side of both cameras (Point $T1$)
2. Target at the left side of CAM2 and right-side of CAM1 (Point $T2$)
3. Target at right-side of both cameras (Point $T3$)

CAM1 is placed at the front side of the tank and the center line of its field of view (FOV) is therefore perpendicular to the tank while CAM2 that is aligned with CAM1 is tilted with an angle ($\theta$), as illustrated. Calculations of the camera-target distance at different scenarios only depend on two main parameters; the total distance between CAM1 and the tank's wall ($D_T$) and the distance (S) between CAM1 and CAM2.

The distance $D_m$ between CAM1 and the target can be calculated from

$$D_m = D_T - C \times D_{f_n} \tag{6.1}$$

where $C$ is a calibration factor which maps the distance measurements in pixels to millimeters and $D_{f_n}$ represents the distance (in pixels) between the target and tank's wall at the above-mentioned scenarios in which the value of $D_{f_n}$ is represented by $D_{f_1}$, $D_{f_2}$, and $D_{f_3}$ that are defined as follows:

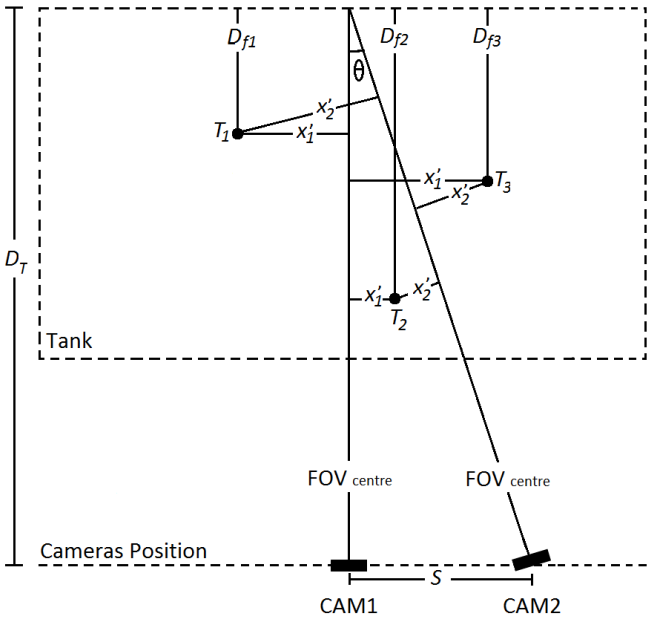


FIGURE 6.1: Geometric model of the camera-target distance $(x'_1, x'_2)$: distances between the target and the FOV centers)

- Target centre is located at the left hand-side of the FOV centres for CAM1 and CAM2. Mathematically, the distance between the target and back-end of the tank $D_{f_1}$ that is derived from Figure 6.2(a). Taking the triangular ABC, the distance AB which represents the desired distance (i.e. the distance between the target and the tank's wall), $D_{f_1}$is given by

$$D_{f_1} = \frac{D_T(x'_2 \sec\theta - x'_1)}{S} \tag{6.2}$$

- Target centre is located between the FOV centres for CAM1 and CAM2. Mathematically, the distance between the target and back-end of the tank $D_{f_2}$ that is derived from Figure 6.2(b). Similarly, the distance AB (i.e. $D_{f_2}$) is given by

$$D_{f_2} = \frac{D_T(x'_1 + x'_2 \sec\theta)}{S} \tag{6.3}$$

- Target centre is located at the right hand-side of the FOV centres for CAM1 and CAM2. Mathematically, the distance between the target and back-end

of the tank $D_{f_3}$ that is derived from Figure 6.2(c). Similarly, the distance AB (i.e. $D_{f_3}$) is given by

$$D_{f_3} = \frac{D_T(x'_1 - x'_2 \sec\theta)}{S} \tag{6.4}$$

### 6.2.2 Calibration

Distance measurements $D_m$ given in Eq. 6.1, combines two components; $D_T$ measure in millimeters and $D_f$ measured in pixels. In order to obtain actual distance in millimeters, $D_f$ should be converted from pixels to millimeters. This is achieved through obtaining a relationship between two different views (shown in Figure 6.2); the tank's view and the camera's view (i.e the captured frame).

From the projection of the fish-length in both views, the calibration factor ($C$) can be initially obtained from

$$C = \frac{L_{T_{mm}}}{W} \tag{6.5}$$

where $L_{T_{mm}}$ represents the tank's length in millimeters, shown in Figure 6.3(a), and $W$ is the image width in pixels, shown in Figure 6.3(b). Now, in Figure 6.3(a), the value of $L_{Tmm}$ can be obtained from

$$L_{T_{mm}} = 2D_m \tan\beta \tag{6.6}$$

where $\beta$ represents half of the camera FOV angle and $D_m$ represents camera-fish distance in tank as explained earlier. Substituting equation 6.6 in equation 6.5 yields

$$C = \frac{2D_m \tan\beta}{W} \tag{6.7}$$

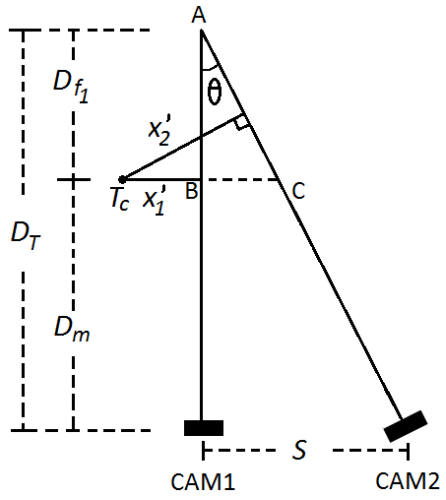


(a) Target $T_c$ at left

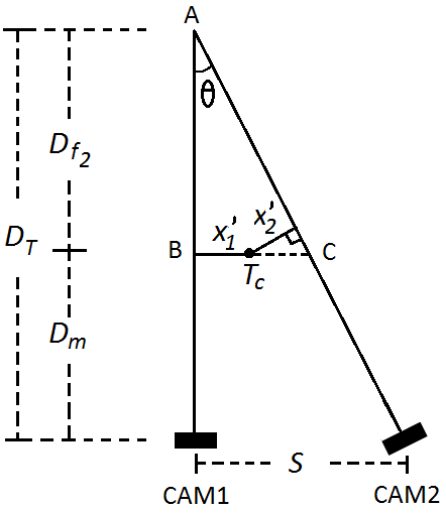


(b) Target $T_c$ in between

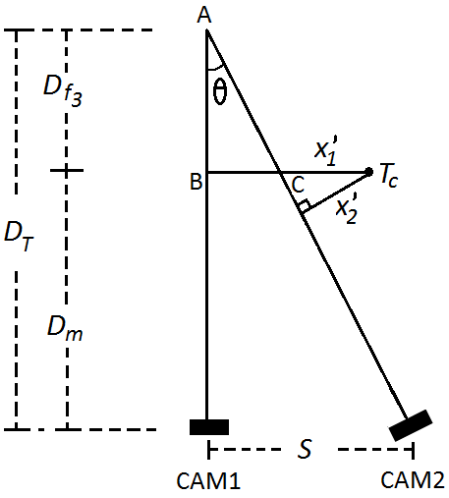


(c) Target $T_c$ at right

FIGURE 6.2: Geometric model scenarios for camera-target distance calculation

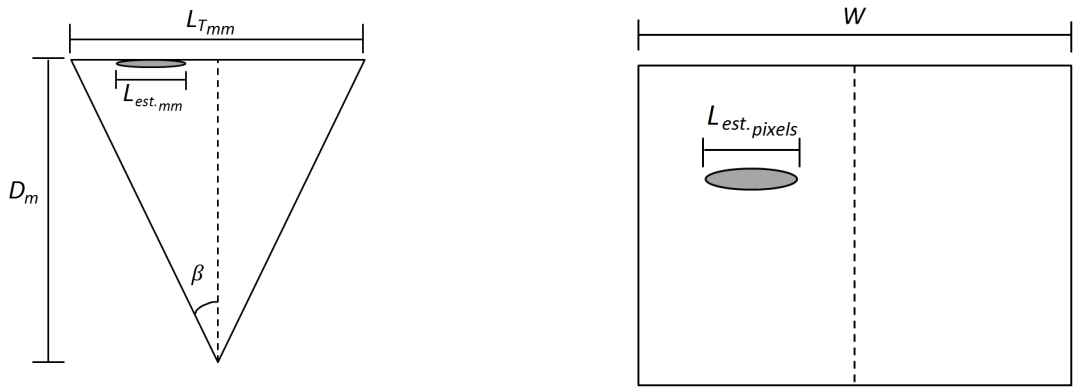


(a) Physical view (mm) (b) Camera view (pixels)

FIGURE 6.3: Geometric representation of the tank and camera views

Substituting for $D_{f_n}$ from Eq. 6.2 and Eq. 6.5 in Eq. 6.1 yields:

$$D_m = D_T - C\,\frac{D_T\,(\,x'_2 + x'_1 \sec\theta)}{S} \tag{6.8}$$

where $x'_1$ and $x'_2$ can take different polarities (i.e.$\pm x_1$, $\pm x_2$), depending on the centre of the target's position in the tank. Now, substituting equation 6.7 in equation 6.8, and rearranging yields

$$D_m = \frac{D_T S W}{SW + 2D_T \tan\beta\,(\,x'_2 + x'_1 \sec\theta)} \tag{6.9}$$

Now, the obtained calibration ration $C$ in equation 6.7 can also be used to calculate the target's length (i.e. length of the fish under test) in millimetres from

$$L_{est.mm} = L_{est._{pixels}} \times \frac{2D_T S \tan\beta}{SW + 2D_T \tan\beta\,(\,x'_2 + x'_1 \sec\theta)} \tag{6.10}$$

where $L_{est.mm}$ represents the estimated length of the fish in millimetres and $L_{est.pixels}$ represents the measured length of the fish in pixels.

## 6.3 Materials and Method

Experimental setup of the stereo imaging system comprises from the same hardware which is used in the presented orthogonal model but, with different cameras setup as illustrated in Figure 6.4. The web cameras that are used for video recording are fixed on a stand outside the tank with a height of 200 mm to cover the desired view angle to minimize the efforts of cameras set up. The desired field of view for the subject's detection is found to be at 95 cm from the tank's wall. This experimental testbed is considered adequate for small size fish length measurements and monitoring which is of particular interest in this study as well as other studies at the laboratory level such growth monitoring and welfare evaluation. In this setup, the distance between the camera and swimming object is dynamic and its accurate estimation represents a significant challenge in this study.

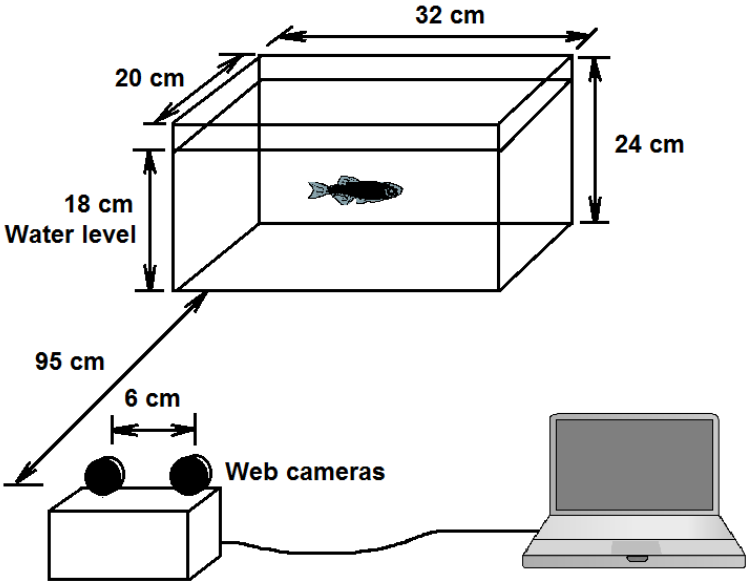


FIGURE 6.4: Experimental setup

Unlike equivalent studies that require a relatively complex setup and parameters adjustments for the angle of alignment for both cameras, the constructed testbed requires a simple setup and alignment of a single camera.

The proposed method of the vision system comprises two distinct stages: pre-processing fish-length estimation. These stages are shown in the block diagram of in Figure 6.5 and are described as follows.

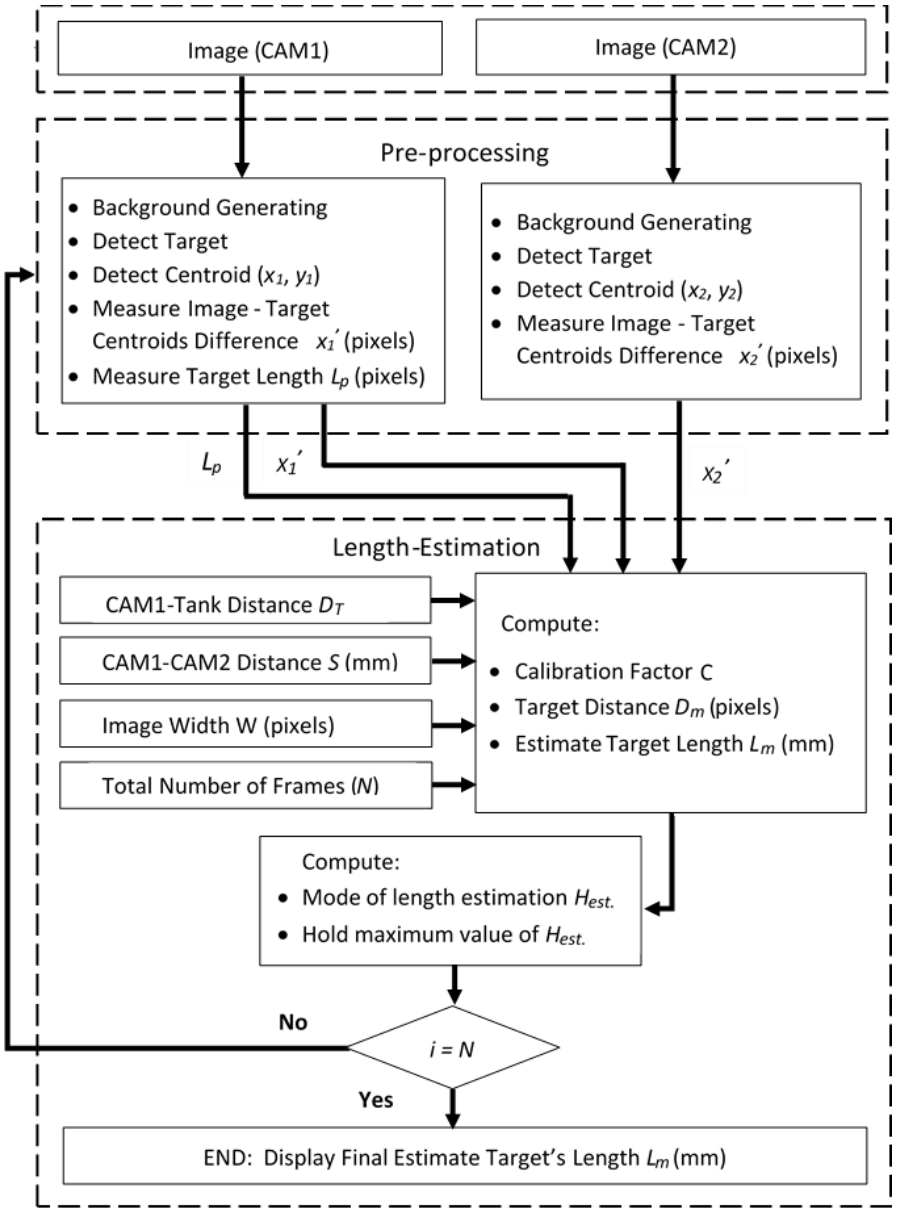


FIGURE 6.5: Block diagram of fish-length estimation process

### 6.3.1 Pre-processing and segmentation

The video frames acquired from CAM1 and CAM2 are pre-processed through two similar background detection and segmentation stages which are presented previously in Chapter 5 (section 5.4). Figure 6.6 shows an example of an image segmentation showing target images detected from both cameras in which the centroid and body length are clearly illustrated. The relative horizontal differences ($x_1^{'}$ and $x_2^{'}$) between the image centre and the obtained target centre for both camera-frames (see Figure 6.1) are then obtained.

(a) Centroids detection

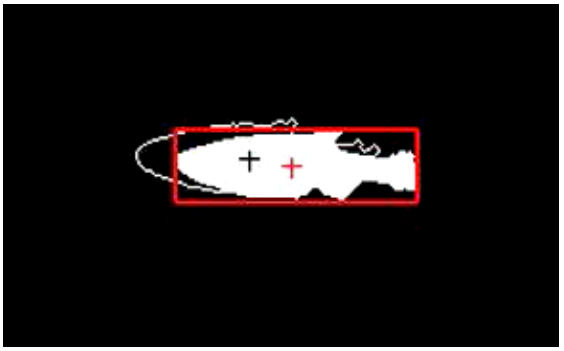

(b) CAM1 Length-measurement

FIGURE 6.6: Example of an image segmentation showing target detection in terms of its centroid and body length. White object: target image of CAM1; Transparent object: target image of CAM2

### 6.3.2 Fish-length estimation

As illustrated in Figure 6.4, the obtained values of ($x'_1$ , $x'_2$) and the measured target length in pixels ($L_{est._{pixels}}$) are fed to this module along with other-specified constants that include the CAM-Tank distance ($D'_T$). Several key parameters are then computed including

1. Calibration factor ($C$)
2. Instantaneous distance (in millimeter) between CAM1 and the swimming target ($D_m$)
3. Length of the target ($L_{est.mm}$) in millimeter

An example of the instantaneously estimated values of the target's length is shown in Figure 6.6 where targets centroids are initially detected, Figure 6.6(a). Next, the target's length is measured in pixels using the image of CAM1, Figure 6.6(b). In this process, the instantaneously estimated length is obtained depending upon computing the above mentioned key parameters.

Figure 6.7 demonstrates an example of instantaneous length estimation for a free-swimming target. The fluctuations appear in Figure 6.7(a) reflect instantaneous variations in the target's movement in various directions. The estimated maximum-length values are therefore directly affected by the target orientation as it appears in front of CAM1. Post estimation of instantaneous maximum lengths, the mode of the estimated values is computed and used to obtain the most frequent value which represents the final value of the target's length, as illustrated in Figure 6.7(b).

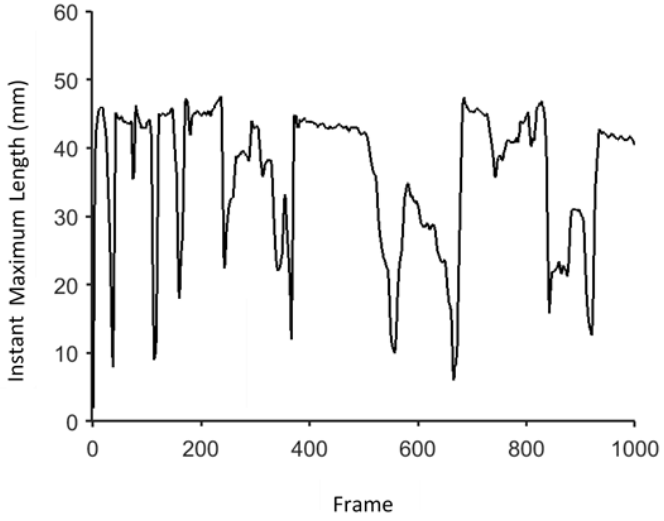


(a) Instantaneous maximum-length estimation

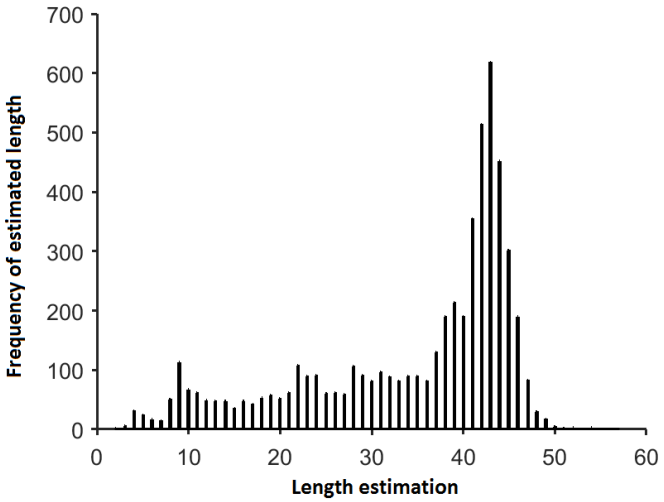


(b) Histogram of length estimation

FIGURE 6.7: Example of fish-length estimation based on histogram mode

## 6.4 Results and Discussion

Two free-swimming adult zebrafish with lengths of 42 and 44 mm are individually used in this study. A flat plastic object was used to temporary confine the fish under test in a certain desired area close to a ruler scale fixed at the side of the tank, as illustrated in Chapter 5. The actual length of the fish under test can therefore be measured accurately through capturing multiple frames from which the average measurement value is considered as a reference in this experiment. On the other

hand, the fish length is also estimated automatically, using the developed vision system as shown in Figure 6.4, and compared to that measured manually. The obtained results demonstrate a relatively small difference between the automatic and manual measurements of the fish length. This finding does not only confirm validity of the proposed model but also addresses the above-mentioned challenges of small-fish sizing.

Ten experiments were initially carried out to estimate the length of each of the subjects under test. Figure 6.8 compares the actual and estimated fish-length measurements. As illustrated, a difference in the range of $6-6.5\%$ is demonstrated at this stage. This error can be caused by several factors including utilization of inadequate camera resolution, camera sensor instability, rapid movement of the fish, and distortion relevant to image segmentation at large depth distance and morphological operations.

In order to minimize this estimation error, a correction is performed using the similar formula (Eq. 5.15) that is used in the orthogonal system in Chapter 5 to obtain the final value of the corrected length estimation $L_{cor}(mm)$.The optimum value of $\varepsilon$ is obtained experimentally by numerous experiments with different values of $\varepsilon$. The obtained results revealed that the best-estimated length could be obtained when $\varepsilon$ value is in the range of 4 to 5. Sample results for different values of $\varepsilon$ settings are shown in Table 1. It can be noticed that the average length estimation error dropped from 6% (Figure 6.8) to 1.19% for Fish1 (42 mm) and 1.36% for Fish2 (44 mm). The results in this study has also significant performance improvement in length-estimation for small and large fish as compared to that systems reported in [49, 44, 44], where the average error in length estimation from 3% to 14%.

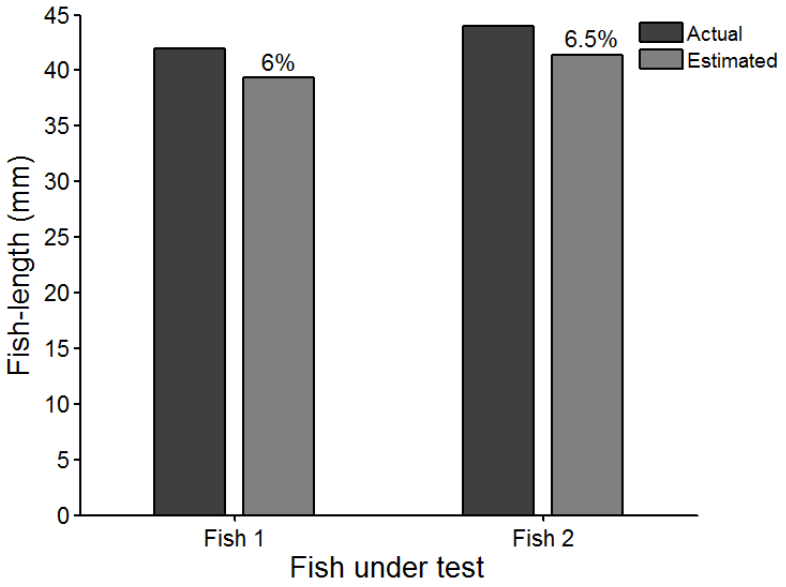


FIGURE 6.8: Comparison between estimated and actual fish-length

TABLE 6.1: Relative percentage error RE% for two fish with different lengths

| **Test** | **Actual Length 42 mm** | | | | | **Actual Length 44 mm** | | | | |
|---|---|---|---|---|---|---|---|---|---|---|
| | **RE%** | | | | | **RE%** | | | | |
| | $\varepsilon = 0$ | $\varepsilon = 3$ | $\varepsilon = 4$ | $\varepsilon = 5$ | $\varepsilon = 6$ | $\varepsilon = 0$ | $\varepsilon = 3$ | $\varepsilon = 4$ | $\varepsilon = 5$ | $\varepsilon = 6$ |
| 1 | 7.14 | 3.37 | 2.12 | 0.86 | 0.38 | 4.54 | 0.00 | 1.51 | 3.03 | 4.54 |
| 2 | 4.76 | 0.99 | 0.25 | 1.51 | 2.76 | 6.81 | 2.27 | 0.75 | 0.75 | 2.27 |
| 3 | 4.76 | 0.99 | 0.25 | 1.51 | 2.76 | 9.09 | 4.54 | 3.03 | 1.51 | 0.00 |
| 4 | 7.14 | 3.37 | 2.12 | 0.86 | 0.38 | 6.81 | 2.27 | 0.75 | 0.75 | 2.27 |
| 5 | 7.14 | 0.99 | 0.25 | 1.51 | 2.76 | 6.81 | 2.27 | 0.75 | 0.75 | 2.27 |
| 6 | 7.14 | 3.37 | 2.12 | 0.86 | 0.38 | 9.09 | 4.54 | 3.03 | 1.51 | 0.00 |
| 7 | 7.14 | 3.37 | 2.12 | 0.86 | 0.38 | 4.54 | 2.27 | 0.75 | 0.75 | 2.27 |
| 8 | 4.76 | 0.99 | 0.25 | 1.51 | 2.76 | 4.54 | 1.51 | 3.03 | 4.54 | 0.00 |
| 9 | 4.76 | 0.99 | 0.25 | 1.51 | 2.76 | 6.81 | 2.27 | 0.75 | 0.75 | 2.27 |
| 10 | 7.14 | 3.37 | 2.12 | 0.86 | 0.38 | 6.81 | 2.27 | 0.75 | 0.75 | 2.27 |
| **Av.** | 6.19 | 2.18 | **1.19** | **1.19** | 1.5 | 6.59 | 2.27 | **1.36** | **1.36** | 2.27 |

Although the proposed system offers an acceptable range of accuracy compared with related application for large fish size as reported in [44], it has similar limitations which are represented in the orthogonal sizing system in terms of required time for each experiment and the use of fixed generated background and detection threshold in the detection process. This makes the system prone to

error due to variations in the light intensity that can be addressed through using dynamic adaptation of both the background and the detection threshold.

## 6.5 Stereo System Validation

This part of work aims at addressing the setup complexity challenge of 3D tracking systems while maintaining a tracking accuracy level that is favorably compared with the state-of-the art for free-swimming zebrafish. This is achieved by developing a new vision system that comprises two fixed cameras takes two images separated by a baseline as dimensioned previously. Centroids of the target to be tracked at both images are identified and used to extract the third coordinate of the 3D model using simple triangulation to derive the targets depth as illustrated in Figure 6.9.

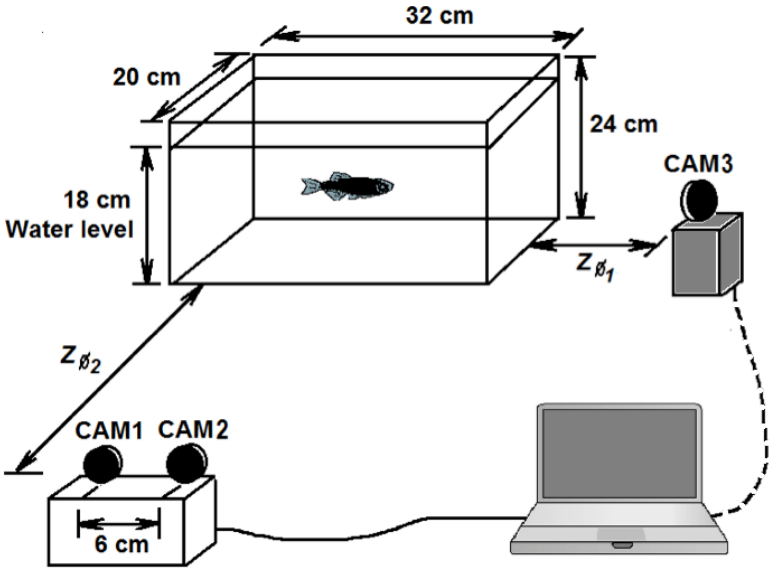


FIGURE 6.9: Setup of system evaluation

Validity of the derived stereo model is assessed experimentally and compared to an existing orthogonal model. Examples of 3D trajectories for a 5-minute

free-swimming zebrafish is shown in Figure 6.10 using both stereo and orthogonal trajectories. In Figure 6.11, it can be noticed that the stereo system has successfully detected the third dimension (i.e. fish depth) using the model derived described earlier in Section 6.1. The performance of the developed stereo vision system is compared to that obtained from a 3D orthogonal vision system.

In this study, the latter system is only used for test and validation purposes. In this experiment, a third camera (CAM3) was used along with CAM1 and CAM2 of the stereo vision system for simultaneous recording of 3 video clips. 3D trajectories of the fish under test are obtained by tracing the positional coordinates of the fish at each frame as illustrated in Figure 6.10(a), (b) and (c). The results presented in these figures compare 3D trajectories of stereo and orthogonal tracking systems.

In Figure 6.11, the estimated depth of both stereo and orthogonal systems are compared where it can be noticed that there is a high correlation between the performances of both systems. In this experiment, only 1200 out of 4500 samples are presented for demonstration purposes. The obtained results from the developed stereo vision system are found to be highly correlated with that obtained from the orthogonal system. This confirms the validity of both models but with a significant reduction in the required system setup with a less experimentation space.

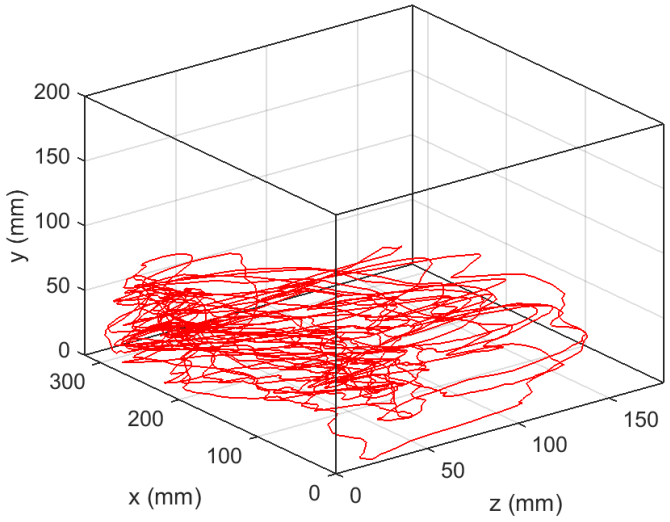


(a) Stereo tracking trajectory

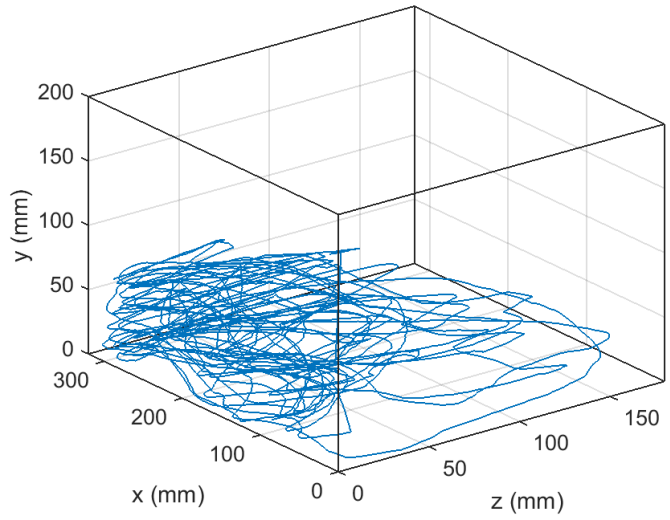


(b) Orthogonal tracking trajectory

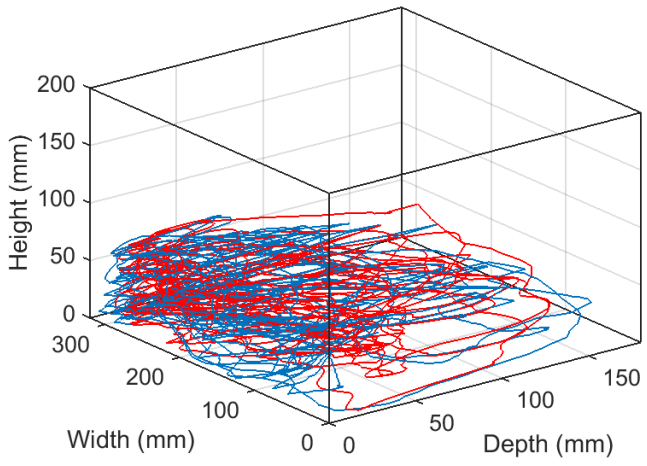


(c) stereo and orthogonal tracking trajectories

FIGURE 6.10: Comparison between 3D trajectories of stereo and orthogonal tracking systems

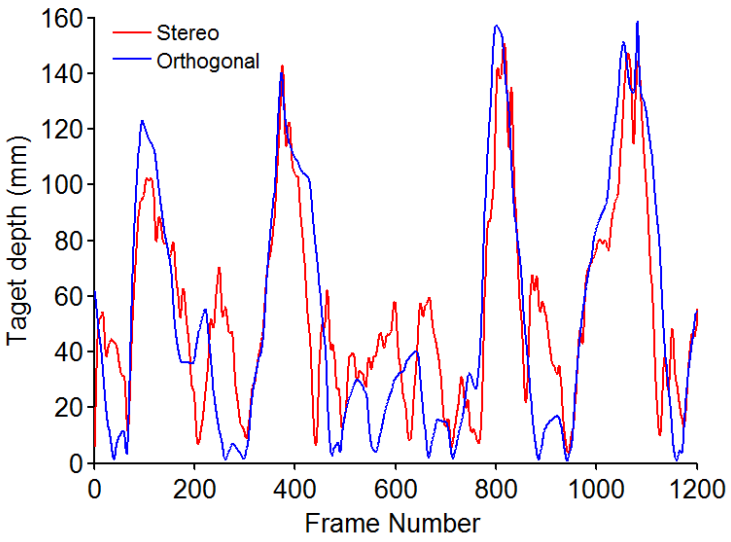


FIGURE 6.11: Correlation between stereo and orthogonal of estimated target depth

## 6.6 Conclusion

Overall, the developed stereo prototype can be considered cost effective and easy to use for small experimental tanks in laboratory settings to estimate fish length. It also allows for accurate fish mass calculation using related length-mass relationships. This pilot study, however, is expected also to support further future studies on the welfare of small fish which have not been thoroughly explored in the literature yet.

# Chapter 7

# Fish Recognition

## 7.1 Introduction

In this chapter, a new non-destructive methods for recognizing and extracting of a new feature in zebrafish is proposed and implemented as an alternative to the physical tagging. The proposed methods aim at extracting unique fish feature using Colour Space CIELAB feature extraction method and Speed-Up Robust Feature (SURF) matching method. Utilization of these methods in fish identification is not thoroughly explored in literature yet is considered in this chapter.

## 7.2 Colour Space Feature Extraction Method

This method comprises several sequential stages including data collection, preprocessing, color space transform, clustering and feature extraction. These stages are shown

in Figure 7.1 and are describes as follows.

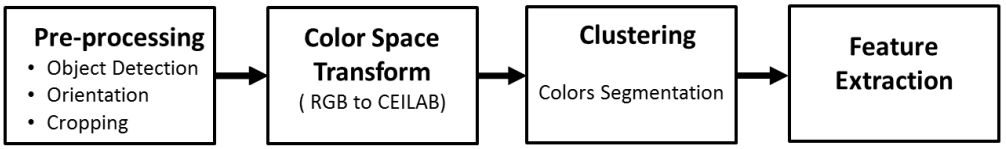


FIGURE 7.1: Steps of the work methodology

### 7.2.1 Data Collection

Twenty five side images with size of (1500 × 3500) pixels for four individual zebrafish were captured manually. Due to fast motion of the objects under study, 18 images are blurred and then discarded from the original images set. Therefore, 4 clear images are used and labeled in the present technique. Figure 7.2 shows an example of side captured image.

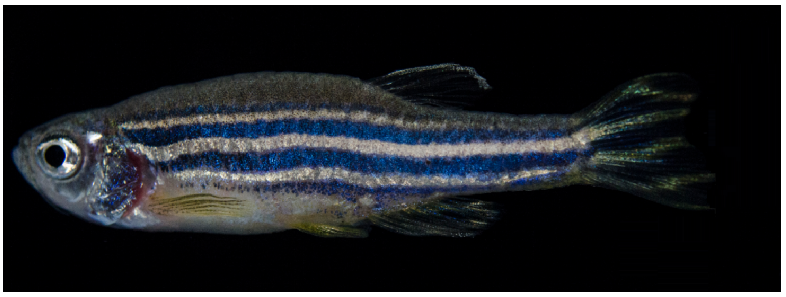

FIGURE 7.2: Example of a side image of zebrafish

### 7.2.2 Preprocessing

Pre-processing is considered a key stage for other sequential stages of the proposed method. In this stage, the raw acquired RGB image is converted to gray intensities

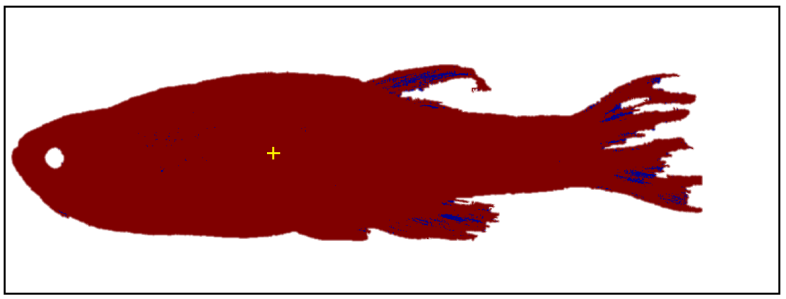

(a) Segmentation, alignment and centre detection

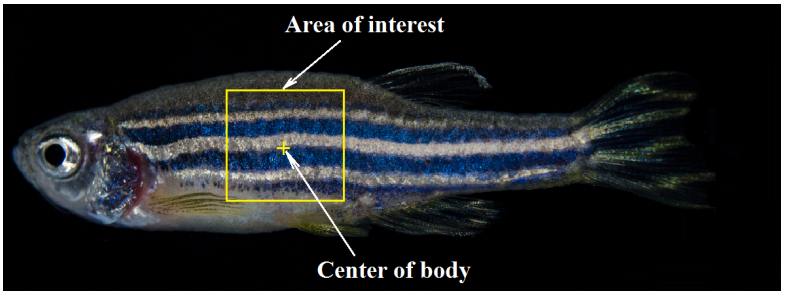


(b) Identification of the area of interest

FIGURE 7.3: Image pre-processing

$[0-1]$ with double precision. Then, after labelling process, all areas with their corresponding centroids in the image are determined. The desired object is segmented with its centroid using maximum detected areas in the image as shown in Figure 7.3(a). After this step, the orientation of detected body is corrected by resting the angle of the longitudinal body axis. The importance of this step is to reduce the distortion that might appear in the blue stripes pattern stage. The final step of pre-processing is to use the detected centroid to obtain a $600 \times 600$ sub-image from the original colored one as illustrated in Figure 7.3(b).

### 7.2.3 Colour space transform

RGB to CIELAB colour space transform process is required to obtain more colour information in image than the in RGB colour space as described earlier in Chapter

2. This stage aims as extracting a new feature from the distribution of the blue colour in the selected sub-image. The default RGB colour of the identified area is transformed into L*a*b* colour space (also called CIELAB space), which provides an enhanced pixel-level presentation for the colour of the area of interest.

1. Clustering - in this stage, the converted L*a*b* colour space is reduced to *a and *b by discarding lightness component L*. By using this reduction, the clustering for new two dimensions patched image can be then performed easily with aid of $k$-means algorithm which is previously mentioned in Chapter 2. Figure 7.4 shows an example of the segmented blue stripes from the the raw patched image.

2. **Feature Extraction** - four sequential processing steps; distribution vector generation of pixels values in blue image, vector smoothing, peaks detection and standard deviation of peaks are used in this stage to extract a feature in each object. The summation of pixels values in this pattern is used to represent the distribution of blue colour in the segmented colour image as follows. Let $(n, m)$ are the dimensions of the image and $r(x, y)$ represents the instance value of pixel in the image. Then, a vector $v(x)$ is assumed to represent the distribution of blue segmented pattern in y-axis and can be represented as follows

$$v(x) = \sum_{y=1}^{m} r(x, y), \qquad x = 1, 2, \cdots, n \tag{7.1}$$

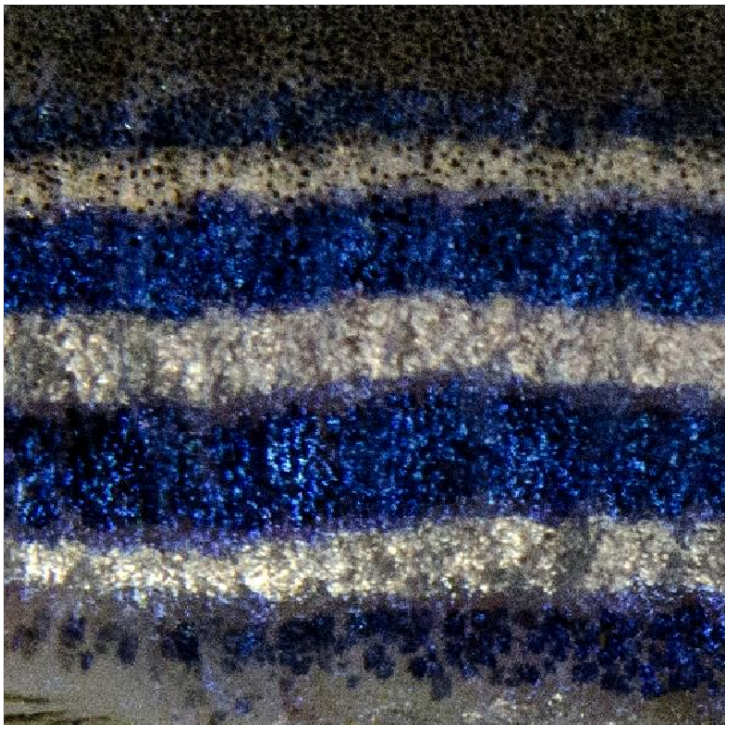

(a) Raw patched image

(b) Segmented image

FIGURE 7.4: An example of the segmented blue stripes from the the raw patched image

Moving average process is used to obtain smoothed $v(x)$ vector by computing series of averages of different subsets of the full data [77] as follows:

$$\tilde{v}(x) = \frac{1}{d}\sum_{r=0}^{d-1} v(x-r) \tag{7.2}$$

where $d$ depends on the chosen subset number.

The standard deviation $\sigma$ of positive peaks values $P^+$ in $\tilde{v}(x)$ is then used as a unique statistical feature that is given by

$$\sigma = \sqrt{\frac{1}{T}\sum_{t=1}^{T}(P^+(t) - \mu P^+)} \tag{7.3}$$

where $\mu P^+$ is the mean value and $T$ represents the length of $P^+$ vector.

## 7.3 Speed-Up Robust Feature Matching

The proposed recognition system aims at developing a painless and zero stress method for individual recognition of zebrafish as shown in block diagram of Figure 7.5. However, application of this technique to fish identification has not been explored in literature yet. The recognition method in this study is based on point matching of the SURF features as described earlier in Chapter 2. A (moderately) high-resolution web camera ($1080 \times 720$) pixels is used in this study for image capturing in two phases:

1. Building a reference feature database
2. Individual identification

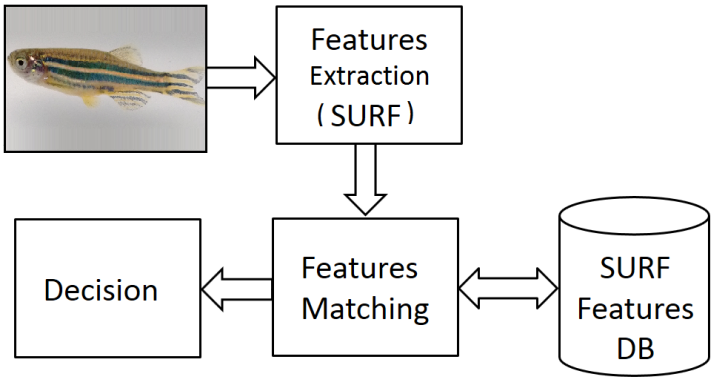


FIGURE 7.5: Block diagram of the proposed system

In this study, a reference feature database of 300 images are built and used for feature matching. The collected raw image for each fish is augmented to 50 images. Reference key points (i.e. features) of each fish-class are initially extracted and saved in the database. For each input image of the fish under test, key points are then extracted and compared to reference key points. If a feature match within a prespecified threshold exists, the system identifies the fish under test. Otherwise, the system displays unmatched status, thus the fish under test is considered unknown and should be enrolled/registered in the reference database.

This matching threshold is a percentage ratio of the total matched features of both the reference and processed images to the total number of key points that are stored in the reference database ($DB$).

The proposed fish recognition approach consists of two main phases; namely feature extraction phase and matching phase. As illustrated in Figure 7.5, the proposed system begins with the feature extraction in which the collected number of points of interest (features) is used as reference in the next matching stage. These two stages are described briefly as follows.

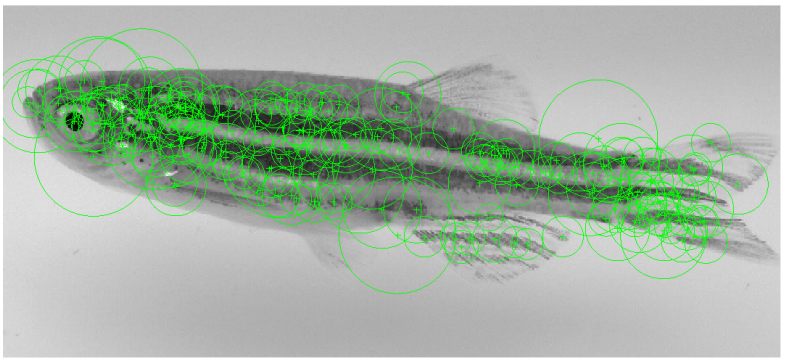

FIGURE 7.6: Example of feature extraction (187 SURF features for Fish 1)

### 7.3.1 Feature extraction

The key points are first extracted from images of all the fish used in this study. This leads to obtaining 70 to 190 key points per fish, depending on the quality and clarity of the acquired image. Next, the extracted key points are used to compute SURF feature vectors for each of the collected images. The feature vectors represent a unique identifying signature for each fish. This is justified by the fact that the total number and positions of the extracted key points are different in each fish image. An example which demonstrate the feature extraction process based on SURF is shown in Figure 7.6. In this example, a total of 187 key points were extracted for one of the fish (labelled Fish 1) used in this study.

### 7.3.2 Feature matching

The matching process between the computed features of the current image and corresponding features that are stored in the reference are performed at this stage. Now, defining $S$ and $F$ as vector arrays for key-points of the reference and query

(test) key points respectively. These arrays are given by

$$S = \{s_1,\ s_2,\ s_3,\ ...,\ s_m\} \tag{7.4}$$

$$F = \{f_1,\ f_2,\ f_3,\ ...,\ f_n\} \tag{7.5}$$

where $s_i$ and $f_j$ are the feature vectors of key point i in $S$ and that of key point $j$ in $F$ respectively. The biggest ration of matching pairs between two images the greater similarity between those images. Mathematically, the matching conditions are given by

$$N_i = \left\{ \begin{array}{ll} 1 & \rho \geqslant \delta \geqslant \gamma \\ 0 & else \end{array} \right\} \tag{7.6}$$

where $N_i$ represents condition of the matched pairs of key points and features vectors of $F$ and $S$, $\rho$ and $\gamma$ are the predefined threshold band to achieve high recognition accuracy and, $\delta$ represents the pre-specified threshold percentage. For each tested image, the percentage accuracy $Acc$ is then calculated by

$$Acc = \frac{Total\ number\ of\ the\ matched\ pairs\ keypoints}{Total\ number\ of\ the\ keypoints\ in reference\ image} \times 100\% \tag{7.7}$$

A set of reference features database of 300 images is used to assess the performance of the proposed method by obtaining the relationship between the average accuracy percentage of recognition versus the prespecified percentage threshold as will be described in next section.

## 7.4 Results and discussion

### 7.4.1 Colour space feature extraction

The differences in the whole shape and size of the object are used as main features in many fish species discrimination approaches and systems. However, these features will not be effective to recognise objects which have a similar shape and size as well as colour. The proposed method attempts to address this problem. By using the blue stripes pattern distribution on the central side of fish image, a unique identifier is extracted. Additionally, the location of these strips is found to be critical in obtaining clear sub-image sets. It is therefore taken into account in the design of proposed vision system.

In this study, a set of several individual fish is considered. Images of the subjects used in this study are handled through applying the sequential steps of the methodology described earlier in Section 2. The results demonstrated steps of the feature extraction for a single fish that are applied to the clustered blue-pattern image. These steps as illustrated in Figure 7.7 include:

- Distribution of pixels summation
- Peaks detection
- Peaks distribution

The former step which essentially a pre-filtering step is applied to the distribution vector $(x)$ to obtain smoothed pixels distribution $v(x)$ vector, as shown in Figure 7.7.

In Figure 7.8, the positive-peaks ($P^+$) represents a new trend for $v(x)$distribution. These data processing steps allows for extracting a new discrimination feature for fish using standard deviation, as illustrated in Figure 7.9. Such an important finding demonstrates validity of the proposed approach towards discriminating individual fish via machine vision, which is compared, favorably to the existing painful and stressful physical tagging methods.

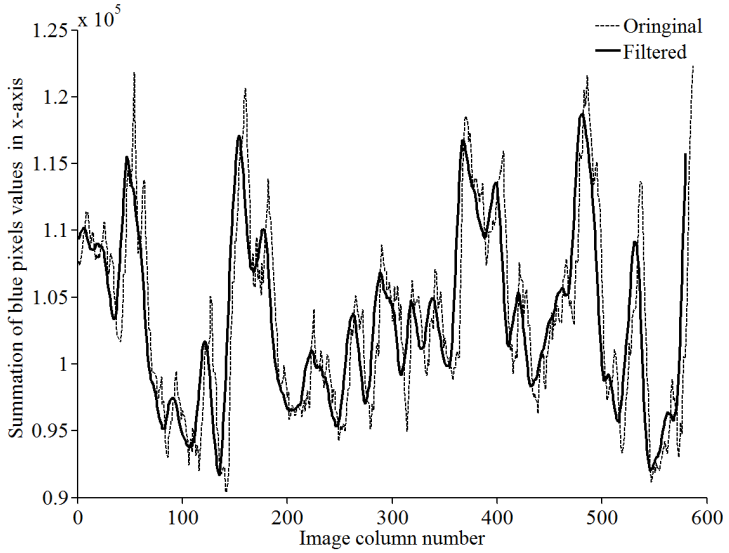


FIGURE 7.7: Distribution of pixels summation

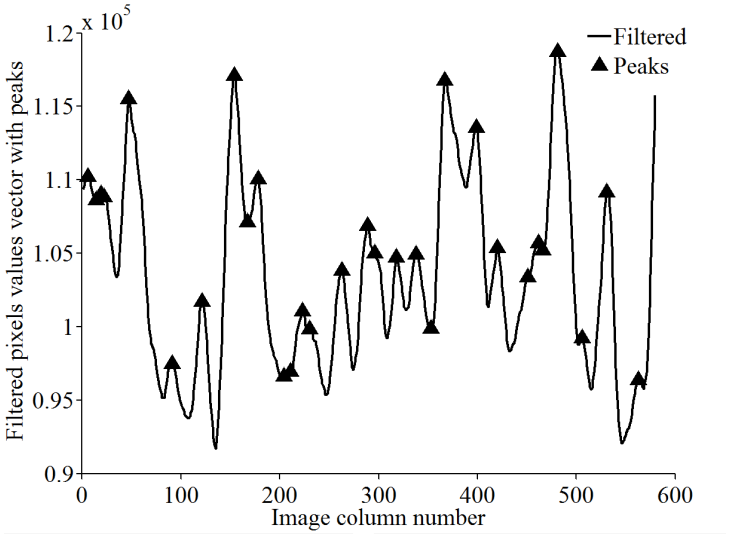


FIGURE 7.8: Peaks detection and distribution

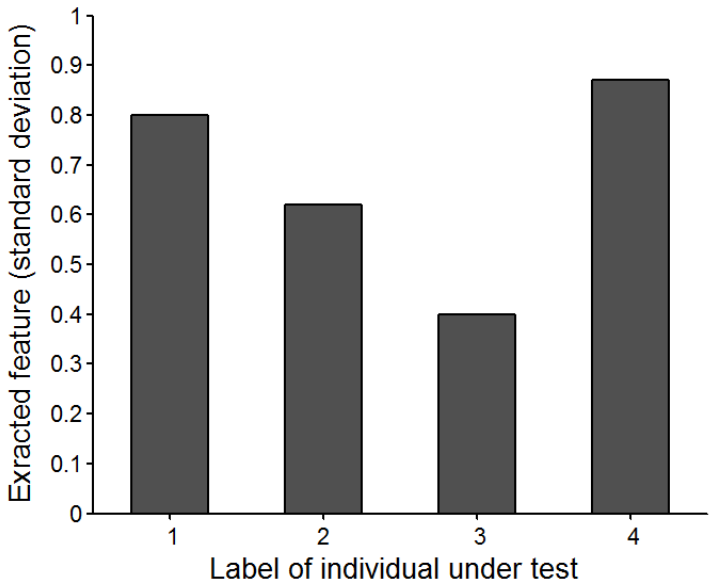


FIGURE 7.9: Extracted feature for four individual fish

### 7.4.2 Speed-up robust feature matching

Examples for different key point matching scenarios are shown in Figure 7.10. In Figure 7.10(a), 187 key points are matched (i.e. 100%) while in Figure 7.10(b) and in Figure 7.10(c) only partial key points are matched; 57 (30%) and 9 (5%) key points matching, respectively. However, depending on the threshold set which is 16% percent in this case, the image of Figure 7.10(b)is considered successfully matched while the image of Figure 7.10(c) is unmatched.

Figure 7.11 demonstrate the recognition accuracy of the developed system versus the matching threshold ($\delta$). It can be noticed that maximum recognition accuracy can be obtained through proper setting of the key points matching threshold that should be selected within the boundaries ($\rho$ and $\gamma$) as defined earlier in Eq. 7.6. In the current study, an accuracy of approximately 90% is obtained with a threshold value, $\delta = 16\%$ . However, an acceptable recognition accuracy can be obtained when the threshold is set to be around this value.

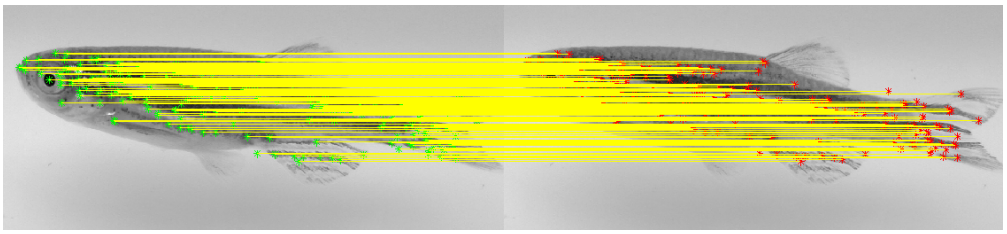

(a) Features matching for same fish images (Full successful matching)

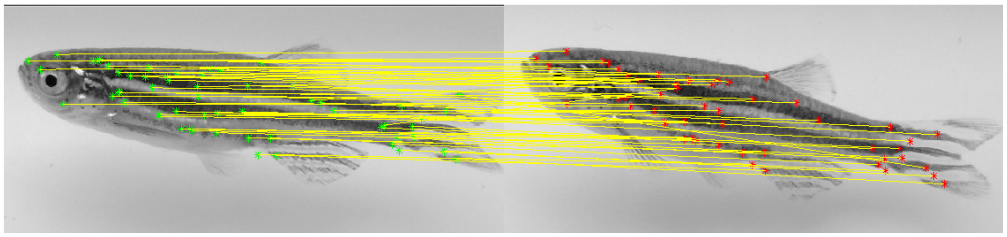

(b) Features matching for same fish but different image (Partial successful matching)

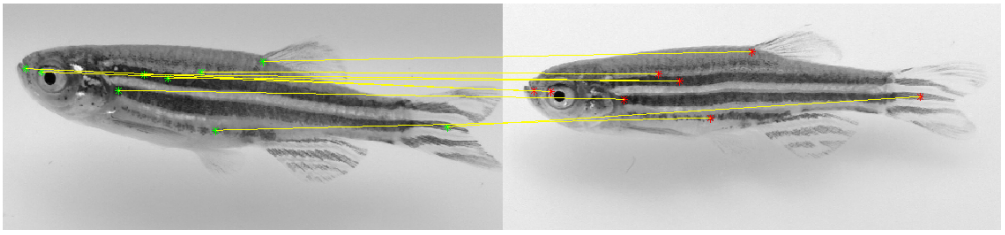

(c) Features matching for different fish (Partial unsuccessful matching)

FIGURE 7.10: Examples of key points matching for same and different fish

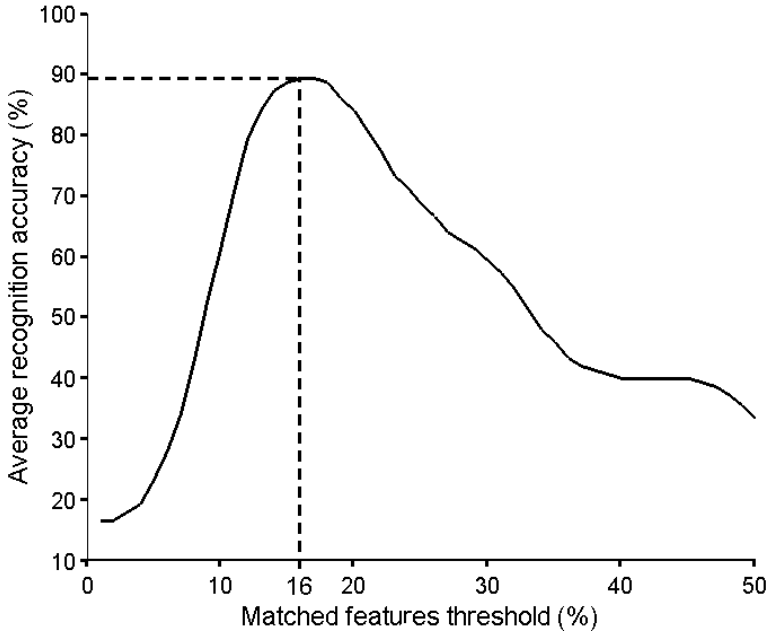


FIGURE 7.11: Average accuracy of recognition versus matching features threshold (%)

Despite that recognition of individual adult zebrafish using colour space feature extraction method provided higher recognition accuracy than SURF, it was found prone to recognition error due its complex pre-processing requirement and highly affected by body orientation of the subject under test. In contrast, the SURF method overcomes these limitations and provides a promising potential for real time recognition for zebrafish individuals.

## 7.5 Conclusions

Novel computer vision methods for the individual adults zebrafish recognition have been developed and implemented successfully. The results of both approaches have been demonstrated the capability of being a viable real-time alternative to the traditional physical tagging in terms of a significant reduction of experts efforts and improvement of animal welfare by using non-contact recognition methods. The methods also can easily be extended and applied to recognise other fish species or other organisms under similar experimental conditions.

# Chapter 8

# Conclusions and Future Work

## 8.1 Conclusions

This project is the result of extensive multidisciplinary work. It proposed a set of successfully implemented behaviour analysis, sizing and recognition systems based on computer vision which has been used in various research areas and industrial applications. The importance of this work is in novelty of the proposed system, the merge of two different fields to solve common problems, and the impact of this work on provides solutions to important challenges using various image/video analysis techniques. The main conclusions generated from the work presented in this thesis can be summarized as follows.

1. The developed platform for physical activity monitoring opens the door for a better understanding of the behaviour of zebrafish larvae when they are exposed to different types of painful stimulation; electrical, chemical and thermal. Impact of the developed platform in zebrafish larvae behavioural

analysis is reflected throughout publication of novel articles in this field as well as its current utilization as an efficient tool for the biologist at the University of Liverpool. This will not only used for painful stimulation experiments but also for other types studies including fear and stress.

The utilization of the platform have also led to developing a novel larvae behavioural analysis. The method is capable to assess the effect of voltage intensity on the larvae response as a group in terms of occurrence of the larvae in the outer zones in the arena. This in turn has opened the door to further investigate the larvae pain perception when expose to electrical stimulation experiment.

2. A non-destructive cost-effective and easy to use computer vision systems using orthogonal and stereo cameras setup have been proposed and implemented successfully for length estimation of small fish. Mathematical models for both vision systems have been derived and implemented.

   Both models incorporate auto-calibration feature where the image pixels are mapped to metric dimensions and accounts for variable camera subject and subject orientation throughout its free swimming activity in the test tank. The obtained results clearly demonstrated validity of the developed models which is reflected by accurate estimation of small-fish length. However, the stereo vision system is found to be more practical in terms of complexity of the system setup and required space for the experimentation. Furthermore, the high correlation of tracking parameters between both proposed systems demonstrate not only the accuracy of detection also forms a solid foundation for 3D tracking and behavior analysis of such small animals. These developments are expected to improve knowledge and facilitate further studies on growth, food optimization, and welfare of small fish, in particular, zebrafish.

3. New fish recognition methods for individual adult zebrafish recognition have been proposed and implemented successfully using L*a*b* colour space feature extraction and speed-up robust feature matching techniques. The performance of the proposed tagging methods is assessed experimentally using six free-swimming zebrafish. The obtained results demonstrated that developed methods can be considered as a promising fingerprint for zebrafish individual recognition.

## 8.2 Future Work

The original contributions and developments reported in this thesis are still open for further studies and improvement. Potential areas of extensions can be summarized as follows.

1. The suggested object tracking algorithm can be further improved through: (i) using real-time tracking rather than using a per-recorded video clips to recognize and classify various behavioral patterns for the subjects under test and (ii) investigating the instant impact of voltage intensity level on the behaviour of each subject under test in order to gain more insight on the fish response to this kind of stimulation.

2. The developed vision systems for fish-sizing estimation can also be further improved through conducting (i) multi-fish tracking and behavioural analysis, (ii) 3D fish-body reconstruction through detection of both the front and longitudinal cross-section areas of the fish body, and (iii) adopting the image feature matching approach, which was applied in this thesis for fish recognition, as a tagging tool for fish-sizing that is still a standing challenge for multi-fish.

3. Finally, possible avenues for further improvement of fish-recognition can be achieved through combining the proposed new feature set along with other known features such as visual texture. The nature of the processing involved, and the speed at which the computation can be executed lends these approach to modularisation and deployment using hand-held computing platforms. For example, such systems could be incorporated into a smartphone app that could potentially identify fish in real time using the built-in phone camera. Alternatively, a stand-alone Raspberry Pi system could be developed at an even lower cost to constantly monitor the fish in a tank, and provide real-time monitoring data such as size, feeding patterns and swimming behaviour. Combining fish size and individual recognition allows growth profiles and behavioural trends to be monitored over time for individual fish, and can be of tremendous value in a commercial fish farm or in an aquaculture research laboratory setting.

# Bibliography

[1] Rupert J Egan, Carisa L Bergner, Peter C Hart, Jonathan M Cachat, Peter R Canavello, Marco F Elegante, Salem I Elkhayat, Brett K Bartels, Anna K Tien, David H Tien, et al. Understanding behavioral and physiological phenotypes of stress and anxiety in zebrafish. *Behavioural brain research*, 205(1):38–44, 2009.

[2] Liqun Zhu and Wei Weng. Catadioptric stereo-vision system for the real-time monitoring of 3d behavior in aquatic animals. *Physiology & behavior*, 91(1):106–119, 2007.

[3] Chiranjib Chakraborty, Chi H Hsu, Zhi Hong Wen, Chang Shing Lin, and Govindasamy Agoramoorthy. Zebrafish: a complete animal model for in vivo drug discovery and development. *Current drug metabolism*, 10(2):116–124, 2009.

[4] Boaz Zion. The use of computer vision technologies in aquaculture–a review. *Computers and electronics in agriculture*, 88:125–132, 2012.

[5] Ingrid Torjesen. Number of animals used in science increased slightly in 2013, home office reports. *BMJ: British Medical Journal*, 349, 2014.

[6] Lynne U Sneddon. The evidence for pain in fish: the use of morphine as an analgesic. *Applied Animal Behaviour Science*, 83(2):153–162, 2003.

[7] Siobhan C Reilly, John P Quinn, Andrew R Cossins, and Lynne U Sneddon. Behavioural analysis of a nociceptive event in fish: Comparisons between three species demonstrate specific responses. *Applied Animal Behaviour Science*, 114(1):248–259, 2008.

[8] I Karplus, M Gottdiener, and B Zion. Guidance of single guppies (poecilia reticulata) to allow sorting by computer vision. *Aquacultural engineering*, 27(3):177–190, 2003.

[9] I Karplus, V Alchanatis, and B Zion. Guidance of groups of guppies (poecilia reticulata) to allow sorting by computer vision. *Aquacultural engineering*, 32(3):509–520, 2005.

[10] Anthony J Siccardi III, Heath W Garris, Warren T Jones, Dorothy B Moseley, Louis R D'Abramo, and Stephen A Watts. Growth and survival of zebrafish (danio rerio) fed different commercial and laboratory diets. *Zebrafish*, 6(3):275–280, 2009.

[11] Vassilis M Papadakis, Ioannis E Papadakis, Fani Lamprianidou, Alexios Glaropoulos, and Maroudio Kentouri. A computer-vision system and methodology for the analysis of fish behavior. *Aquacultural engineering*, 46:53–59, 2012.

[12] Qussay Al-Jubouri, Waleed Al-Nuaimy, Majid A Al-Taee, Javier L Luna, and Lynne U Sneddon. Automated electrical stimulation and physical activity monitoring of zebrafish larvae. In *Applied Electrical Engineering and*

*Computing Technologies (AEECT), 2015 IEEE Jordan Conference on*, pages 1–6. IEEE, 2015.

[13] Toni A Beddow, Lindsay G Ross, and John A Marchant. Predicting salmon biomass remotely using a digital stereo-imaging technique. *Aquaculture*, 146(3):189–203, 1996.

[14] JA Lines, RD Tillett, LG Ross, D Chan, S Hockaday, and NJB McFarlane. An automatic image-based system for estimating the mass of free-swimming fish. *Computers and Electronics in Agriculture*, 31(2):151–168, 2001.

[15] Sachit Butail and Derek A Paley. Three-dimensional reconstruction of the fast-start swimming kinematics of densely schooling fish. *Journal of the Royal Society Interface*, 9(66):77–88, 2012.

[16] BP Ruff, JA Marchant, and AR Frost. Fish sizing and monitoring using a stereo image analysis system applied to fish farming. *Aquacultural engineering*, 14(2):155–173, 1995.

[17] DJ White, C Svellingen, and NJC Strachan. Automated measurement of species and length of fish by computer vision. *Fisheries Research*, 80(2):203–210, 2006.

[18] Javier Lopez-Luna, Qussay Al-Jubouri, Waleed Al-Nuaimy, and Lynne U Sneddon. Impact of analgesic drugs on the behavioural responses of larval zebrafish to potentially noxious temperatures. *Applied Animal Behaviour Science*, 2017.

[19] Javier Lopez-Luna, Martin N Canty, Qussay Al-Jubouri, Waleed Al-Nuaimy, and Lynne U Sneddon. Behavioural responses of fish larvae modulated by

analgesic drugs after a stress exposure. *Applied Animal Behaviour Science*, 2017.

[20] Javier Lopez-Luna, Qussay Al-Jubouri, Waleed Al-Nuaimy, and Lynne U Sneddon. Reduction in activity by noxious chemical stimulation is ameliorated by immersion in analgesic drugs in zebrafish. *Journal of Experimental Biology*, 220(8):1451–1458, 2017.

[21] Marcos A López-Patiño, Lili Yu, Howard Cabral, and Irina V Zhdanova. Anxiogenic effects of cocaine withdrawal in zebrafish. *Physiology & behavior*, 93(1):160–171, 2008.

[22] Caio Maximino, Annanda Waneza Batista da Silva, Juliana Araújo, Monica Gomes Lima, Vanessa Miranda, Bruna Puty, Rances Benzecry, Domingos Luiz Wanderley Picanço-Diniz, Amauri Gouveia Jr, Karen Renata Matos Oliveira, et al. Fingerprinting of psychoactive drugs in zebrafish anxiety-like behaviors. *PloS one*, 9(7):e103943, 2014.

[23] Lee D Ellis, Evelyn C Soo, John C Achenbach, Michael G Morash, and Kelly H Soanes. Use of the zebrafish larvae as a model to study cigarette smoke condensate toxicity. *PLoS One*, 9(12):e115305, 2014.

[24] S Padilla, DL Hunter, B Padnos, S Frady, and RC MacPhail. Assessing locomotor activity in larval zebrafish: Influence of extrinsic and intrinsic variables. *Neurotoxicology and teratology*, 33(6):624–630, 2011.

[25] TD Irons, RC MacPhail, DL Hunter, and S Padilla. Acute neuroactive drug exposures alter locomotor activity in larval zebrafish. *Neurotoxicology and teratology*, 32(1):84–90, 2010.

[26] Uwe Strähle, Stefan Scholz, Robert Geisler, Petra Greiner, Henner Hollert, Sepand Rastegar, Axel Schumacher, Ingrid Selderslaghs, Carsten Weiss, Hilda Witters, et al. Zebrafish embryos as an alternative to animal experimentsa commentary on the definition of the onset of protected life stages in animal welfare regulations. *Reproductive Toxicology*, 33(2):128–132, 2012.

[27] Adrian J Hill, Tisha C King Heiden, Warren Heideman, and Richard E Peterson. Potential roles of arnt2 in zebrafish larval development. *Zebrafish*, 6(1):79–91, 2009.

[28] Sean D Pelkowski, Mrinal Kapoor, Holly A Richendrfer, Xingyue Wang, Ruth M Colwill, and Robbert Creton. A novel high-throughput imaging system for automated analyses of avoidance behavior in zebrafish larvae. *Behavioural brain research*, 223(1):135–144, 2011.

[29] Pascal I Bang, Pamela C Yelick, Jarema J Malicki, and William F Sewell. High-throughput behavioral screening method for detecting auditory response defects in zebrafish. *Journal of neuroscience methods*, 118(2):177–187, 2002.

[30] Robbert Creton. Automated analysis of behavior in zebrafish larvae. *Behavioural brain research*, 203(1):127–136, 2009.

[31] Sara M Lindsay and Richard G Vogt. Behavioral responses of newly hatched zebrafish (danio rerio) to amino acid chemostimulants. *Chemical Senses*, 29(2):93–100, 2004.

[32] Yohaan Fernandes and Robert Gerlai. Long-term behavioral changes in response to early developmental exposure to ethanol in zebrafish. *Alcoholism: Clinical and Experimental Research*, 33(4):601–609, 2009.

[33] Clinton L Cario, Thomas C Farrell, Chiara Milanese, and Edward A Burton. Automated measurement of zebrafish larval movement. *The Journal of physiology*, 589(15):3703–3708, 2011.

[34] Yangzhong Zhou, Richard T Cattley, Clinton L Cario, Qing Bai, and Edward A Burton. Quantification of larval zebrafish motor function in multi-well plates using open-source matlab® applications. *Nature protocols*, 9(7):1533, 2014.

[35] NBT. Zebrafish Larvae Activity Monitoring. `http://www.nbtltd.com/products/zebrafish-larvae-activity-monitoring/`, 2015. [Online; accessed 10th September 2015].

[36] NBT. Viewpoint Behavior Technology. `http://www.viewpoint.fr/en/p/equipment/zebrabox/`, 2015. [Online; accessed 24th September 2015].

[37] Actual Analytics. Actual Track for Fish Larvae. `http://www.actualanalytics.com/actualtrack/fish/larvae/`, 2015. [Online; accessed 24th September 2015].

[38] loligo Systems. `http://www.loligosystems.com/`, 2015. [Online; accessed 28th September 2015].

[39] Euan Harvey, Mike Cappo, Mark Shortis, Stuart Robson, Jeff Buchanan, and Peter Speare. The accuracy and precision of underwater measurements of length and maximum body depth of southern bluefin tuna (thunnus maccoyii) with a stereo–video camera system. *Fisheries Research*, 63(3):315–326, 2003.

[40] Ching-Lu Hsieh, Hsiang-Yun Chang, Fei-Hung Chen, Jhao-Huei Liou, Shui-Kai Chang, and Ta-Te Lin. A simple and effective digital imaging

approach for tuna fish length measurement compatible with fishing operations. *Computers and Electronics in Agriculture*, 75(1):44–51, 2011.

[41] Francesca Odone, Emanuele Trucco, and Alessandro Verri. A trainable system for grading fish from images. *Applied Artificial Intelligence*, 15(8):735–745, 2001.

[42] JR Martinez-de Dios, C Serna, and A Ollero. Computer vision and robotics techniques in fish farms. *Robotica*, 21(3):233–243, 2003.

[43] C Costa, A Loy, S Cataudella, D Davis, and M Scardi. Extracting fish size using dual underwater cameras. *Aquacultural Engineering*, 35(3):218–227, 2006.

[44] Shinsuke Torisawa, Minoru Kadota, Kazuyoshi Komeyama, Katsuya Suzuki, and Tsutomu Takagi. A digital stereo-video camera system for three-dimensional monitoring of free-swimming pacific bluefin tuna, thunnus orientalis, cultured in a net cage. *Aquatic Living Resources*, 24(2):107–112, 2011.

[45] Boaz Zion, Victor Alchanatis, Viacheslav Ostrovsky, Assaf Barki, and Ilan Karplus. Real-time underwater sorting of edible fish species. *Computers and electronics in agriculture*, 56(1):34–45, 2007.

[46] Corrado Costa, Michele Scardi, Valerio Vitalini, and Stefano Cataudella. A dual camera system for counting and sizing northern bluefin tuna (thunnus thynnus; linnaeus, 1758) stock, during transfer to aquaculture cages, with a semi automatic artificial neural network tool. *Aquaculture*, 291(3):161–167, 2009.

[47] Kresimir Williams, Christopher N Rooper, and Rick Towler. Use of stereo camera systems for assessment of rockfish abundance in untrawlable areas and for recording pollock behavior during midwater trawls. *Fishery Bulletin*, 108(3):352–362, 2010.

[48] B Zion, V Alchanatis, V Ostrovsky, A Barki, and I Karplus. Classification of guppies(poecilia reticulata) gender by computer vision. *Aquacultural engineering*, 38(2):97–104, 2008.

[49] Austin A Rizzo, Stuart A Welsh, and Patricia A Thompson. A paired-laser photogrammetric method for in situ length measurement of benthic fishes. *North American Journal of Fisheries Management*, 37(1):16–22, 2017.

[50] Etienne Baras, Christelle Malbrouck, Marc Houbart, Patrick Kestemont, and Charles Mélard. The effect of pit tags on growth and physiology of age-0 cultured eurasian perch¡ i¿ perca fluviatilis¡/i¿ of variable size. *Aquaculture*, 185(1):159–173, 2000.

[51] Xavier Cousin, Tarek Daouk, Samuel Pan, Laura Lyphout, Marie-Elise Schwartz, and Marie-Laure Bégout. Electronic individual identification of zebrafish using radio frequency identification (rfid) microtags. *The Journal of experimental biology*, 215(16):2729–2734, 2012.

[52] Jessica S Blackburn, Sali Liu, Aubrey R Raimondi, Myron S Ignatius, Christopher D Salthouse, and David M Langenau. High-throughput imaging of adult fluorescent zebrafish with an led fluorescence macroscope. *Nature protocols*, 6(2):229–241, 2011.

[53] Katherine Leon, Domingo Mery, Franco Pedreschi, and Jorge Leon. Color measurement in l a b units from rgb digital images. *Food research international*, 39(10):1084–1091, 2006.

[54] Timothy J Cavanaugh. *Applications of Spectrophotometry for Paleoclimate Interpretations from Lacustrine Sediment Records*. PhD thesis, Middlebury College.

[55] Renato Cordeiro De Amorim and Boris Mirkin. Minkowski metric, feature weighting and anomalous cluster initializing in k-means clustering. *Pattern Recognition*, 45(3):1061–1075, 2012.

[56] Siddheswar Ray and Rose H Turi. Determination of number of clusters in k-means clustering and application in colour image segmentation. In *Proceedings of the 4th international conference on advances in pattern recognition and digital techniques*, pages 137–143. Calcutta, India, 1999.

[57] Herbert Bay, Andreas Ess, Tinne Tuytelaars, and Luc Van Gool. Speeded-up robust features (surf). *Computer vision and image understanding*, 110(3):346–359, 2008.

[58] Geng Du, Fei Su, and Anni Cai. Face recognition using surf features. In *Sixth International Symposium on Multispectral Image Processing and Pattern Recognition*, pages 749628–749628. International Society for Optics and Photonics, 2009.

[59] Rebecca Dunlop and Peter Laming. Mechanoreceptive and nociceptive responses in the central nervous system of goldfish (carassius auratus) and trout (oncorhynchus mykiss). *The journal of pain*, 6(9):561–568, 2005.

[60] Jared R Eckroth, Øyvind Aas-Hansen, Lynne U Sneddon, Helena Bichão, and Kjell B Døving. Physiological and behavioural responses to noxious stimuli in the atlantic cod (gadus morhua). *PloS one*, 9(6):e100150, 2014.

[61] Lynne U Sneddon, Victoria A Braithwaite, and Michael J Gentle. Novel object test: examining nociception and fear in the rainbow trout. *The Journal of Pain*, 4(8):431–440, 2003.

[62] Andrew Curtright, Micaela Rosser, Shamii Goh, Bailey Keown, Erinn Wagner, Jasmine Sharifi, David W Raible, and Ajay Dhaka. Modeling nociception in zebrafish: a way forward for unbiased analgesic discovery. *PloS one*, 10(1):e0116766, 2015.

[63] Monica Gomes Lima, Caio Maximino, Evander de Jesus Oliveira Batista, Karen Renata Matos Oliveira, and Anderson Manoel Herculano. Nocifensive behavior in adult and larval zebrafish. *Zebrafish Protocols for Neurobehavioral Research*, pages 153–166, 2012.

[64] Veronica Gonzalez-Nunez and Raquel E Rodríguez. The zebrafish: a model to study the endogenous mechanisms of pain. *ILAR journal*, 50(4):373–386, 2009.

[65] William Moy Stratton Russell, Rex Leonard Burch, et al. The principles of humane experimental technique. *The principles of humane experimental technique.*, 1959.

[66] Valentina Malafoglia, Marco Colasanti, William Raffaeli, Darius Balciunas, Antonio Giordano, and Gianfranco Bellipanni. Extreme thermal noxious stimuli induce pain responses in zebrafish larvae. *Journal of cellular physiology*, 229(3):300–308, 2014.

[67] Jessica J Mettam, Catherine R McCrohan, and Lynne U Sneddon. Characterisation of chemosensory trigeminal receptors in the rainbow trout, oncorhynchus mykiss: responses to chemical irritants and carbon dioxide. *Journal of Experimental Biology*, 215(4):685–693, 2012.

[68] Jonathan AC Roques, Wout Abbink, Gaétan Chereau, Aurélie Fourneyron, Tom Spanings, Dirk Burggraaf, Ruud van de Bos, Hans van de Vis, and Gert Flik. Physiological and behavioral responses to an electrical stimulus in mozambique tilapia (oreochromis mossambicus). *Fish physiology and biochemistry*, 38(4):1019–1028, 2012.

[69] Christie Ramos Andrade Leite-Panissi, Norberto Cysne Coimbra, and Leda Menescal-de Oliveira. The cholinergic stimulation of the central amygdala modifying the tonic immobility response and antinociception in guinea pigs depends on the ventrolateral periaqueductal gray. *Brain Research Bulletin*, 60(1):167–178, 2003.

[70] Aletheia Lee, Ajay S Mathuru, Cathleen Teh, Caroline Kibat, Vladimir Korzh, Trevor B Penney, and Suresh Jesuthasan. The habenula prevents helpless behavior in larval zebrafish. *Current biology*, 20(24):2211–2216, 2010.

[71] AS Kane, JD Salierno, and SK Brewer. Fish models in behavioral toxicology: automated techniques, updates and perspectives. *Methods in aquatic toxicology*, 2:559–590, 2005.

[72] Christiane Nusslein-Volhard and Ralf Dahm. *Zebrafish*. Oxford University Press, 2002.

[73] Rafael C Gonzalez and Richard E Woods. Digital image processing prentice hall. *Upper Saddle River, NJ*, 2002.

[74] Mark S Nixon and Alberto S Aguado. *Feature extraction & image processing for computer vision*. Academic Press, 2012.

[75] Jonathan Cachat, Adam Stewart, Eli Utterback, Peter Hart, Siddharth Gaikwad, Keith Wong, Evan Kyzar, Nadine Wu, and Allan V Kalueff. Three-dimensional neurophenotyping of adult zebrafish behavior. *PloS one*, 6(3):e17597, 2011.

[76] Jonathan Cachat, Evan J Kyzar, Christopher Collins, Siddharth Gaikwad, Jeremy Green, Andrew Roth, Mohamed El-Ounsi, Ari Davis, Mimi Pham, Samuel Landsman, et al. Unique and potent effects of acute ibogaine on zebrafish: the developing utility of novel aquatic models for hallucinogenic drug research. *Behavioural brain research*, 236:258–269, 2013.

[77] E Alessio, A Carbone, G Castelli, and V Frappietro. Second-order moving average and scaling of stochastic time series. *The European Physical Journal B-Condensed Matter and Complex Systems*, 27(2):197–200, 2002.

# Appendix A:

# IR camera setup

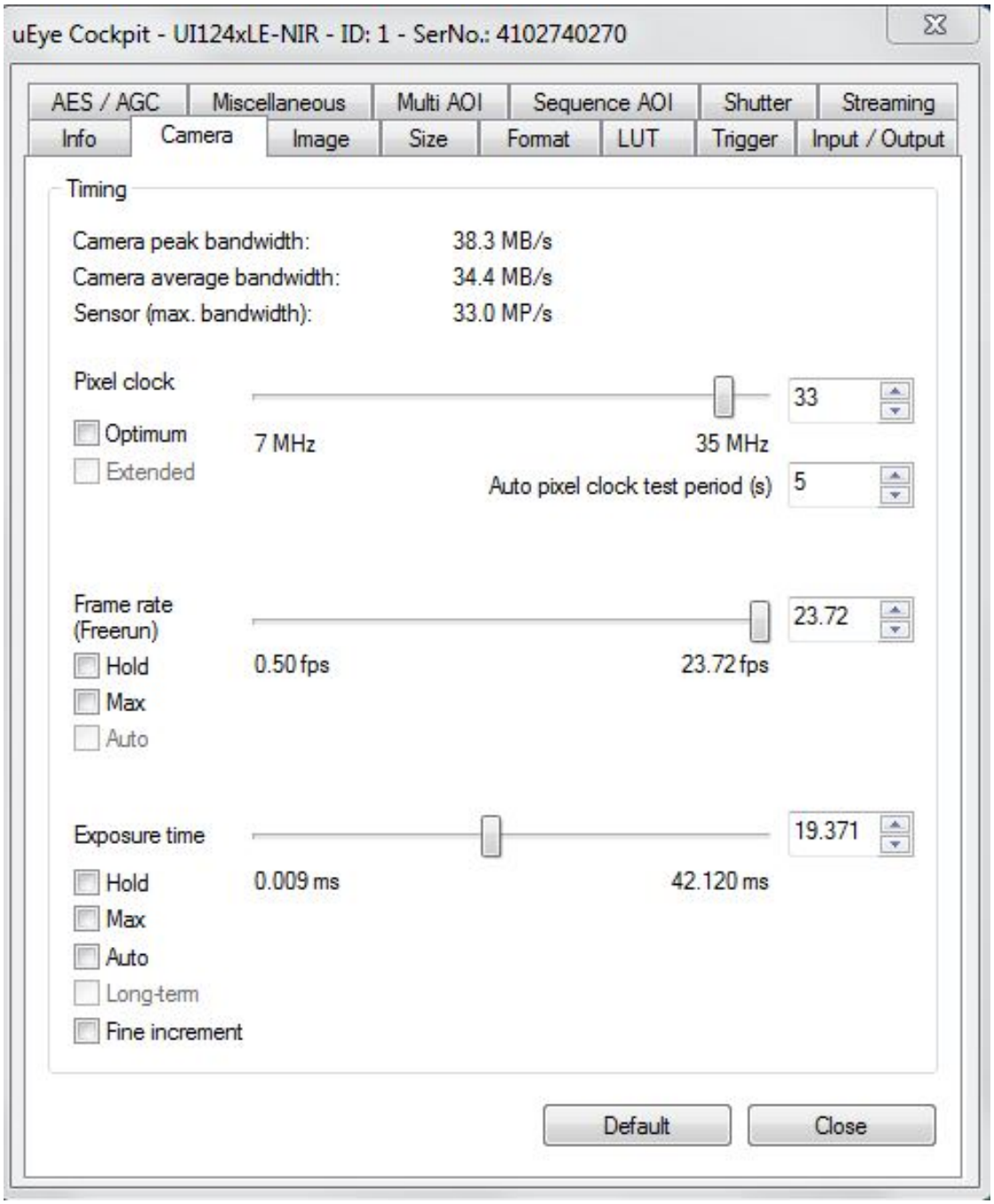
uEye Cockpit - UI124xLE-NIR - ID: 1 - SerNo.: 4102740270
AES / AGC
Miscellaneous
Multi AOI
Sequence AOI
Shutter
Streaming
Info
Camera
Image
Size
Format
LUT
Trigger
Input / Output
Timing
Camera peak bandwidth: 38.3 MB/s
Camera average bandwidth: 34.4 MB/s
Sensor (max. bandwidth): 33.0 MP/s
Pixel clock
33
Optimum
Extended
7 MHz
35 MHz
Auto pixel clock test period (s)
5
Frame rate (Freerun)
23.72
Hold
Max
Auto
0.50 fps
23.72 fps
Exposure time
19.371
Hold
Max
Auto
Long-term
Fine increment
0.009 ms
42.120 ms
Default
Close

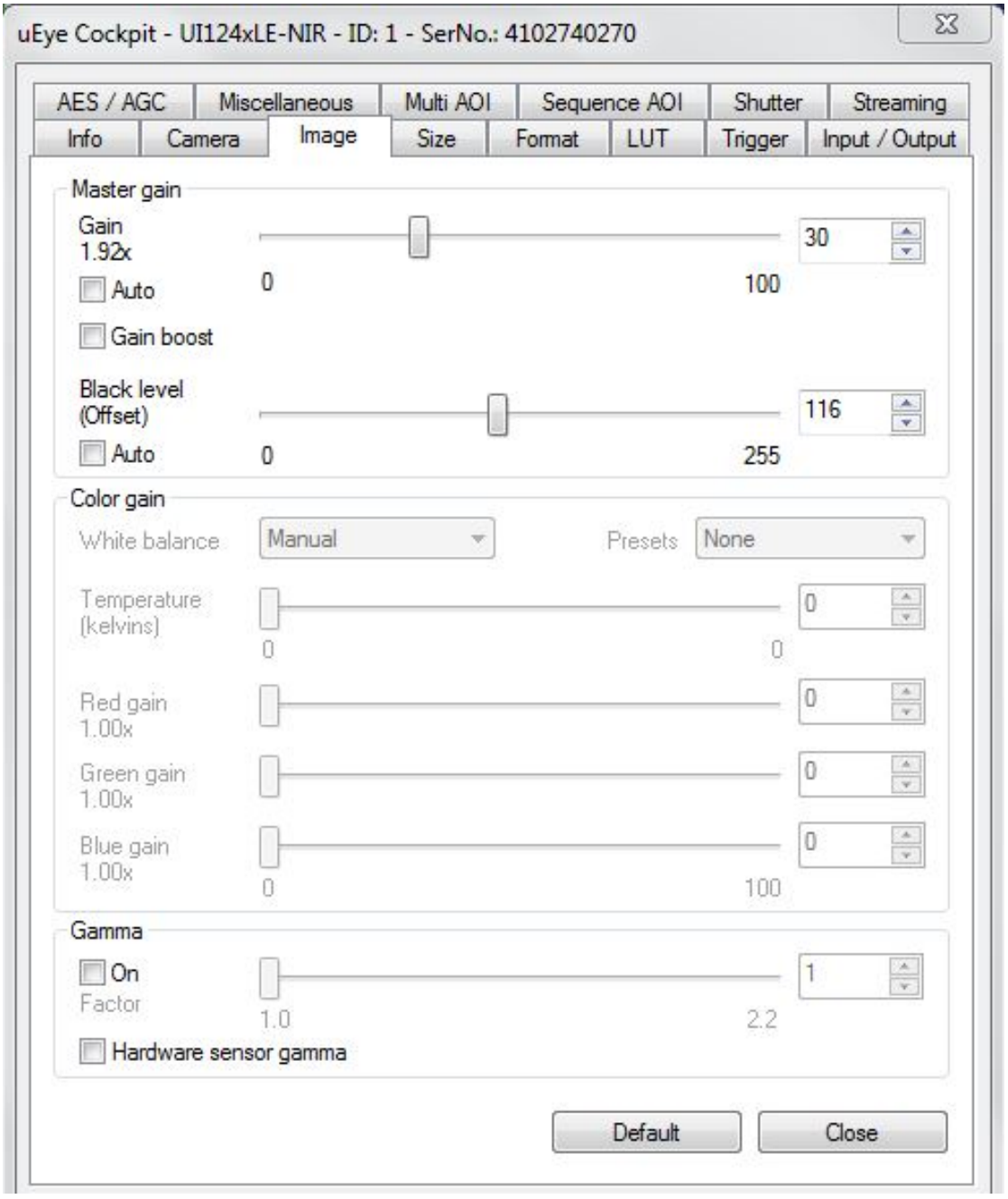
uEye Cockpit - UI124xLE-NIR - ID: 1 - SerNo.: 4102740270
AES / AGC
Miscellaneous
Multi AOI
Sequence AOI
Shutter
Streaming
Info
Camera
Image
Size
Format
LUT
Trigger
Input / Output
Master gain
Gain
1.92x
30
Auto
0
100
Gain boost
Black level
(Offset)
116
Auto
0
255
Color gain
White balance
Manual
Presets
None
Temperature
(kelvins)
0
0
0
Red gain
1.00x
0
Green gain
1.00x
0
Blue gain
1.00x
0
0
100
Gamma
On
1
Factor
1.0
2.2
Hardware sensor gamma
Default
Close

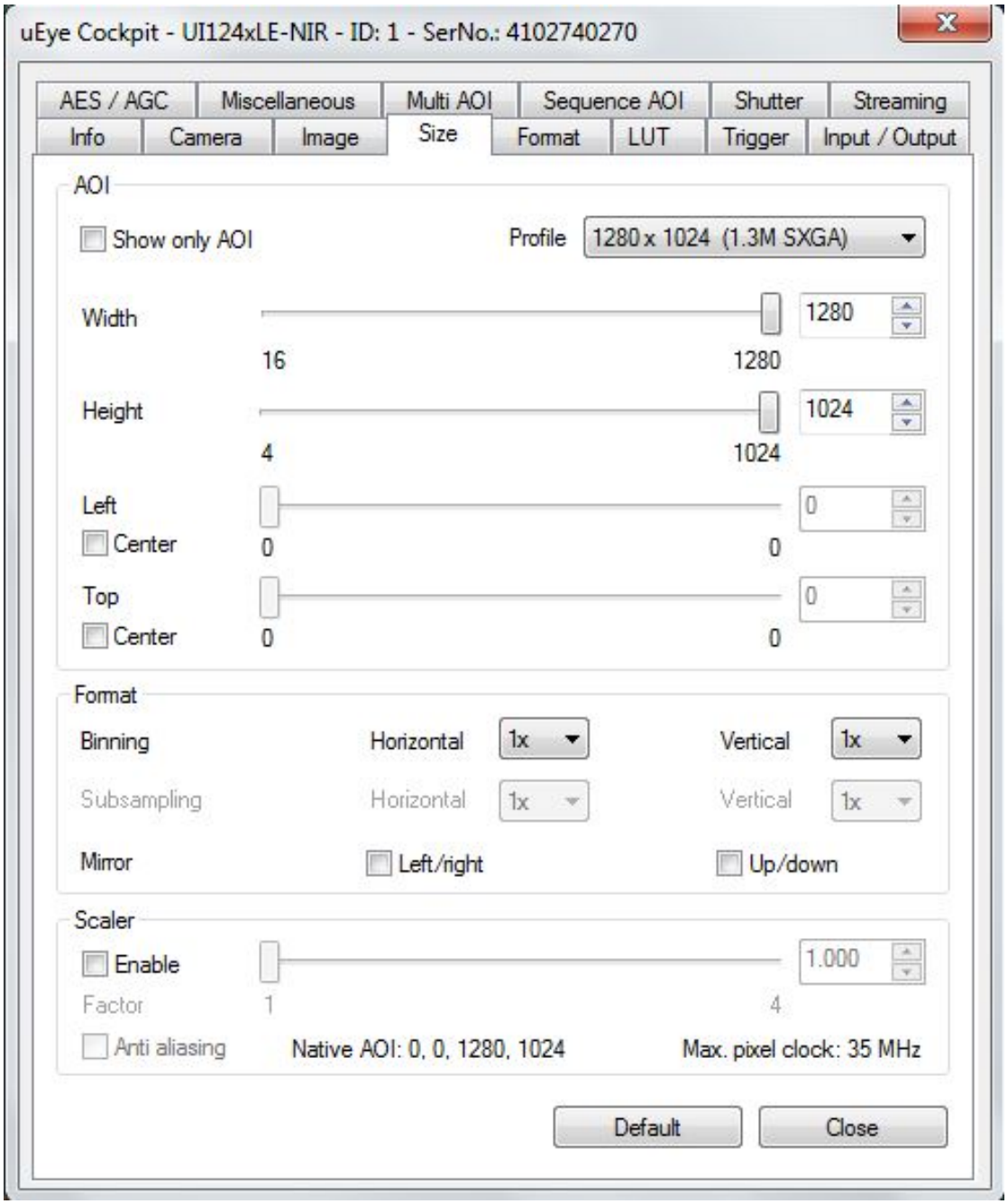
uEye Cockpit - UI124xLE-NIR - ID: 1 - SerNo.: 4102740270
AES / AGC
Miscellaneous
Multi AOI
Sequence AOI
Shutter
Streaming
Info
Camera
Image
Size
Format
LUT
Trigger
Input / Output
AOI
Show only AOI
Profile
1280 x 1024 (1.3M SXGA)
Width
1280
16
1280
Height
1024
4
1024
Left
0
Center
0
0
Top
0
Center
0
0
Format
Binning
Horizontal
1x
Vertical
1x
Subsampling
Horizontal
1x
Vertical
1x
Mirror
Left/right
Up/down
Scaler
Enable
1.000
Factor
1
4
Anti aliasing
Native AOI: 0, 0, 1280, 1024
Max. pixel clock: 35 MHz
Default
Close

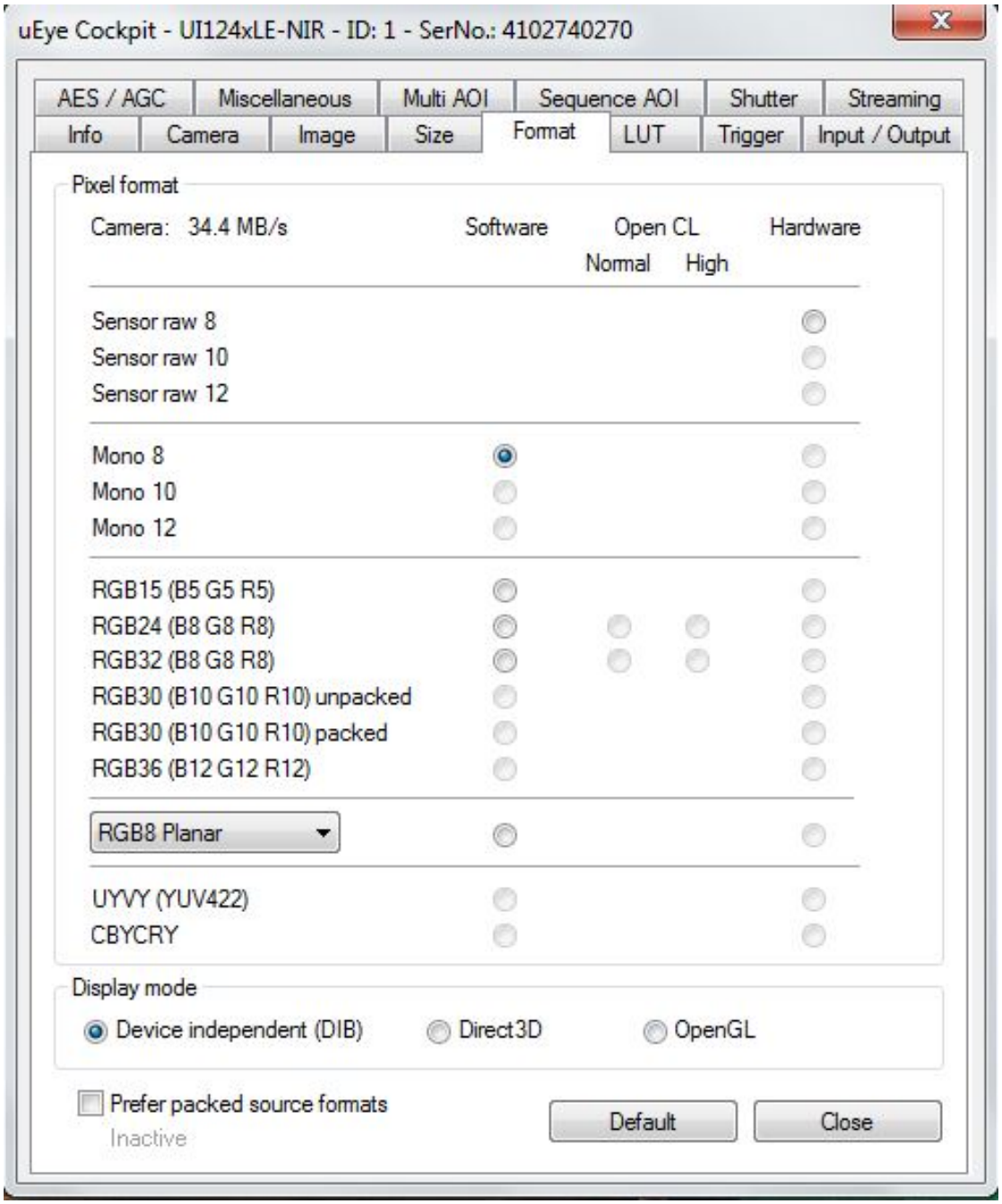
uEye Cockpit - UI124xLE-NIR - ID: 1 - SerNo.: 4102740270
AES / AGC
Miscellaneous
Multi AOI
Sequence AOI
Shutter
Streaming
Info
Camera
Image
Size
Format
LUT
Trigger
Input / Output
Pixel format
Camera: 34.4 MB/s
Software
Open CL
Normal
High
Hardware
Sensor raw 8
Sensor raw 10
Sensor raw 12
Mono 8
Mono 10
Mono 12
RGB15 (B5 G5 R5)
RGB24 (B8 G8 R8)
RGB32 (B8 G8 R8)
RGB30 (B10 G10 R10) unpacked
RGB30 (B10 G10 R10) packed
RGB36 (B12 G12 R12)
RGB8 Planar
UYVY (YUV422)
CBYCRY
Display mode
Device independent (DIB)
Direct3D
OpenGL
Prefer packed source formats
Inactive
Default
Close

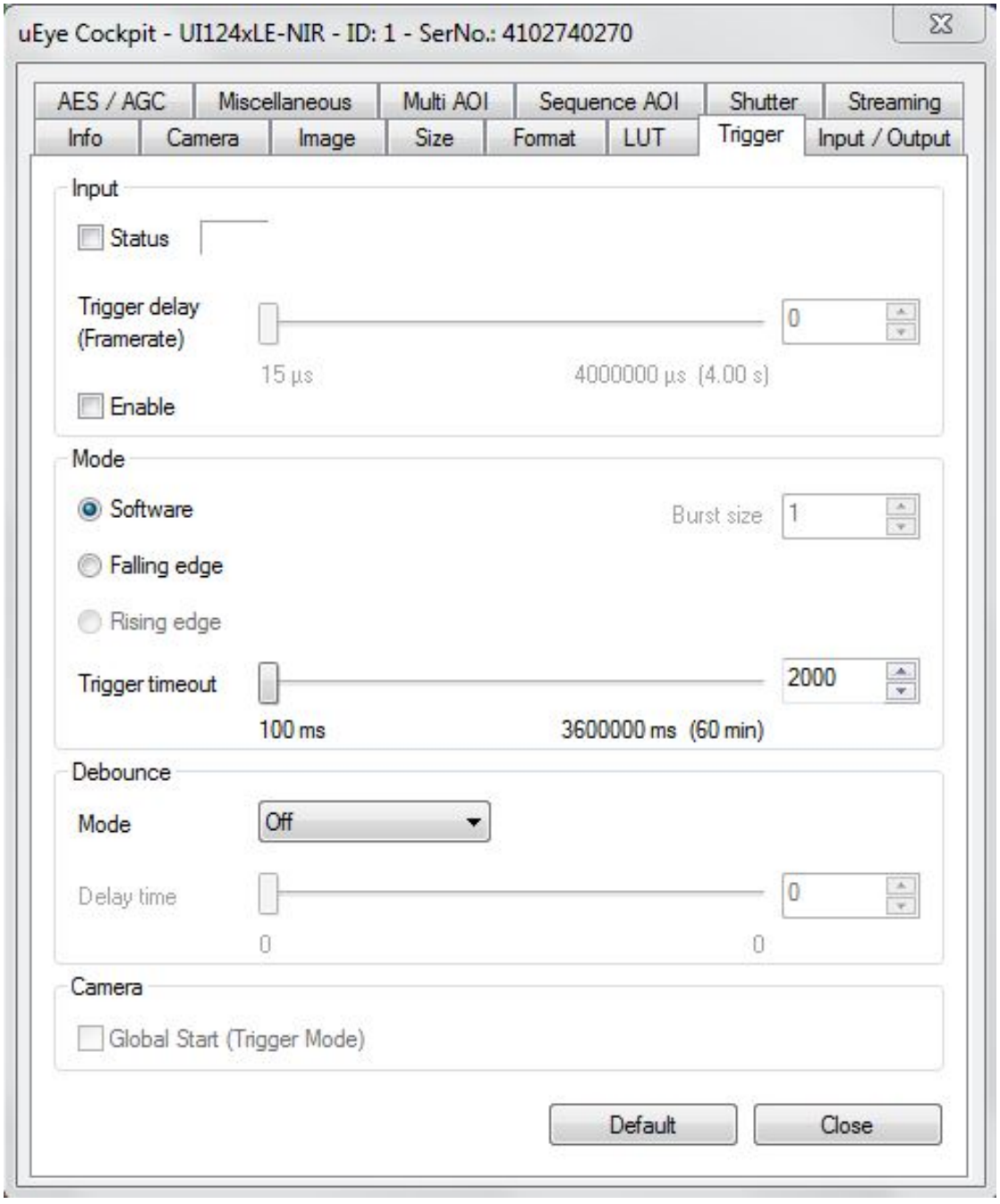
uEye Cockpit - UI124xLE-NIR - ID: 1 - SerNo.: 4102740270
AES / AGC
Miscellaneous
Multi AOI
Sequence AOI
Shutter
Streaming
Info
Camera
Image
Size
Format
LUT
Trigger
Input / Output
Input
Status
Trigger delay (Framerate)
0
15 µs
4000000 µs (4.00 s)
Enable
Mode
Software
Burst size
1
Falling edge
Rising edge
Trigger timeout
2000
100 ms
3600000 ms (60 min)
Debounce
Mode
Off
Delay time
0
0
0
Camera
Global Start (Trigger Mode)
Default
Close

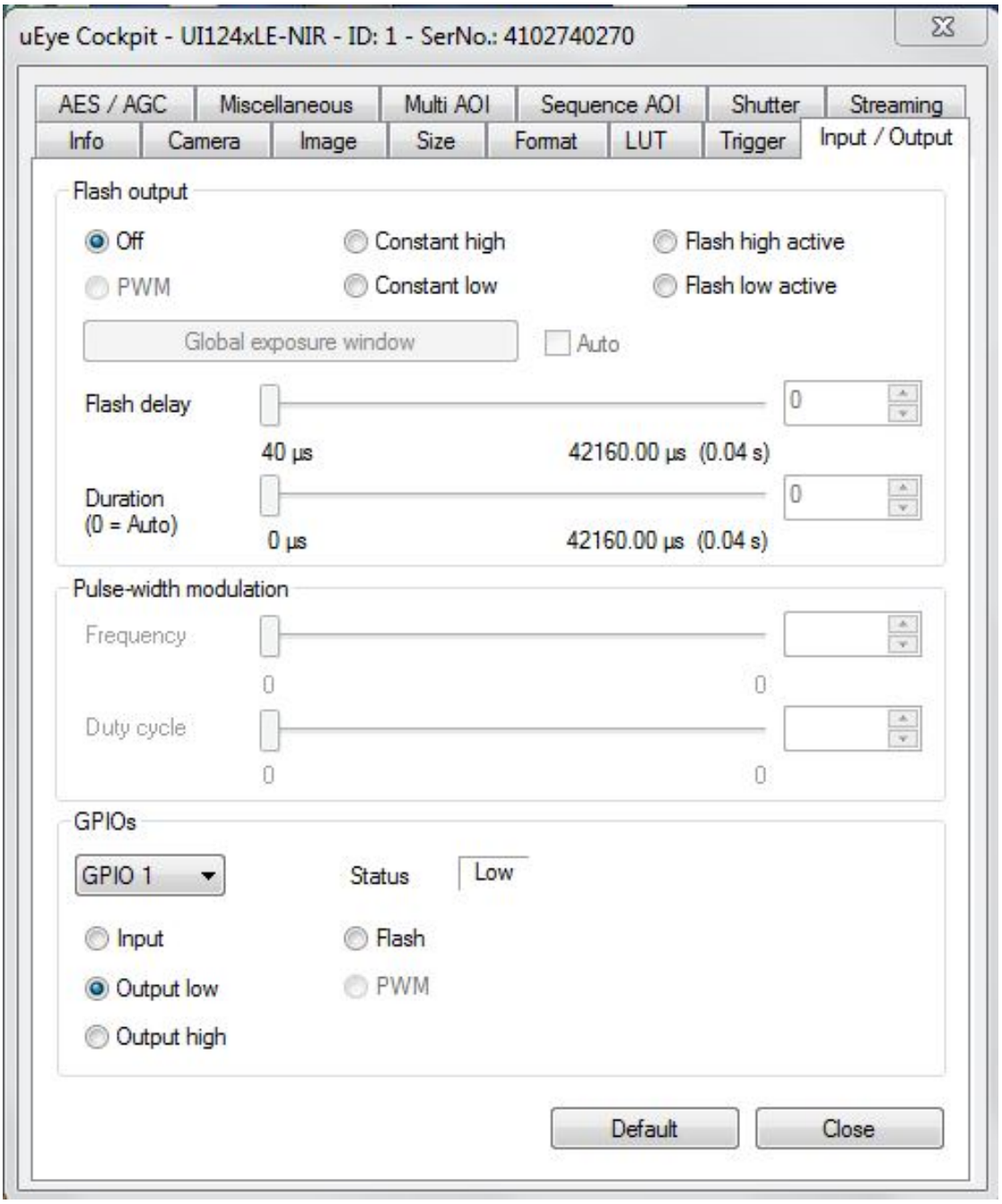
uEye Cockpit - UI124xLE-NIR - ID: 1 - SerNo.: 4102740270
AES / AGC
Miscellaneous
Multi AOI
Sequence AOI
Shutter
Streaming
Info
Camera
Image
Size
Format
LUT
Trigger
Input / Output
Flash output
Off
Constant high
Flash high active
PWM
Constant low
Flash low active
Global exposure window
Auto
Flash delay
0
40 µs
42160.00 µs (0.04 s)
Duration
(0 = Auto)
0
0 µs
42160.00 µs (0.04 s)
Pulse-width modulation
Frequency
0
0
Duty cycle
0
0
GPIOs
GPIO 1
Status
Low
Input
Flash
Output low
PWM
Output high
Default
Close

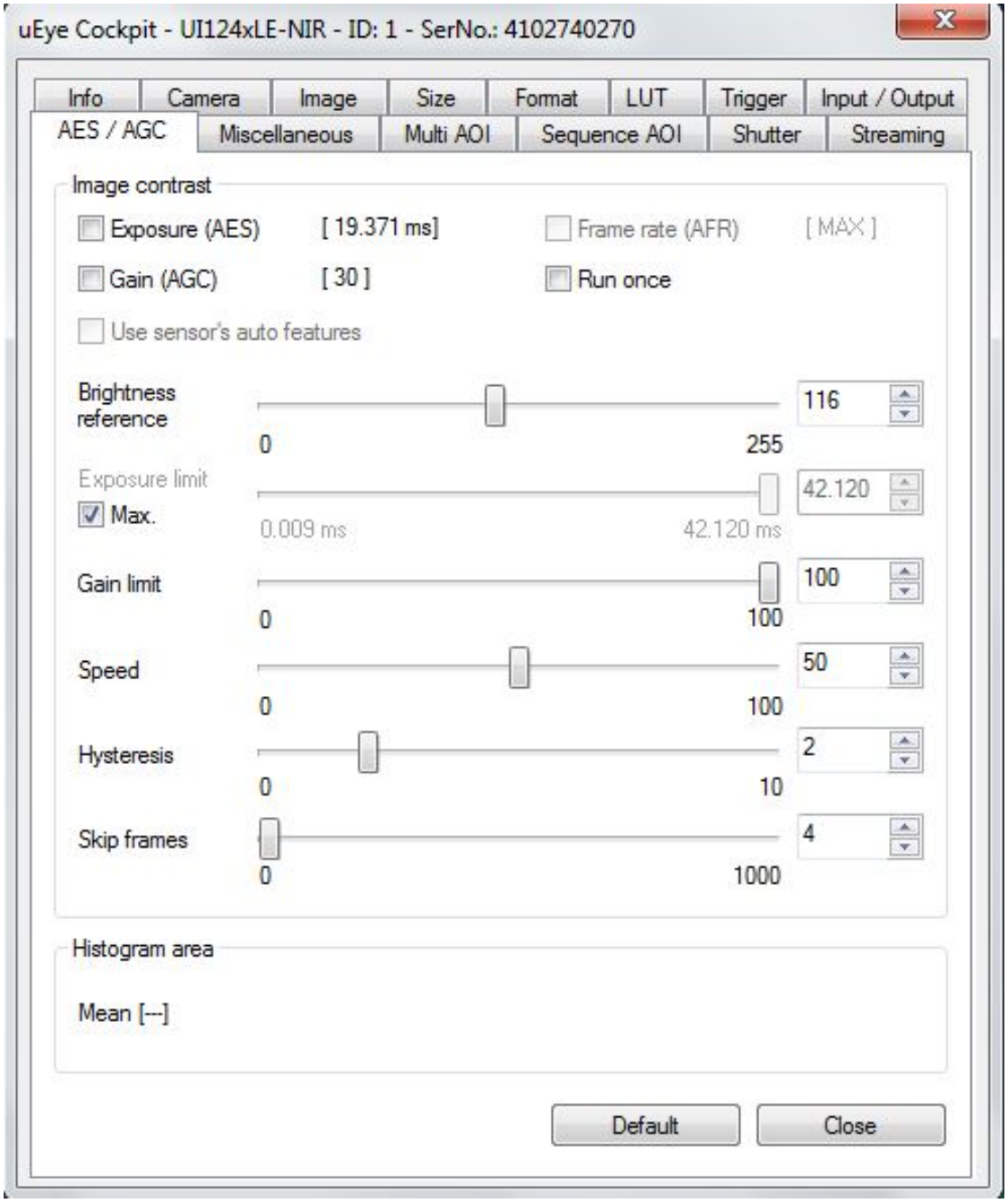
uEye Cockpit - UI124xLE-NIR - ID: 1 - SerNo.: 4102740270
Info
Camera
Image
Size
Format
LUT
Trigger
Input / Output
AES / AGC
Miscellaneous
Multi AOI
Sequence AOI
Shutter
Streaming
Image contrast
Exposure (AES)
[ 19.371 ms]
Frame rate (AFR)
[ MAX ]
Gain (AGC)
[ 30 ]
Run once
Use sensor's auto features
Brightness reference
116
0
255
Exposure limit
Max.
42.120
0.009 ms
42.120 ms
Gain limit
100
0
100
Speed
50
0
100
Hysteresis
2
0
10
Skip frames
4
0
1000
Histogram area
Mean [---]
Default
Close

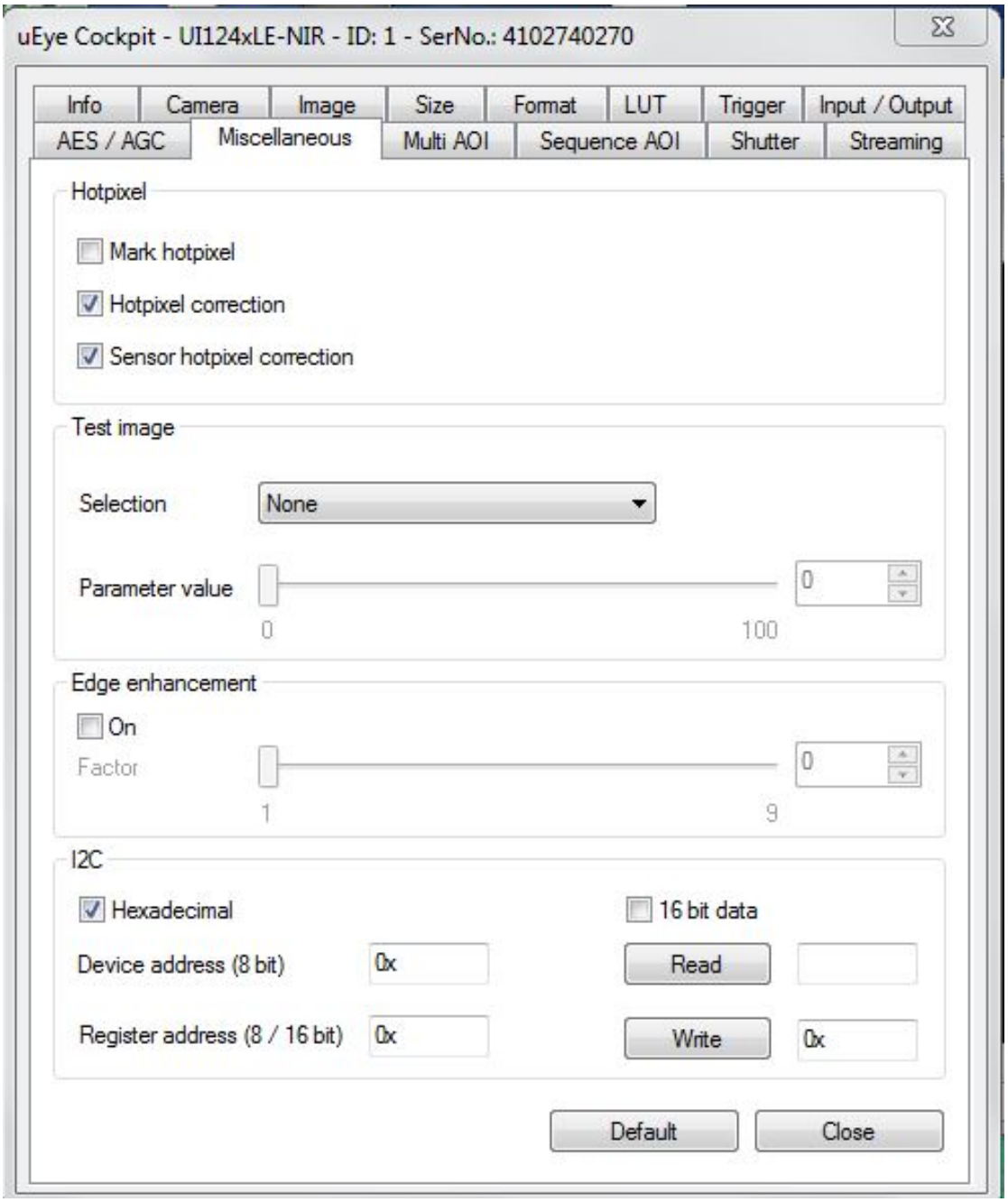
uEye Cockpit - UI124xLE-NIR - ID: 1 - SerNo.: 4102740270
Info
Camera
Image
Size
Format
LUT
Trigger
Input / Output
AES / AGC
Miscellaneous
Multi AOI
Sequence AOI
Shutter
Streaming
Hotpixel
Mark hotpixel
Hotpixel correction
Sensor hotpixel correction
Test image
Selection
None
Parameter value
0
0
100
Edge enhancement
On
Factor
0
1
9
I2C
Hexadecimal
16 bit data
Device address (8 bit)
0x
Read
Register address (8 / 16 bit)
0x
Write
0x
Default
Close

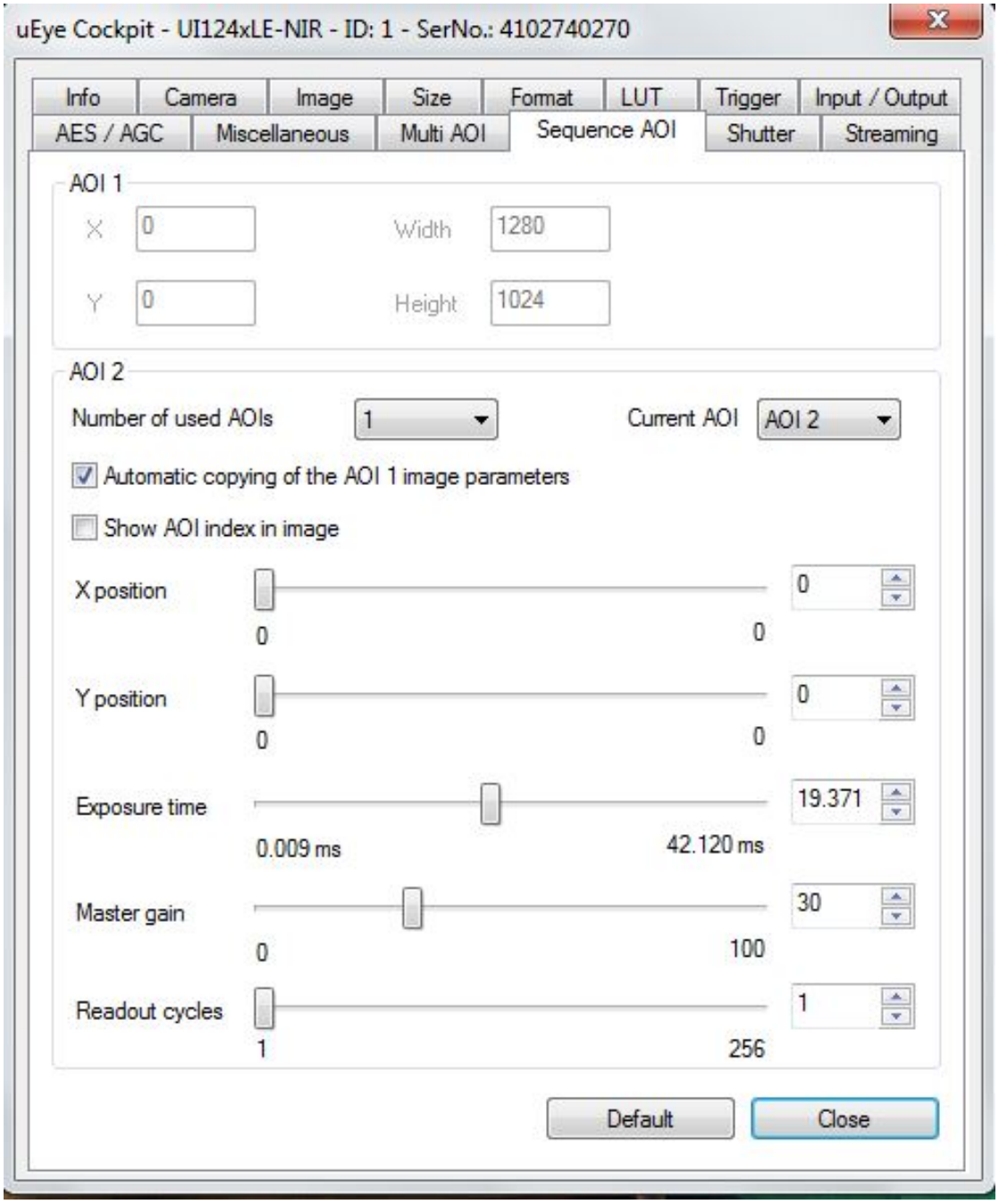
uEye Cockpit - UI124xLE-NIR - ID: 1 - SerNo.: 4102740270
Info
Camera
Image
Size
Format
LUT
Trigger
Input / Output
AES / AGC
Miscellaneous
Multi AOI
Sequence AOI
Shutter
Streaming
AOI 1
X
0
Width
1280
Y
0
Height
1024
AOI 2
Number of used AOIs
1
Current AOI
AOI 2
Automatic copying of the AOI 1 image parameters
Show AOI index in image
X position
0
0
0
0
Y position
0
0
0
0
Exposure time
19.371
0.009 ms
42.120 ms
Master gain
30
0
100
Readout cycles
1
1
256
Default
Close

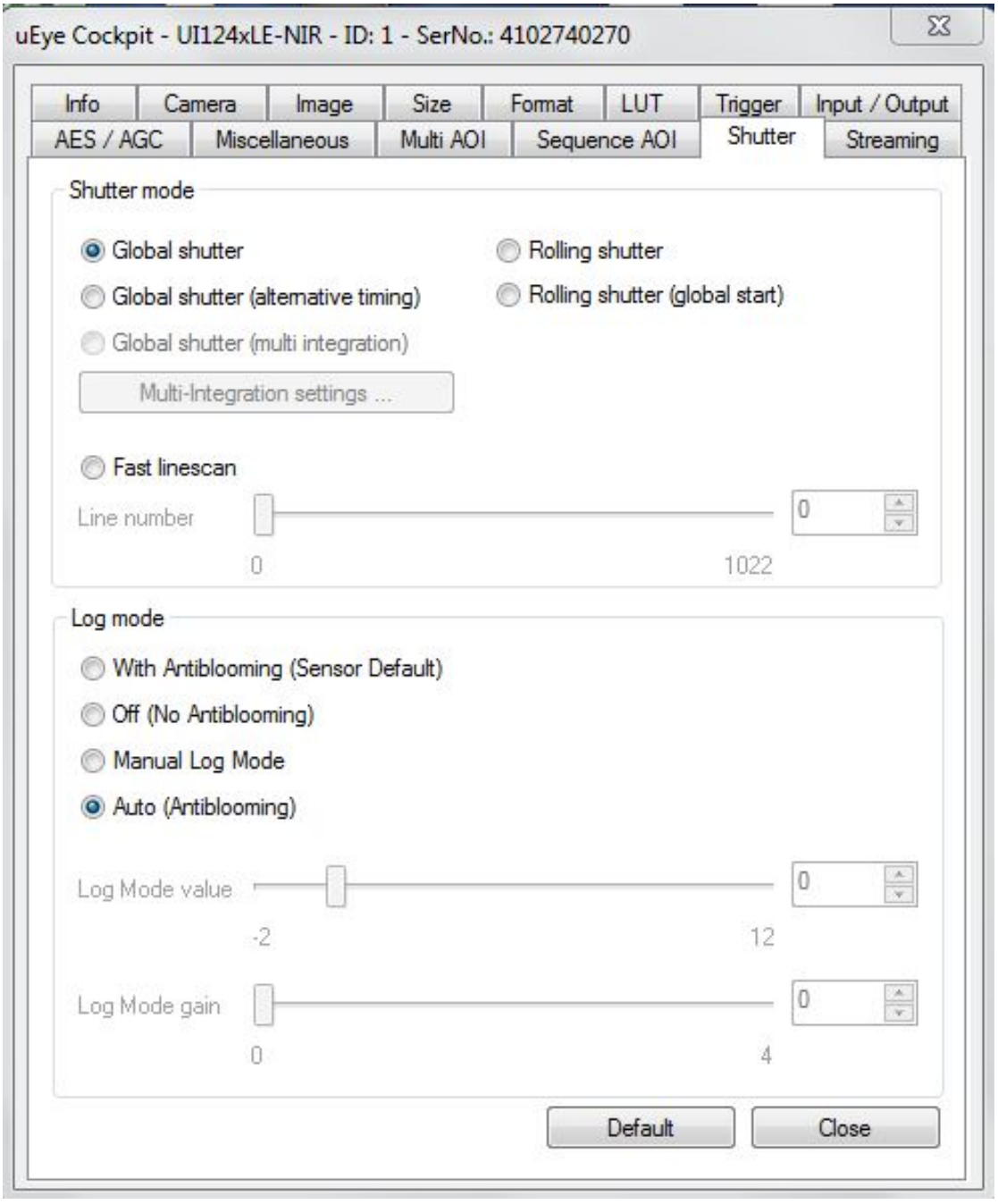
uEye Cockpit - UI124xLE-NIR - ID: 1 - SerNo.: 4102740270
Info
Camera
Image
Size
Format
LUT
Trigger
Input / Output
AES / AGC
Miscellaneous
Multi AOI
Sequence AOI
Shutter
Streaming
Shutter mode
Global shutter
Rolling shutter
Global shutter (alternative timing)
Rolling shutter (global start)
Global shutter (multi integration)
Multi-Integration settings ...
Fast linescan
Line number
0
0
1022
Log mode
With Antiblooming (Sensor Default)
Off (No Antiblooming)
Manual Log Mode
Auto (Antiblooming)
Log Mode value
0
-2
12
Log Mode gain
0
0
4
Default
Close

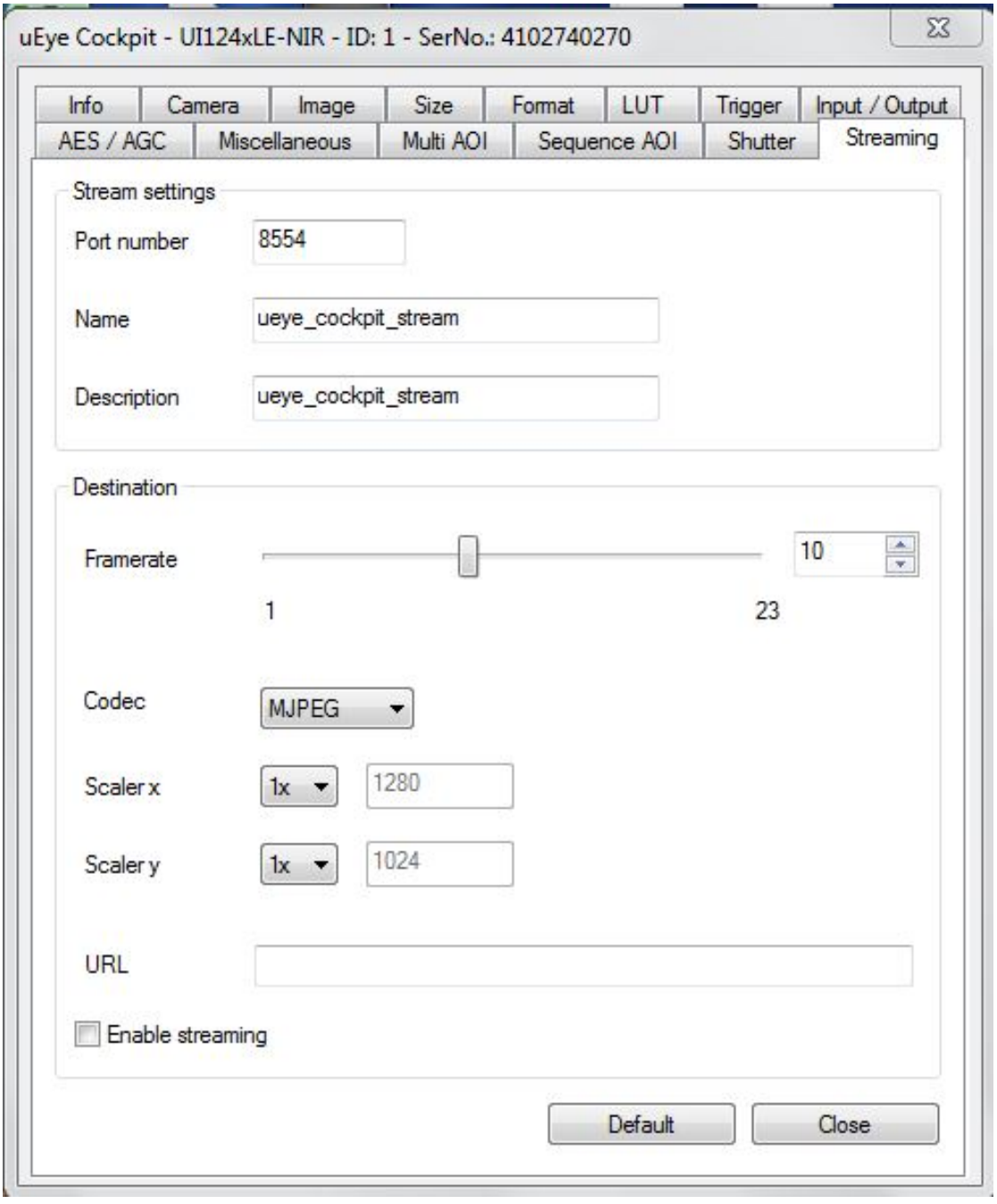
uEye Cockpit - UI124xLE-NIR - ID: 1 - SerNo.: 4102740270
Info
Camera
Image
Size
Format
LUT
Trigger
Input / Output
AES / AGC
Miscellaneous
Multi AOI
Sequence AOI
Shutter
Streaming
Stream settings
Port number
8554
Name
ueye_cockpit_stream
Description
ueye_cockpit_stream
Destination
Framerate
10
1
23
Codec
MJPEG
Scaler x
1x
1280
Scaler y
1x
1024
URL
Enable streaming
Default
Close

# Appendix B:

# Developed Tracking Software for Physical Activity Analysis

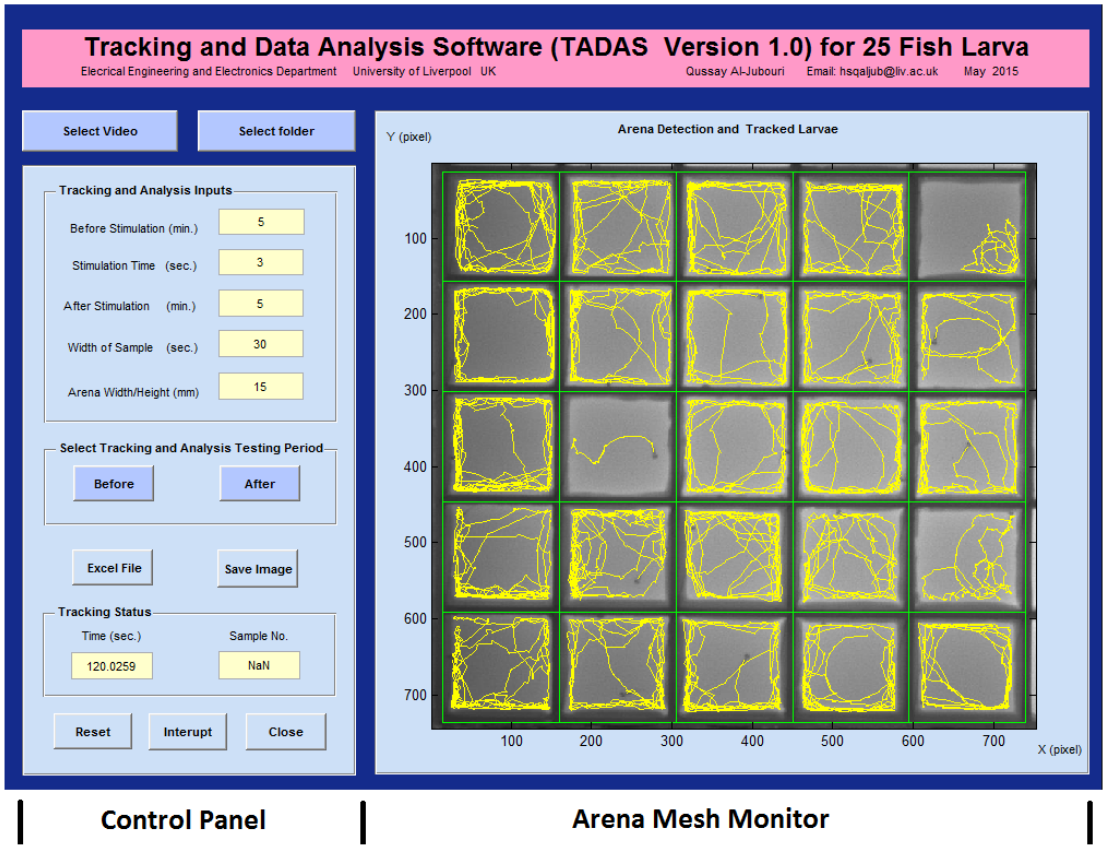


FIGURE C.1: Developed GUI

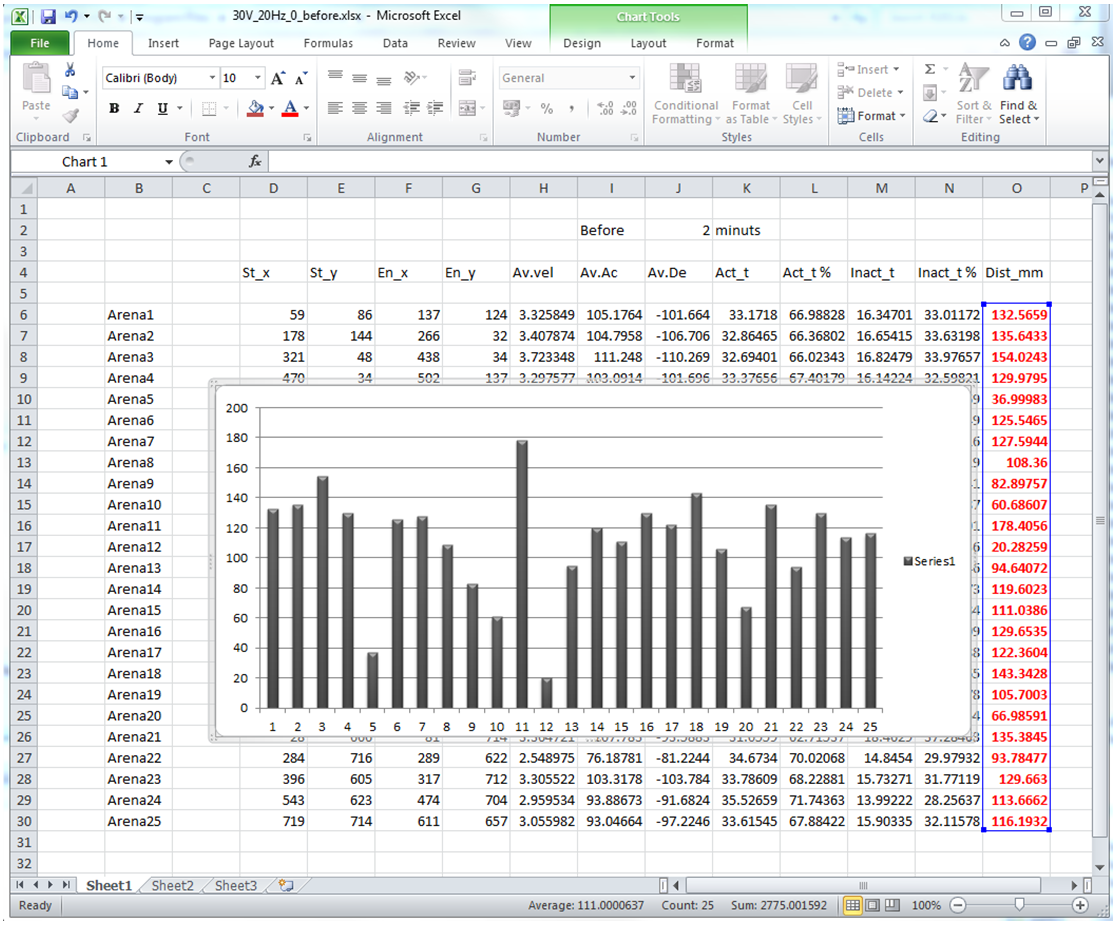


FIGURE C.2: Example of physical activity analysis of tracked fish larvae

# Appendix C:

# Experimental Setup and Estimated Cost of The Developed Electrical Stimulation Testbed

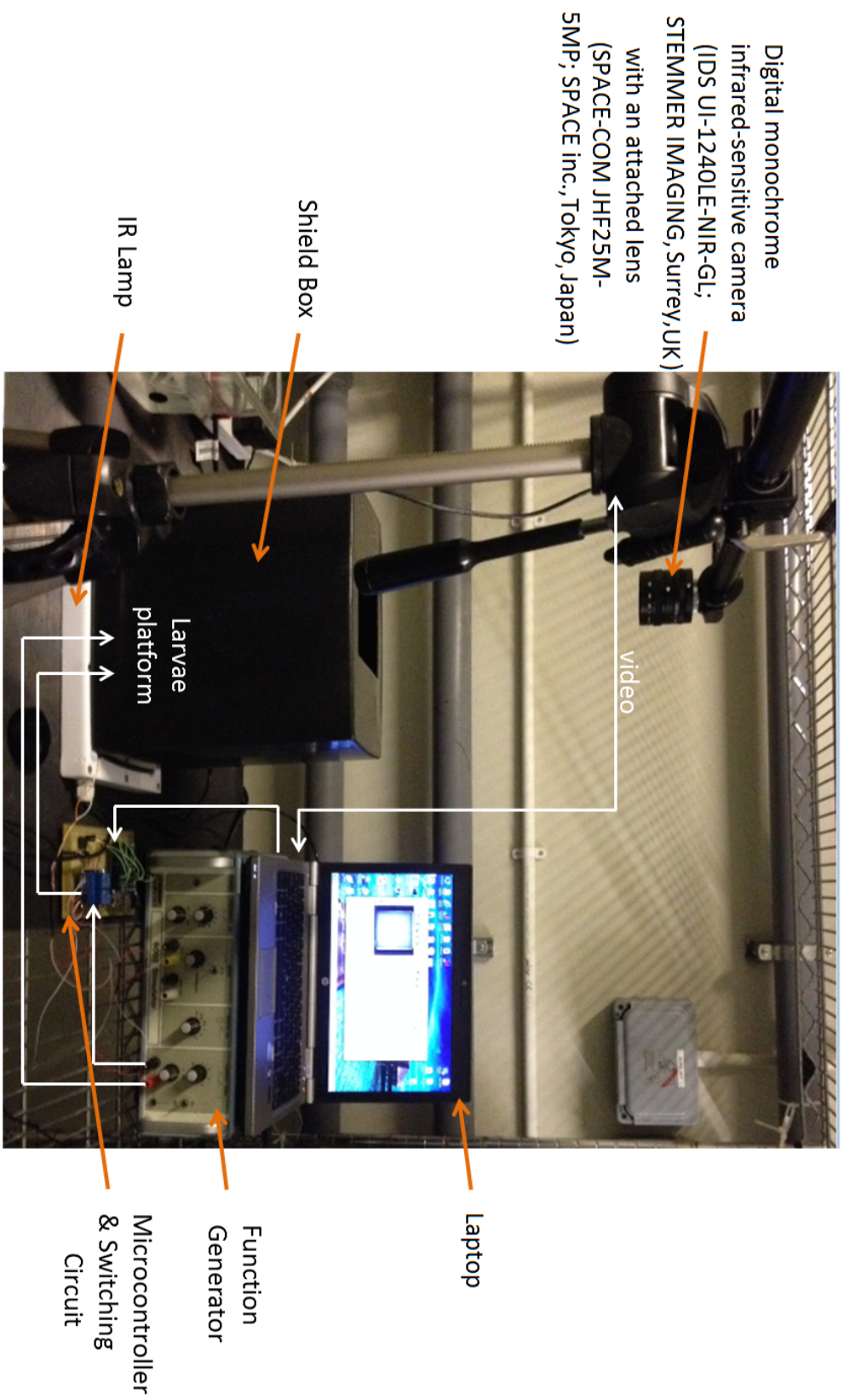


FIGURE D.1: Experimental setup of the developed testbed

| Item Number | Item Description | Item Price (pounds) |
|---|---|---|
| 1 | digital monochrome infrared-sensitive camera (IDS UI-1240LE-NIR-GL; STEMMER IMAGING, Surrey, UK) | 308.00 |
| 2 | lens (SPACE-COM JHF25M-5MP; SPACE inc., Tokyo, Japan) | 115.00 |
| 3 | Laptop, HP EliteBook Intel Core i5 2.4GHz - 2.6 GHz 8.0 GB | 450.00 |
| 4 | Camera tripod with slider | 96.00 |
| 5 | Harvard – research experimental stimulator (series 6000) | 150.00 |
| 6 | Arduino UNO A000066 ATMEGA328 Microcontroller Board | 20.24 |
| 7 | 1 Channel 5V Relay Module Shield | 1.99 |
| 8 | InfraRed Lighting illuminator | 35.00 |
| 9 | Plastic shield box | 2.00 |
| 10 | Built plastic plate of 25 square wells (length: 16.5 mm; width: 16.5 mm; depth: 8 mm) | 10.00 |
| 11 | 2 mm cables Wire (50 cm length) | 2.00 |
| 12 | PCB Experiment Matrix Circuit Board 5x7cm | 1.00 |
| | **Total Price (pounds)** | **1191.23** |

FIGURE D.2: Estimated cost of the developed testbed